The Role of Retained Austenite on the Performance of High Chromium White Cast Iron and Carbidic Austempered Nodular Iron for Grinding Ball Applications

by

JOSEPH SHUMANE MOEMA

Student no 26569087

Submitted in partial fulfilment of the requirements for the degree

MSc (Applied Science) (Metallurgy)

in the

Department of Materials Science and Metallurgical Engineering, Faculty of Engineering, Built Environment and Information Technology

UNIVERSITY OF PRETORIA

OCTOBER 2018

Declaration by author

This dissertation is composed of my original work, and contains no material previously published or written by another person except where due reference has been made in the text. I have clearly stated the contribution by others to jointly-authored works that I have included in my thesis.

I acknowledge that copyright of all material contained in my dissertation resides with the copyright holder(s) of that material.

Publications during candidature

Peer-reviewed and International papers:

1. **Moema JS**, Stumpf WE and Papo MJ. 2011. Effect of chromium addition on the abrasive wear behaviour of austempered ductile iron (ADI). *Microscopy Society of Southern Africa Proceedings*. vol. 41 pp21. (MSSA 2011). 5th-8th December 2011. DST/CSIR Nanotechnology Innovation Centre. National Centre for Nanostructured Materials. Pretoria, Gauteng, South Africa.

   ISSN 0250-0418 and ISBN 978-0-620-73767-8

2. **Moema J.S.**, Papo M.J., Stumpf W.E. and Slabbert D., "The role of retained austenite on performance of grinding media", *First International Conference on Tribology*, 24 to 26 November 2010, Copacabana, Rio de Janeiro, Brazil and Conference proceedings published in 2011, pp319 - 333: **ISSN 2178-3956**

Conference papers:

1. **Moema, J.S.**, Papo, M.J., Slabbert, G.A., and Zimba, J. Grinding media quality assurance for the comminution of gold ores. *World Gold Conference 2009*, The Southern African Institute of Mining and Metallurgy (SAIMM), 2009., Misty Hills, Cradle of Humankind, Johannesburg. South Africa, pp27 - 33

Acknowledgements

Firstly, I thank God the Almighty, who is worthy of my eternal praise and love.

To the following institutions and people, I am sincerely grateful for their contributions

- Dr Jones Malesela Papo of the Advanced Materials Division (AMD) within Mintek for offering financial support and providing world class conditions to conduct this MSc project. It is an honour to be a member of such a reputable research institution. Also my appreciation to Mintek for the opportunity to complete the project.
- My academic supervisor, Prof. Charles Siyasiya for his precise advice, encouragement, and patience in dealing with my overly enthusiastic behaviour.
- My wife Noko Rynett (Tlabela) Moema, who has left everything behind to marry me and for loving me and being my best friend (making me smile even when things turn bad). To you, I also apologise for making you feel the bitterness of my frustrations during this dissertation journey. To our lovely son Kgomotso Ditshego Moema who complained but understood why I had to miss some of his activities.

Lastly and most of all, I would like to thank my parents Mr Aaron Ramangadi Moema and Mrs Elizabeth Sesi (Ditshego) Moema for their unconditional love and all the sacrifices they made to raise my sister, four brothers and I. There are no words that I could use to describe my immense gratitude to you, other than, I love you.

The Role of Retained Austenite on the Performance of High Chromium White Cast Iron (HCWCI) and Carbidic Austempered Nodular Iron (CANI) for Grinding Ball Applications

by

Joseph Shumane Moema

Supervisor: Prof Charles W Siyasiya [1]

Co-supervisors: Prof Roelf J. Mostert[1]

Dr Malesela J Papo[2]

1. Department: Department of Materials Science and Metallurgical Engineering

   University: University of Pretoria

2. - Mintek – The Advanced Materials Division (AMD)

Abstract

The role of retained austenite on the performance of cast iron based grinding media (balls) is somewhat controversial. One school of thought is that retained austenite improves the performance through work hardening and transformation to martensite. Others argue again that the same phenomenon compromises the performance of the balls through spalling. In this study, high chrome white cast iron (HCWCI) and carbidic austempered nodular iron (CANI) grinding balls were subjected to different heat treatments to yield various amounts of retained austenite, after which they were subjected to abrasive wear testing. The tests involved were high stress abrasion (pin-on-belt abrasion test), low stress abrasion (rubber wheel abrasion test according to ASTM G65), combined abrasion-impact conditions (ball mill) and impact tests (drop test). As expected, it was found that the percentage retained austenite increases with an increase in austenitising temperature due to the dissolution of carbides. The surface hardness again decreases as the destabilisation temperature and amount of retained austenite increases.

The retained austenite content of the alloy before the high stress abrasion wear (pin on belt test, POB) was found to be significantly higher if compared to that after testing. The decrease in retained austenite was due to the transformation from austenite (γ_{rest}) to strain induced martensite (α') that occurs during the high stress abrasion wear test. The austenitising temperature of 1000 °C resulted in low percentage mass loss values or a lower wear rate from the ball mill test. The best high stress abrasive wear resistance for HCWCI, which was due to optimum properties, was achieved when the retained austenite content was reduced to 22.6%. It was found that the high stress abrasion resistance decreased abruptly once the retained austenite content decreased to lower than 10%.

The CANI alloy which was austempered at 275 °C (with graphite spheroids and carbides in the ausferrite matrix and 17.4% retained austenite) performed better under both low and wet abrasive wear (ball mill) conditions.

Keywords: Retained austenite, HCWCI, ADI, CANI, low stress abrasion, pin-on-belt, dry rubber wheel abrasion, ball mill.

TABLE OF CONTENTS

LIST OF FIGURES

LIST OF TABLES

LIST OF ACRONYMS

ADI – Austempered Ductile Iron

HCWCI – High Chromium White Cast Iron

CNI – Carbidic Nodular Iron

DI – Ductile Iron

CANI – Carbidic Austempered Nodular Iron

SEM – Scanning Electron Microscopy

POB – Pin on Belt

DRWAT – Dry Rubber Wheel Abrasion Wear Test

XRD – X-Ray Diffraction

AG – Autogenous

SAG – Semi-Autogenous

SAM – Sala Agitated Mill

BIC – Bushveld Igneous Complex

PGMs – Platinum Group Metals

UG2 – Upper Group 2 Reef

PGEs – Platinum Group Elements

R&D – Research and Development

ASTM – American Society for Testing and Materials

DIN – Deutsches Institut für Normung (German Institute for Standardization)

BS – British Standards

HRC – Rockwell C Hardness

BH – Brinell Hardness

MBWT – Marked Ball Wear Test

EDM – Electrical Discharge Machining

Q&P – Quenched and Partitioning

De-MQ-Sct – Multicycle Quenching sub-critical treatment

NOR – Normalization

TRIP – Transformation Induced Plasticity

NDT – Non-Destructive Testing

TTT – Time Transformation Temperature

CCT – Continuous Cooling Transformation

FAQ – Forced Air Quenching

EBSD – Electron Backscatter Diffraction

RAR – Relative Abrasion Resistance

MPa – Megapascal

AISI – American Iron and Steel Institute

SAE – Society of Automotive Engineers

EMPA – Electron Microprobe Analysis

TEM – Transmission Electron Microscopy

1. CHAPTER 1: INTRODUCTION

1.1. Objectives

The role of retained austenite on the performance of grinding balls was investigated in this project. The major focus was on controlling the amounts of retained austenite in order to optimize wear resistance and toughness in cast iron-based grinding media applications. Two families of cast irons were investigated, namely high chrome white cast irons (HCWCI) and austempered ductile irons (ADI). It was envisaged that the experimental work would establish the effect of retained austenite on the spalling behaviour, toughness and wear resistance of these families of materials. In terms of industrial applications, the balls are meant for use in the Platinum (Pt) mining industry, hence special emphasis was placed on the suitability of these balls for the milling of Pt bearing ores such as UG2 and Merensky Reef ore. Table 1.1 shows the metallurgical properties of the current grinding balls that are used in the platinum mining industry.

Table 1.1. Current Balls used in the Pt mining industry.

Material	HCWCI (*Magotteaux*^{TM})$^{(1)}$
Microstructure	Chromium carbides + Martensite
% Retained austenite	Less than 10%
Hardness	490 – 700HB (Brinell)
No. of drops within a ball mill	≥2000
Ball consumption	~0.93kg Steel/tonne of ore milled
Cost of grinding balls	R16 500 – R22 000/ton of balls (March 2016 price)
Grinding media cost	R13.94 – R16.90/ton of ore ground

The cost associated with this essential consumable depends mainly on two factors: delivered price and durability (quality) of the grinding media. When comparing different operating conditions arising from the changes in ore type or ball supplier (or simply, a trial of new products from the same supplier), there is a well-accepted evaluation criterion that accounts for both media price and quality, referred to as the Effective Grinding Cost or the Cost-Effectiveness of the application.

Any given operating condition is considered to be cost-effective when its unit grinding media cost, normally expressed in R/ton ground, is to some extent reduced, with respect to a nominal reference condition:

Grinding media cost (R/ton ground) **=** **ball price** (R/ton balls) x **ball consumption** (ton of steel balls lost/ton of ore ground)

Under this criterion, an alternative, higher-price grinding media product could be cost-effective if its associated consumption rate is sufficiently lower than the reference media, to yield an also lower grinding cost, as dictated by the equation. Additional costs like power consumption and storage costs are added to calculate the final Rand/ton milled. The plan is to use the grinding balls until they disappear (i.e. wear to small balls/scats), therefore there is really no income from recycling broken balls or scats. When the new ball is worn to the point where the porosity is exposed, it wears very rapidly into the porous section to form a bowl shaped lump that soon wears to a plate. These oddly shaped scats are then competent and wear down at the same general rate as the whole balls.

Even when the **HCWCI ball** is the 'industry standard', for example the platinum group metals (PGMs) mining industry in South Africa, when events like the global financial crisis occur the status quo is challenged based on unit cost of **the raw material** as mining companies pursue cost reduction strategies to maintain their financial viability.

1.2. Project Aim and Methodology

The key objective was to determine the influence of retained austenite on the following properties of the two cast irons, see Figure 1.1.:

- abrasive wear → high stress (pin-on-belt) and low stress (dry rubber wheel abrasion test)
- impact wear (spalling) → drop test (impact test)
- combined abrasive and impact wear → ball mill abrasion/impact test

---

[1] Magotteaux Fond, Patent specification number 1315203 of 1973

Methodology (also graphically shown in Figure 1.2):

An *extensive literature survey* was conducted in order to gain a fairly comprehensive overview of the various materials used in the mining industry, techniques used to evaluate these materials, and phenomena that ought to have been encountered in the course of the project.

Material: Based on the **literature review**, two alloys or cast irons as shown in Figure 1.1 were selected and developed. These alloys are High Chromium White Cast Iron (HCWCI) and Carbidic Nodular Iron (CNI). Pattern preparation and casting of the selected chemistries into wear plates and grinding balls were carried out. The carbon and silicon content, cooling rate of the alloy, heat treatment process and the formation of graphite makes a difference in the cast iron. The forms of eutectic graphite/carbide present in the iron microstructure and the matrix determines the classification. Figure 1.1 shows the six important types of cast iron(2). In this work two cast iron types were studied and compared, namely **high chromium white cast iron** (HCWCI) and **ductile iron** (DI) containing carbides in the ausferrite matrix known as carbidic austempered nodular iron (CANI).

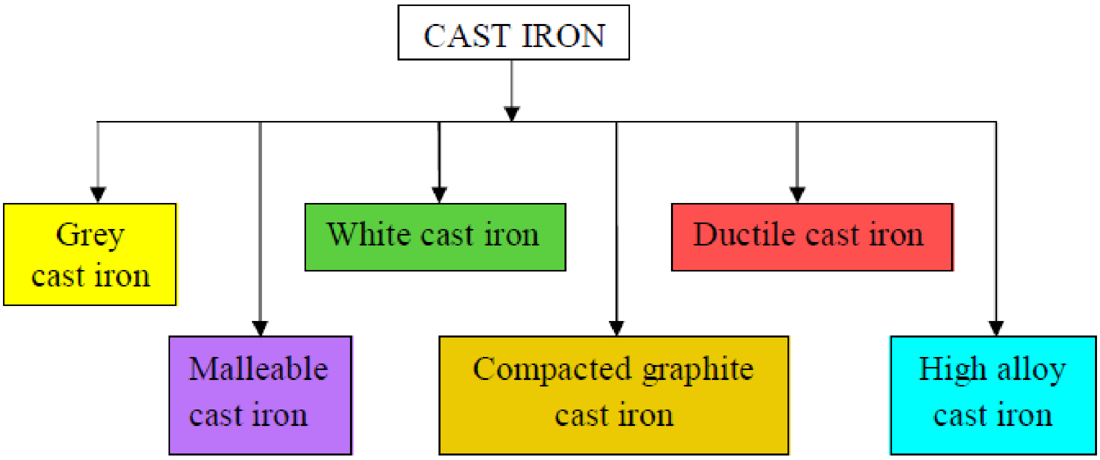

Figure 1.1: Types of cast iron.

---

[2] P. Dhanapal, PhD Thesis: A Study on the Production and Characterization of Carbidic Austempered Ductile Iron, Anna University, 2011

For this work, a high chromium white cast iron (HCWCI) alloy chemistry was selected or used since it does not have a negative effect to down-stream operations, such as flotation. High Cr cast irons are alloys based on the Fe–Cr–C system, usually in the range from 10 to 30wt% Cr and from 1.8 to 4wt% C. Commercial alloys contain up to 1wt% residual Si and additions of Mn, Mo, Ni and Cu to increase hardenability. While a variety of elements can be used to increase the hardenability of the alloys, for most of the alloys a single factor – the C content of the austenite just before quenching – is the main cause determining the hardness of the martensite and the amount of retained austenite after quenching.

Processing: Heat treatment processes to yield different amounts of retained austenite on HCWCI and CNI (to be converted to carbidic austempered nodular iron (CANI)) were performed.

Material Testing: The following tests were carried out on the processed material:

- General metallurgical characterisation tests such as chemical analysis, metallography, hardness and Scanning Electron Microscopy (SEM)
- Abrasive wear → high stress (Pin-on-Belt) and low stress (dry rubber wheel abrasion test, DRWAT)
- Combined abrasive and impact wear → ball mill wet abrasion/impact test
- X-Ray Diffraction (XRD) to determine the amount of retained austenite on the processed materials
- Scanning Electron Microscopy (SEM) to determine the wear mechanisms of the two alloys after abrasive wear testing.

A detailed schematic diagram showing the research methodology for the project is shown in Figure 1.2.

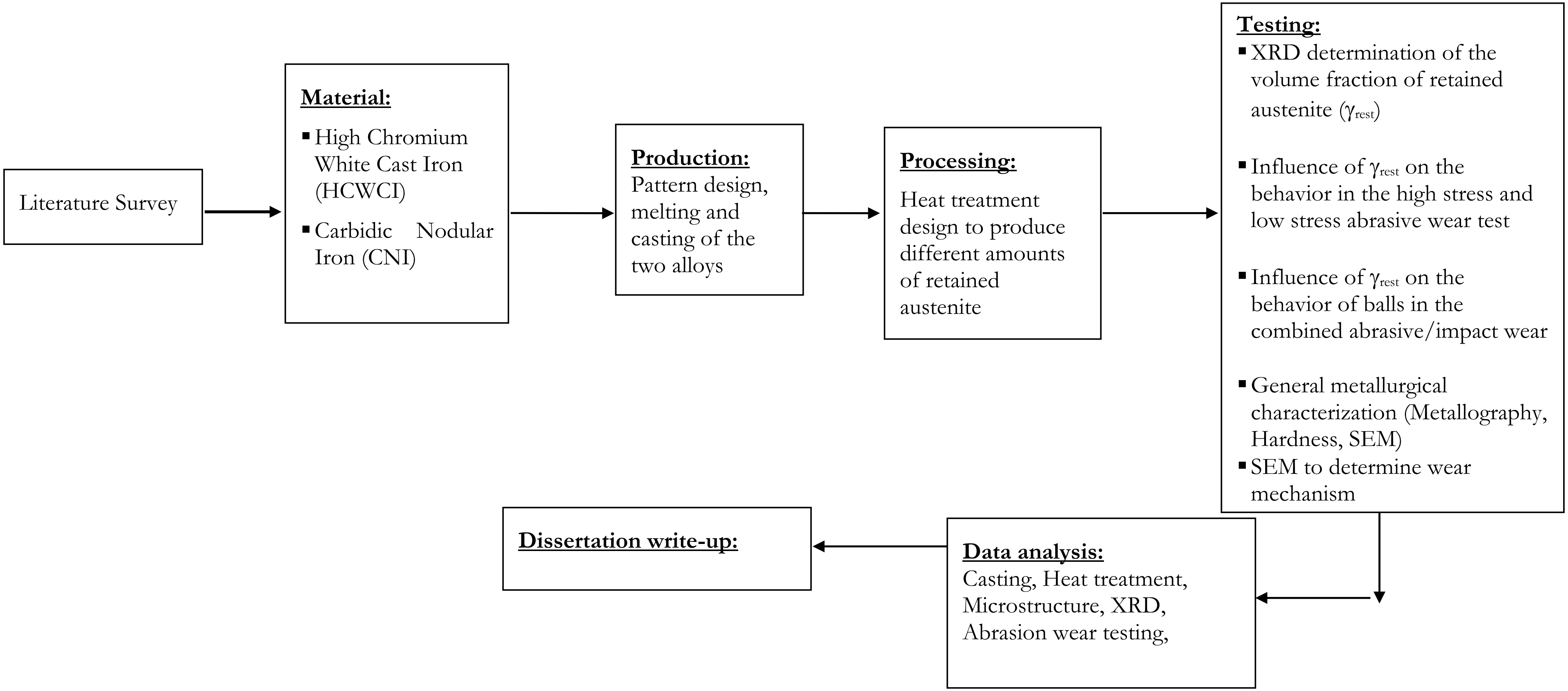

Figure 1.2: Schematic diagram showing the research methodology for the project.

2. CHAPTER 2: LITERATURE REVIEW

The rock crushing and grinding professionals continually seek new **comminution techniques** to gain greater control over their milling processes. By doing this they must ultimately relinquish this command and share their developed technologies with sector colleagues in order to move forward. Different types of grinding media have been used in the mining industry for processing of various natural ores such as:

- Iron
- Platinum
- Gold
- Copper
- Bauxite
- Lead – Zinc
- Rock phosphate and
- Coal.

There is no standard solution for the mineral industry and the wear rate of grinding media varies from mine to mine, ore to ore and even for the same ore from time to time. Due to the diversity of all the literature available, this survey is concentrated on the following key issues:

- **Comminution of minerals by ball grinding**: an overview is given of what ball grinding is about, what are the variables, costs, life times, typical types of alloys, end-of-life determinants, different mining industry needs, etc..
- **General metallurgy of grinding ball alloys**: a review of what is required in general from a grinding ball, typical types of alloys, the Magotteaux^{TM} process, conventional casting details, etc.
- **Wear and erosion mechanisms in ball grinding**: literature on the wear models, variables, determinants, etc. are reviewed.
- **Types of wear and abrasion tests**: In this section different tests, why different tests, how are they compared, etc. are reviewed.

2.1. Preamble

The **comminution process** is one of the biggest cost drivers in the mining industry. Most grinding balls often suffer from high abrasion and impact related problems, see Figures 2.1 and 2.2 [1]. Whether the balls are based on steel or cast iron, proper alloying and/or heat treatment, offer a window for conferring the desired microstructure and with that a long service life to the balls. This literature review examines the role of retained austenite on the performance of high chromium white cast iron (HCWCI) and austempered ductile iron (ADI) for grinding ball applications.

The role of retained austenite on the performance of grinding media is somewhat controversial. One school of thought is that retained austenite improves the performance through work hardening/transformation to martensite. On the other hand, others argue that the same phenomenon compromises the performance of the balls through spalling. A literature survey was therefore conducted with the objective of understanding the effect and role of retained austenite in high chromium white cast iron (HCWCI) and austempered ductile iron (ADI) materials used for grinding balls. The salient findings from this study are detailed below, starting with ductile iron.

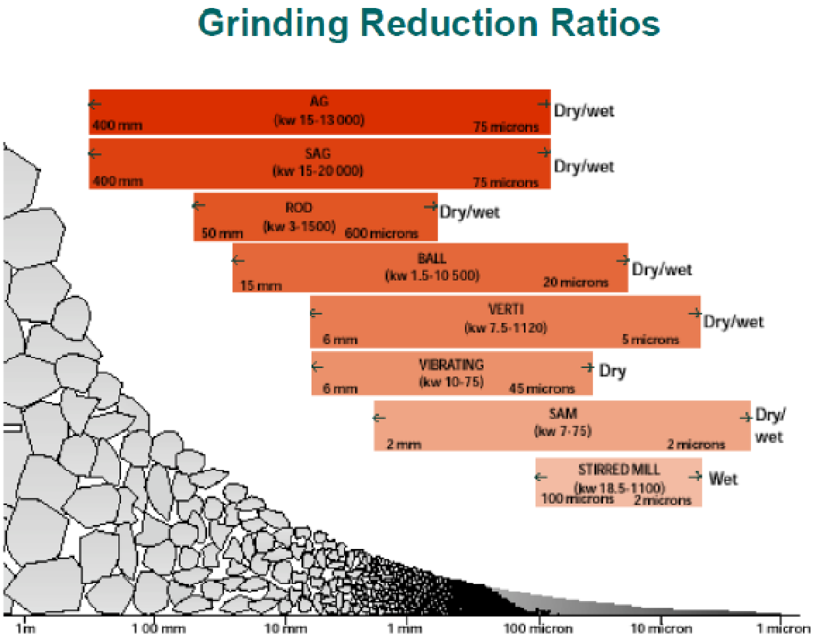

Figure 2.1. Typical comminution operations such as autogenous (AG), semi-autogenous (SAG), rod (ROD) and ball mills (BALL), low speed stirred mills, namely, Vertimill, Sala Agitated Mill (SAM) in the mining industry [1].

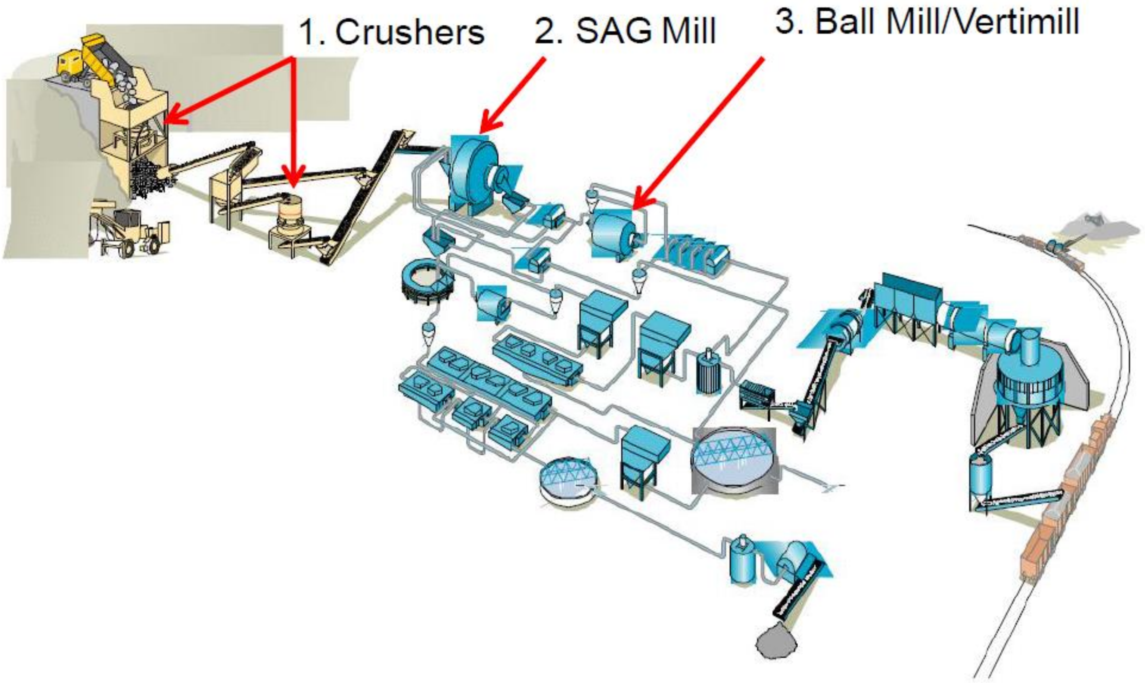

Figure 2.2. Typical comminution operations involving crusher, semi-autogenous (SAG) and stirred vertical ball mills in the mining industry [1].

2.2. Comminution of minerals by ball grinding

This section gives an overview of what ball grinding is about, what are the variables, costs, life times, typical types of alloys, end-of-life determinants, and different mining industry needs.

2.2.1. What ball grinding is about

Grinding is an important process that is used in many industries such as mineral processing, cement production, power plants and pharmaceutical industries. It is an inefficient and costly process in terms of energy and alloy requirements. An enormous amount of research has been done in trying to understand and improve the process [2]. One of the basic operations in minerals processing is grinding of the ore to the point where valuable minerals are liberated from the host rock. Subsequent operations then separate the desirable minerals from the gangue or waste. Grinding usually accounts for at least 50% of a concentrator's energy consumption and as it is essential to the efficient separation of minerals, is the key to good minerals processing [2, 3]. To produce clean concentrates it is necessary to grind the ore fine enough to liberate the minerals, but over-grinding inflates energy costs and can lead to the production of untreatable fine 'slimes' particles. Grinding is therefore a compromise between recovering clean high-grade concentrates, operating costs and fines losses.

2.2.2. The Milling Process

Milling is performed in rotating cylindrical steel vessels shown in Figures 2.3 and 2.4 (usually enclosed with 15~22° tapered ends), normally driven at a fixed speed, and provided with renewable internal liners to protect the shell. The grinding medium varies with the application and can be steel balls or cones, rods, sized rocks (pebbles) and, in some cases, the ore itself. The grinding medium is coaxed to move inside the mill and breaks up the ore particles by a combination of attrition and impact as shown in Figure 2.5. Maximum driving energy is drawn when the load is run between 40% and 50% volume filling and water is added to the feed to assist the flow through the mill [2, 3].

Figure 2.3. Top view of a typical industrial ball mill [2].

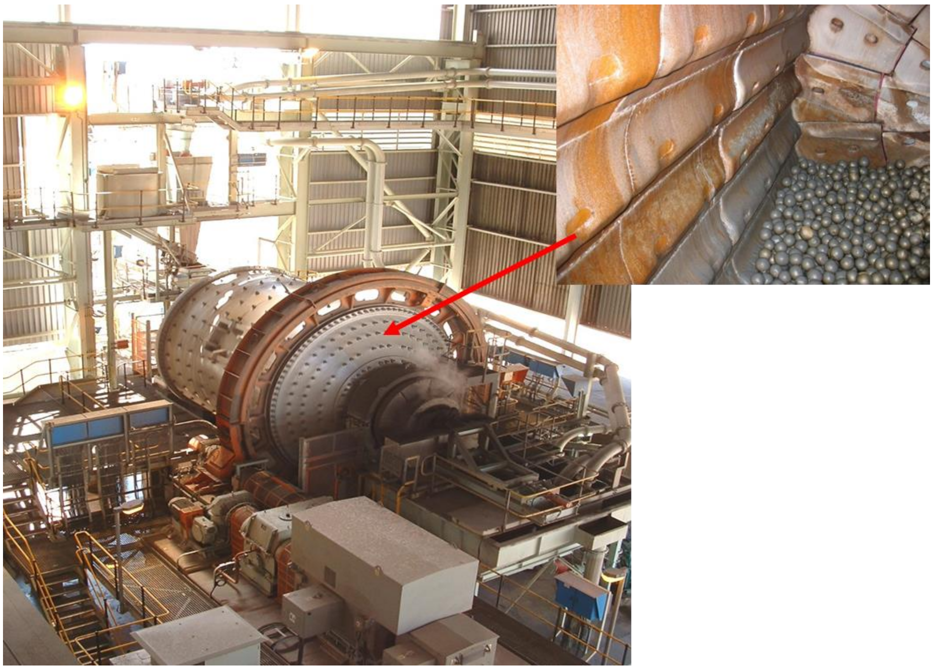

Figure 2.4. External and internal views of a typical industrial ball mill.

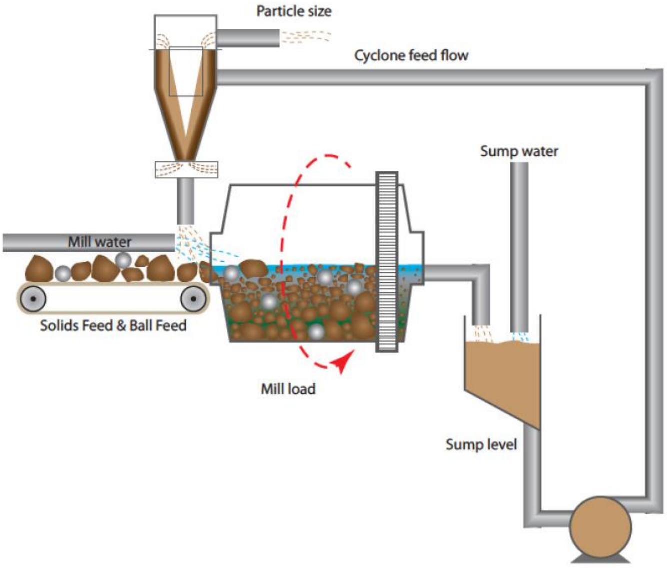

Figure 2.5. A picture showing a single stage closed circuit grinding mill circuit [3].

In the process, incoming feed, which may be straight run of mine (ROM) ore, or may have gone through stages of crushing preparation, is reduced to the required size or mesh of grind. The type of medium used, the nature of the ore feed and the type of circuit control product size are variables from application to application. Mills can operate in either open or, more commonly, closed circuits. In a closed circuit operation the material discharged from the mill is pumped into a cyclone classifier, a device for separating coarse from fine mineral particles. The coarse fraction is then returned to the mill for further grinding. The rotational speed of the ball mill at which the load centrifuges, i.e. sticks to the shell of the mill, is called the critical speed and varies according to the diameter of the mill and the mass density of the load. Mill speed is usually defined as a percentage of the critical speed, normally between 65% and 90%. Finally, the milling operation can be single or multi-stage, determined by the ore type, mesh of grind and economics [3].

2.2.3. Ball mills

A ball mill, as the name implies, uses media for grinding, normally ranging from 25mm to 150mm in diameter. Normally one top-up size is used. However if there are several distinctly different feed streams more than one should be used. The ball mill should operate at between 65% and 80% of the critical speed, but higher speeds have been used on ores which require high impact conditions for improved grinding. Ball mills can be of the grate discharge or overflow type. Grate discharge mills are normally used for primary grinding, and overflow mills for regrinding. Since balls have more discrete breakage events, they are better suited for fine grinding than rods and are thus used for secondary and tertiary stage milling [3].

Ball milling circuits can be designed to be topped-up on- or off-line. 'Polish' grinding, or concentrate regrinding operations often employ cones or cylpebs (cylindrical pebbles) as grinding media because of lower operating costs and reduced slimes production. However, a combination of top-up sizes is required for optimum media size distribution [2].

Description: Ball mills are similar in concept to the rod mill but are charged with steel balls in this environment. The mill consists of a cylindrical drum, sometimes tapered at one end, and usually has a charge of steel balls (up to 40% by volume) ranging in size up to 125mm for larger mills. Product size can be as small as 5µm, but the product size is dependent upon the time the charge spends in the grinding zone and therefore the reduction rate is a function of the throughput. The lining material is of great importance as there is a significant amount of wear taking place due to the action of the steel balls on the liner. The speed of rotation is an optimum at about 75% of the critical speed. Some mills are compartmentalised with each subsequent section having a smaller ball size [4]. The mineral can pass through to the proceeding section, but the balls cannot. This ensures that the smaller particles are effectively ground by the smaller grinding media.

Characteristics*:* Ball milling is a versatile grinding operation and has a wide range of applications. The mill can vary in size from small batch mills up to mills with outputs of hundreds of tons per hour. They are the most widely used of all grinding mills. Small hand operated ball mills are used in Bolivia for preparation of ore, sand and gravel. Mineral processing plants use two main processes; these are comminution and separation [5]. The objective of the comminution process is to break complex particles consisting of numerous minerals into smaller simpler particles where individual particles consist primarily of only one mineral. The process in which the mineral composition distribution in particles changes due to breakage is called liberation. The purpose of separation is to separate particles consisting of the valuable mineral from those containing the non-valuable mineral or gangue [5].

2.2.4. Key Process Variables

Ball milling has for a very long time been a standard procedure for the size reduction of many types of ores, and was introduced into the gold milling plants of South Africa in 1935. Grinding media exert a significant influence on milling performance in terms of product size, energy consumption and grinding costs due to media wear. Grinding ball's mass, surface area and size distribution are considered as the major factors affecting ore size reduction performance during comminution [5].

Milling encompasses so large a number of variables that it is almost a truism to say that it is not possible to specify the optimum plant configuration, mill design, milling conditions, type and load of medium for any given task [6].

Media shape: Early work on grinding media focused exclusively on materials and size. However more recently, the role of media shapes on grinding performance is gaining attention [7]. The acclaimed advantages of non-spherical grinding media are their foundry production costs, which are thought to be lower than those of spheres, and the minimum porosity that can be produced on casting [7]. Cloos stated that the advantage of a particular grinding media shape depends on the area, linear and point contact of the media with each other [7]. However, ideally grinding media should fulfil the following requirements:

- They should have the largest possible surface area to provide suitable contact with the material being ground;
- They should be as heavy as possible to have sufficient energy required for breaking the ore particles.

These requirements must be balanced, since the larger the individual grinding media, the less the specific surface. In a ball mill particles are "nipped" between steel balls as shown in Figure 2.6.

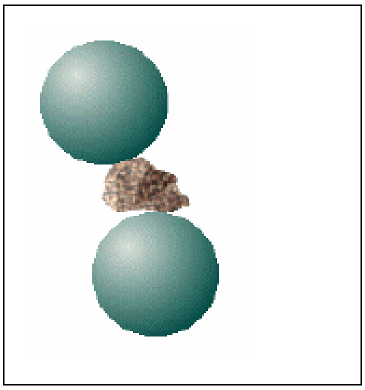

Figure 2.6. Photograph showing the grinding process that occurs in the ball mill [6].

Mill Speed: Two types of charge motion can be described in the ball mill, i.e. the cascading charge at lower speeds and the cataracting mill at higher speeds. The speed is measured as a fraction or percentage of the rotation rate at which gravity is equal to the centrifugal force at the inside of the mill liner [6]. This is called the critical speed

$$Cs = 42.3/\sqrt{D}$$

where: D = diameter (m) inside liners

Cs = critical speed (rpm)

Ball Load: The Ball Load is expressed as the volume fraction occupied after a grind out of 10-15 minutes. This represents approximately a voidage of 30 - 40% by volume (as shown in Figures 2.7 to 2.8) and up to 45% for diaphragm mills [6].

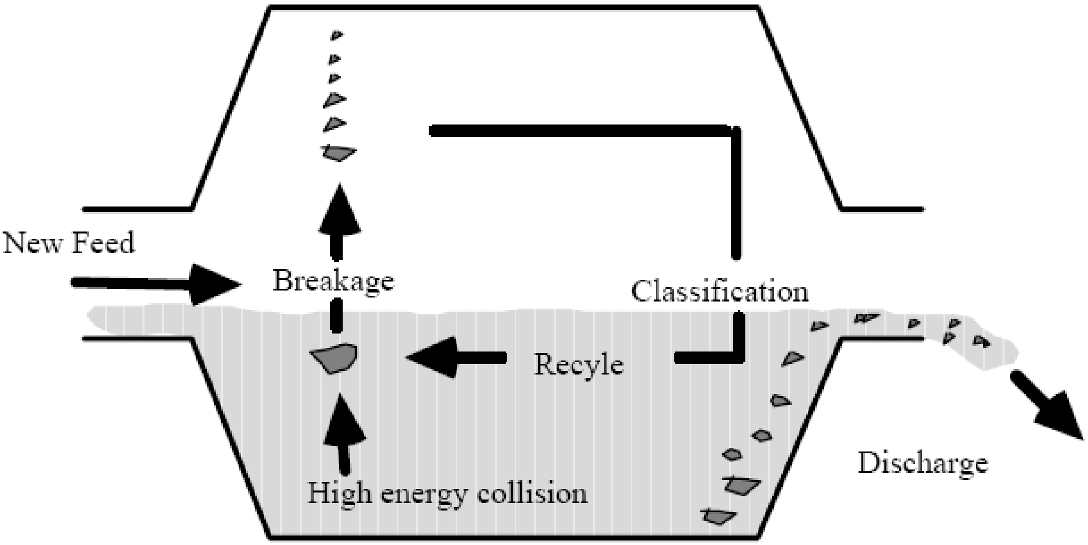

Figure 2.7. Conceptual view of a typical industrial ball mill [6].

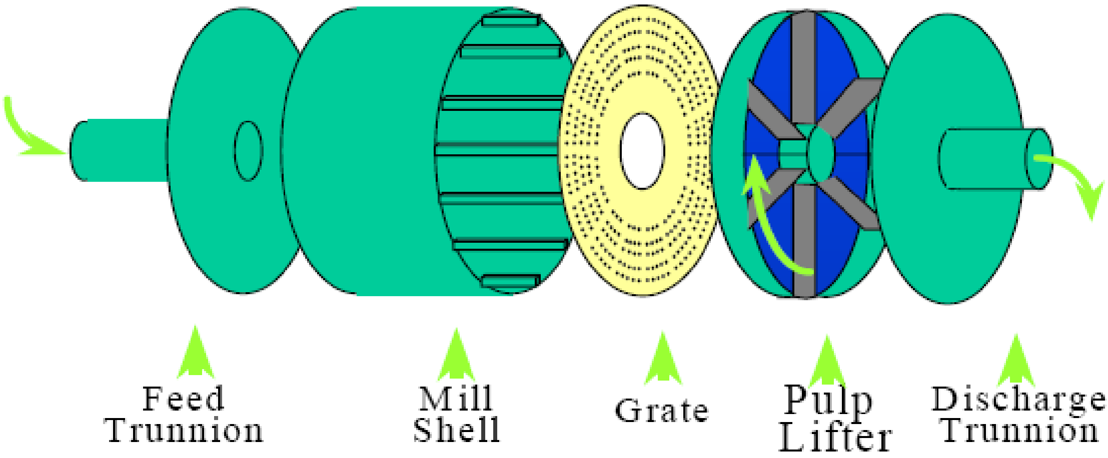

Figure 2.8. Conceptual view of ball mill [6].

Mill efficiency: This is an important parameter which affects the energy utilization during comminution. It is affected by the mechanical energy transition, the breakage mode, and the energy lost in elastic and permanent deformation of the solid particles before breakage. Obviously, energy efficiency does not depend only on the equipment used but it is also dependent on the material itself, especially at smaller sizes [8]. The pulp density is an important parameter which influences the grinding efficiency. The performance of ball mills is very sensitive to the volumetric mill filling which influences grinding media wear rates, throughput, power draw and product grind size [8].

Mill power: Usually plant operators use mill power readings as an indicator of the degree of ball filling and often try to keep it at the maximum level. It is well known that the mill-absorbed-power depends on other operating parameters than ball level, such as pulp density, liner configuration, etc. [9]. As the ball wear rate depends directly on the surface of the media charge, a small variation in power will lead to an important increase of wear rate. The risk of under-loading or overloading the mill could be an issue as well. A direct measurement of the ball level in the mill, more accurate than power readings, as well as a control of it, is highly important as operating costs are directly affected [9].

Ore size reduction in mining operations is a significant contributor to energy consumption and mineral production costs. In fact, more than 50% of the total energy consumed in the production of copper, gold and other mined commodities is spent on size reduction, and this energy intensity is exacerbated as plants process higher tonnages of ores of lower head grade. Semi-autogenous grinding (SAG) mills account for a large portion of the overall grinding energy input in mineral processing [9].

2.3. Type of Wear in Mining Industry

The mining industry involves many problems beyond the initial ore removal and handling of the large size feed. The treatment of an ore body from the run of mine (ROM) to a final product goes through various processes and each stage uses some form of wear or abrasive resistant material, see Figure 2.9 [1]. Run-of-Mine (ROM) ball mills are used for primary grinding applications in operations where it is difficult to get a consistent proportion of coarse competent rocks in the feed to act as grinding media. Different types of wear mechanism occur at each stage as summarised below:

- Crushers
    - High stress abrasion
    - High impact forces
    - Gouging abrasion
- AG/SAG mills and large ball mills
    - High stress grinding abrasion
    - Medium impact forces
    - Scratch and micro-cracking resistant
- Small ball mills and Vertimills
    - Erosion
    - Low stress scratching abrasion
    - Low impact forces.

Figure 2.9. A flow diagram showing type of wear in the mining industry (Comminution) [1].

2.3.1. Grinding media wear

Steel consumption constitutes a significant proportion of grinding cost in industrial ball mills. This steel consumption is mainly attributed to wear of grinding media and liners. The wear of grinding media in a mill is a contentious subject and many theories exist regarding the laws governing this process. It is known that the total media wear in the grinding process results from three recognized wear mechanisms: **abrasion, impact and corrosion**, see Figure 2.10 [1].

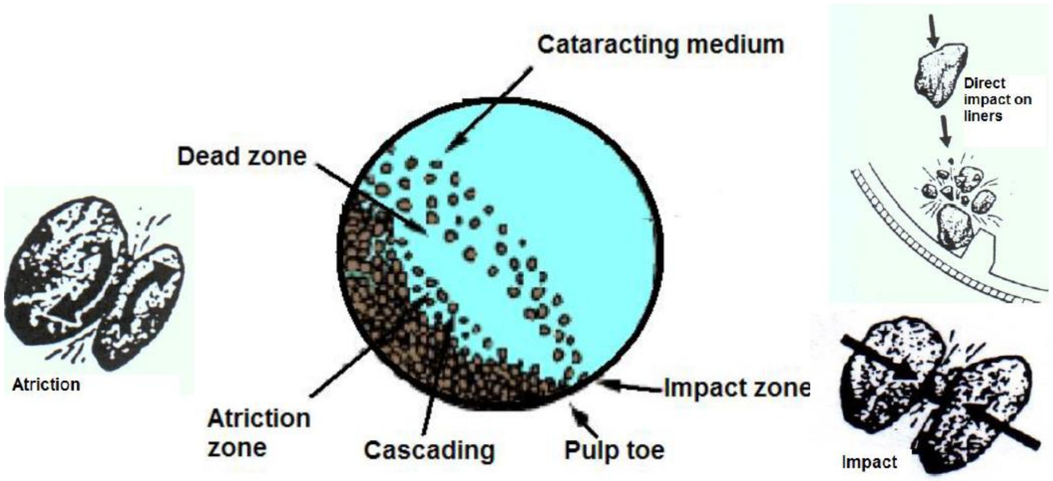

Figure 2.10. A diagram showing the attrition and the impact grinding mechanisms inside a ball mill [1]

Corrosive wear is most significant in wet milling and least significant in dry milling, while abrasion and impact wear dominate in dry milling [10]. It is, however, difficult to isolate their relative contributions toward overall wear under the conditions in a mill; the contribution to total media wear of each of these wear mechanisms has not correctly been established [10]. As the mill speed approaches the critical speed, the ball charge continuously falls from a height of about, or greater, than half of the inner diameter of the mill, and contact is made with ore particles, other balls or mill liners, causing impactive wear of both media and liners, see Figure 2.10.

Attrition plays a large part in all fine grinding operations and has been known and acknowledged [10]. However it is associated with abrasive wear, which occurs through penetration and ploughing of media materials from the media surfaces by hard ore particles. The rate of ball wear during the abrasive process is proportional to the surface area of the ball or the square of the ball diameter.

Electrochemical interactions between abraded and un-abraded areas of the ball surface, as well as between the grinding media and minerals, occur especially in wet grinding; resulting in media corrosion. In attempts to reduce the ball's consumption and the high costs of fine grinding, many studies have focussed on the analysis of factors causing ball wear and a number of theories have been proposed [1, 10]. Bond proposed that galvanic corrosion could contribute to wear owing to differences in electrochemical potential between the metal and the slurry. More recently, other investigators used inhibitors to reduce the corrosion component of wear in laboratory mills. The corrosion rate of the media was found to be a function of the mineral in the slurry [10].

For copper ore grinding, the corrosion of white irons was found to be between about 40 and 60% of the wear. Corrosion was about 25 to 35% of the wear for the same media when grinding iron ores [11].

2.3.2. Models and theories of wear

Grinding media wear is a contentious subject and many theories exist regarding the mechanisms governing the process. Measurement of ball size distribution within a ball mill can provide data on ball wearing mechanisms and indicates the relative intensities of abrasion and impactive forces within the mill. Some work done in trying to establish specific mechanisms dominating wear were also reviewed. Wear itself is complex and there is no generalised wear theory that adequately describes the wearing phenomenon.

However, several authors have made an important contribution to the understanding of the wear process [11, 12]. Among the models and theories put forward are;

- Bond Wear Model (equal film wear)
- Volume Theory (impactive)
- Surface Theory (abrasive).

On the basis of data from a large number of experimental tests and from industrial plant experiences, Bond [12] in 1963 developed the following ball wear loss formulae for wet and dry ball milling [12]:

For wet ball milling:

$$Ball\ Wear\ \left(\frac{kg}{kWh}\right) = 0.16(Ai - 0.015)^{1/2} \text{...............Equation 2.1}$$

And for dry ball mills (grate discharge)

$$Ball\ Wear\ \left(\frac{kg}{kWh}\right) = 0.023(Ai)^{1/2} \text{.........................Equation 2.2}$$

where $\mathbf{A_i}$ is the abrasion index of material determined from ball mill abrasion tests and some figures of the abrasion index for other materials are shown in Table 2.1 [13].

Table 2.1. Abrasion index for other materials [13].

Material	Specific gravity	A_i
Dolomite	2.70	0.016
Shale	2.62	0.021
Limestone	2.70	0.032
Clinker	3.15	0.071
Magnesite	3.00	0.078
Copper ore	2.95	0.147
Hematite	4.17	0.165
Magnetite	3.70	0.222
Granith	2.72	0.388
Taconite	3.37	0.624
Quartzite	2.70	0.775
Alumina	3.90	0.891

Volume theory

The volume theory predicts a hyperbolic size frequency distribution. According to this theory, the rate at which the weight of any ball decreases is proportional to the mass (volume) of a ball [12]. It was established that during impact, work done by a ball to stress an ore particle is proportional to the kinetic energy of a ball when cataracting and cascading during rotary motion of a mill and, therefore, to the mass (m) or volume of a ball. This can be presented mathematically as:

$$-\left(\frac{dm}{dT}\right) = k_m m \text{……………………Equation 2.3}$$

T being the amount of material milled in tons. The constant of proportionality $\mathbf{k_m}$ is termed the tonnage constant of balls, measured in the units as "per ton".

Surface theory

According to the surface theory, the size frequency distribution is flat: the same number of balls is found in every interval when the size range is divided into equal widths [12]. The basic assumption of this theory is that the majority of comminution events are due to abrasive grinding of the particles of ore by the balls, and so suggests that wear rate of balls is proportional to the surface area of a ball. For a ball of mass m, the surface area is proportional to mass to the power of two thirds; so that the rate of mass loss is:

$$-\frac{dm}{dT} = bm^{2/3} \text{ ……………………Equation 2.4}$$

$$m(T) = \{m_0^{1/3} - \tfrac{1}{3}bT\}^3 \text{………..….Equation 2.5}$$

where:

b is a surface wear constant

m$_o$ is the original mass of a ball and

T carries the same meaning as for the volume theory.

These equations are only valid if the sphericity of a ball remains constant and valid only if

$$T < \frac{3m_0^{1/3}}{b} \text{..................................Equation 2.6}$$

2.4. Typical Types of Ores

The composition of the ore itself has an important influence on the pulp chemistry [14]. Moreover, if the ore composition is heterogeneous the pulp chemistry could change quite quickly. Sulphide minerals consume oxygen by sulphur oxidation, e.g., the oxidation reactions of pyrite and pyrrhotite (here written as troilite) are:

$FeS_2(s) + 7/2\ O_2(aq) + H_2O \rightleftharpoons Fe^{2+} + 2SO_4^{2-} + 2H^+$

$FeS(s) + 3/2\ O_2(aq) + H_2O \rightleftharpoons Fe^{2+} + SO_4^{2-} + 2H^+$

Many parameters, such as mineral electrochemical activity and oxidation kinetics, will influence the reactivity of the reactions. The final oxygen concentration will depend on the mineral's sulphide content, the reactivity of the sulphides, the aeration effect in the mill and other factors. The main difference is, of course, that sulphide ores consume more oxygen while oxide and silicate ores consume less. A worst case, in terms of dissolved oxygen, would be an autogenous mill grinding an oxide ore. Conversely, the best is a steel media ball mill grinding a sulphide ore [14]. The mill speed has an astonishingly strong influence on the oxygen level. The reason is probably that a rapidly running mill has more of a mixing action for the charge and, therefore, takes up more oxygen from the air. On the contrary, a slowly rotating mill only moves the charge. This is consistent with the general view that two grinding mechanisms exist in a grinding mill, the cascading charge at lower speeds and the cataracting mill at higher speeds [15].

In grinding the softer copper sulphide types of ore, the introduction of Magotteaux^{TM} balls (high chromium white cast iron) gave greater improvements in performance than before. For ores in decreasing order of hardness, i.e., ores from Black Mountain, copper deposits of the O'okiep District and Palabora, the Magotteaux^{TM} balls were 2.5 times, 3.5 times, and 9 times better than the standard drop-forged carbon-steel balls. Obviously, in grinding softer ores, and ores that may give rise to pulps with pH values of less than 7 (acidic), high-chromium white cast-iron balls may show a decided cost benefit [16, 17].

In the gold mining industry, the high consumption of balls in the milling of quartzite, which is severely abrasive, adds substantially to the milling costs [17]. High chrome white cast iron grinding balls under known economic conditions did not appear to be cost effective in milling the gold ore. From Howat's [17] studies it appears that the use of carbon forged steel balls would be cost effective in milling the siliceous material (gold ore).

2.4.1. UG2 Reef

The upper group 2 reef (UG-2) chromitite ore found in Northern Province is more fragile than the gold ore (Witwatersrand) and this effect can be seen in both the impact and the bed breakage size distributions [17]. The bed breakage produced much more fines with the UG-2 ore than with the gold ore. Additionally there is a distinct bimodal distribution in the UG-2 ore which is absent from the Gold ore – reflecting the difference in the mineralogical structures. The impact breakage produced more small particles in the size range 0.2 to 30mm but almost the same amount of fines. UG-2 ore is much more fragile than the target gold ore and there are also two distinct mineral phases in the UG-2 ore (chromitite and the lower grades in the hanging wall or footwall) that may have an influence on the breakage size distribution [17]. When the ore contains a large amount of waste rock (hanging wall and footwall) the breakage size distribution may change from the distinct bimodal shape of the UG-2 product and become similar to the normal Rosin-Rammler distribution [18].

The Rosin–Rammler distribution is a useful distribution for representing particle size distributions generated by grinding, milling and crushing operations. The difference at the finer end of the size range may largely be attributed to the breakage of the UG-2 on grain boundaries of ore [18].

2.4.2. Platinum-Group Metal Ores

Platinum-group metal (PGMs) ores are concentrated in narrow but extensive strata known as the Merensky reef, the Platreef, and the UG-2 chromatite layer. These three layers in the Bushveld Complex each have their own distinctive associated mineralogy [19]. The first two reefs are found in relation to one another with the generally wider UG-2 reef lying below the Merensly reef by anywhere from 15 meters to 330 meters [20].

South Africa is the world's largest producer of platinum. Most of the PGMs are found in the Merensky and UG2 Reefs of the **Bushveld Igneous Complex** (BIC). The reserves of Merensky and UG2 ores to a depth of 1200 m, have been estimated to be 3 300 million t (Mt) and 5 420 Mt respectively [21].

The UG-2 Reef occurs about 150 m below the Merensky Reef in the Western Belt and up to 400 m below in the Eastern belt of the BIC. Although rich in chromite $[(Fe,Mg)^{2+}O.\ (Cr,Fe,Al)^{3+}{}_2O_3]$, the UG-2 Reef is exploited primarily for the PGM value and not for its chromite content [21]. A generalized map of the BIC shows the major platinum operations and some of the current ferrochrome operations (Figures 2.11 and 2.12).

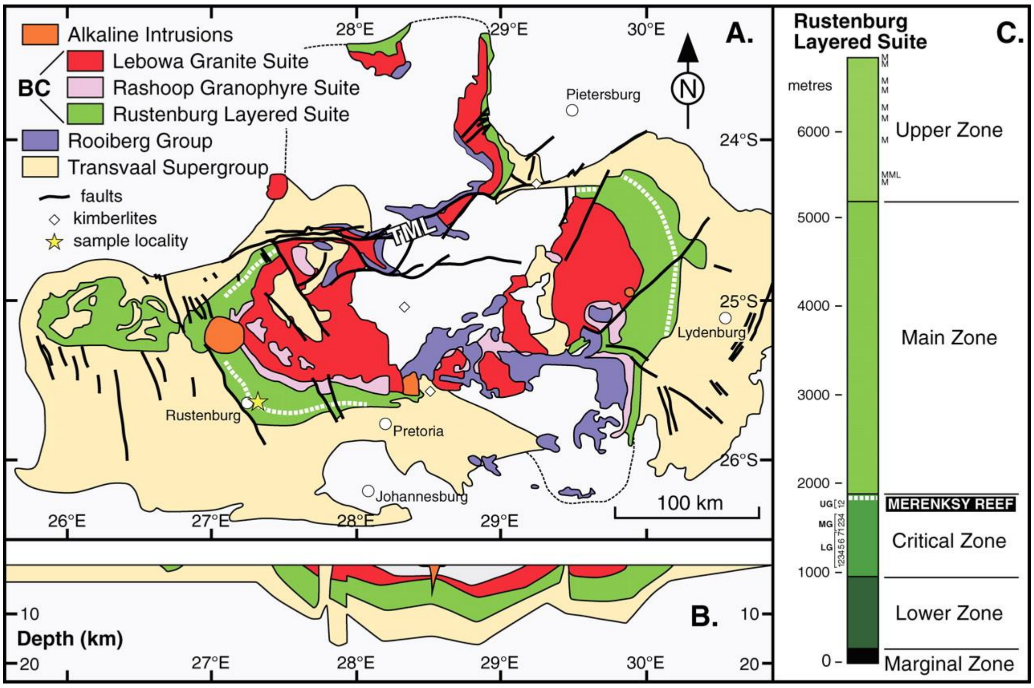

Figure 2.11. South Africa – the Bushveld Igneous Complex (BIC) [21].

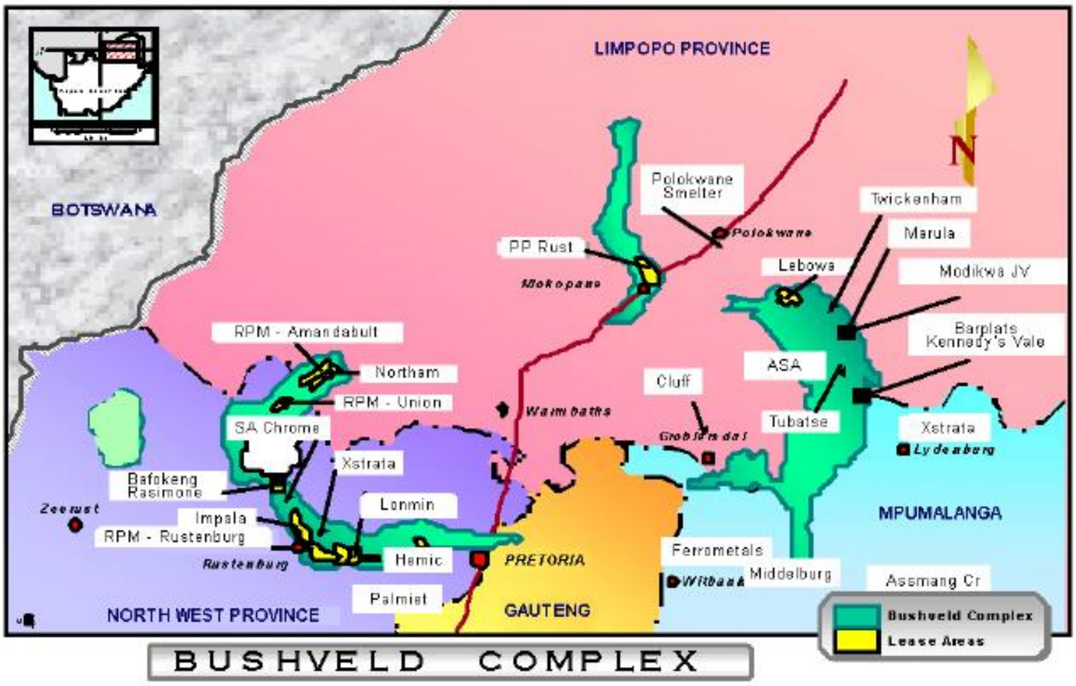

Figure 2.12. Location of key platinum and ferrochrome operations situated on the BIC in 2003 [21].

The Merensky Reef is a layer of igneous rock in the Bushveld igneous complex (BIC) in the North West, Limpopo, Gauteng and Mpumalanga provinces of South Africa which together with an underlying layer, the upper group 2 reef (UG-2), contains most of the world's known reserves of platinum group metals (PGMs) or platinum group elements (PGEs) - platinum, palladium, rhodium, ruthenium, iridium and osmium [21].

Chromite crystals form a large part of the volume of UG-2 and other chrome ores. Base-metal sulphides are much more prevalent in Merensky and Platreef ores than in the UG-2 or chrome ores. In UG-2 processing there are a number of options regarding by-product chromite recovery and blending with the Merensky ore before milling. At present, though, only one South African producer is recovering chromite: this is done after primary milling, with the chromite crystals being liberated at their natural grain size. UG2 ores require finer grinding than Merensky ore for optimum PGM recovery [22].

Typical compositions of Merensky concentrate and a blend of UG-2 concentrates (wt%) for the operations are given in Table 2.2 [23]. It can be seen than the UG-2 concentrate is characterized by high concentrations of Cr_2O_3 and is much more refractory than Merensky concentrate.

Table 2.2. Typical Merensky and UG2 concentrate analyses for the Lonmin operation (wt%) [23].

Ore Type	**Elements (wt.%)**								**ppm**
	Al_2O_3	**CaO**	**Cr_2O_3**	**Cu+Ni**	**Fe**	**MgO**	**S**	**SiO_2**	**PGM**
Merensky	1.8	2.8	0.4	5	18	18	9	41	130
UG2 Blend	3.6	2.7	2.8	3.3	15	21	4.1	47	340

2.4.3. The Platreef

The Platreef is an ore containing platinum group elements and a base metal enriched mafic/ultramafic layer situated along the base of the northern limb of the Bushveld Complex. The Platreef rests on metasedimentary rocks and comprises of three medium-grained units of gabbronorite/feldspathic pyroxenite that are separated by hornfels interlayers. These three platiniferous layers are referred as the Lower, Middle and Upper Platreef [23].

- The Middle Platreef is the main mineralised layer, with total PGM contents up to 4 ppm.
- The Lower and Upper Platreefs are less well mineralised (up to 1.5 ppm).

Trace element and S-isotope data show compositional breaks between the different platiniferous layers suggesting that they represent distinct sill-like intrusions of pyroxene and sulphide enriched crystal mushes. All three Platreef layers are enriched in heavy S of 2.6 to 9.1 per millilitre indicating addition of crustal sulphur, and they have elevated K, Ca, Zr and Y contents and high Zr/Y ratio [23].

2.4.4. Gold Ore Minerals

By far most of the gold that has been mined in South Africa (98%) has come from the Witwatersrand goldfields, see Figure 2.13. The name "Witwatersrand" is Afrikaans (originating out of Dutch, French and German) for "White Waters Ridge". The name was derived from the white quartzite ridge which strikes parallel to the edge of the basin in which the sediment was deposited. The gold mines in this area are situated around an ancient sea (over 2700 million years old) where rivers deposited their sediments in the form of sand and gravel which became the conglomerate containing the gold. The Witwatersrand Basin is approximately 350 km long and 200 km wide [24].

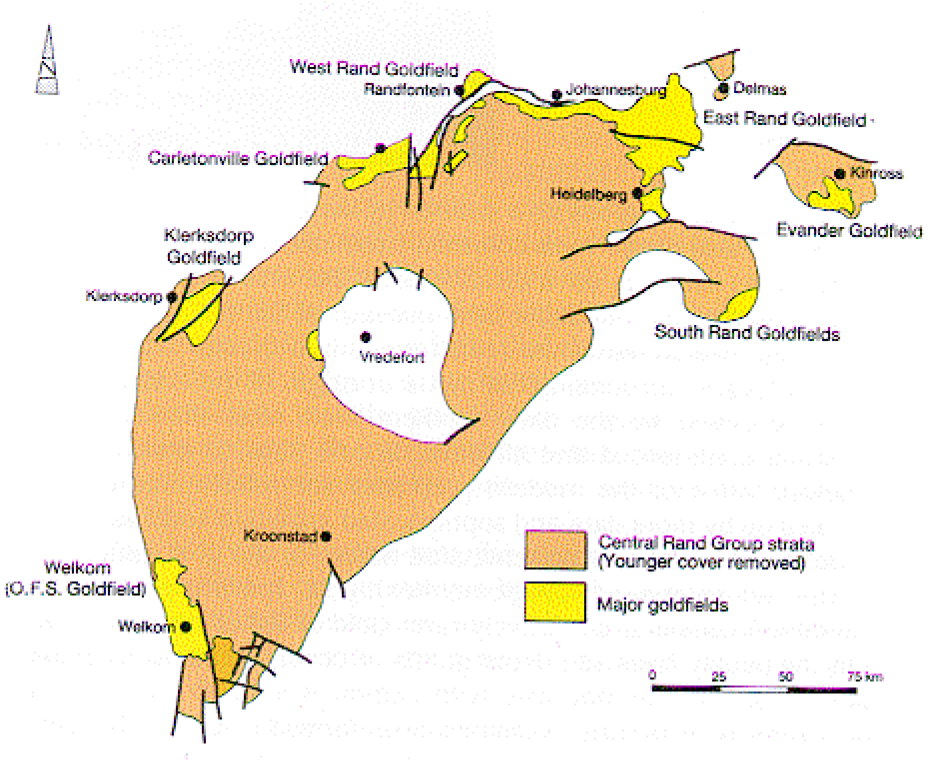

Figure 2.13. Witwatersrand Basin (RSA) [24].

The most prominent form of gold in the Witwatersrand is native gold - most of the native gold contains a small amount of silver, copper, platinum, etc. Telluride minerals are the most common minerals which contain significant gold in their make-up. Gold deposits are often classified according to their association. The first of these may be catalogued as quartzose. This implies that the gangue mineral is acid, i.e. quartz, and that fluorite may abound, or even the other gangue minerals of the alkaline earth group. Not infrequently there appears within the quartz varying amounts of pyrite and even limited quantities of chalcopyrite and galena. The second class of gold ores is auriferous copper ores [25].

Howat [26]. undertook a research programme to provide comparative data on the performance of various types of balls for use in the grinding of gold ores [26]. The focus was to understand the behaviour of different types of ores in ball milling. Quartz ore was used as a reference material to the non-ferrous sulphide ores from Black Mountain, O'okiep and Palaborwa. The results showed that these ores are much softer than quartzite. The grindability of these three ores in relation to quartz was compared and it was found that the ores from Black Mountain and O'okiep have very similar grindability characteristics, whereas Palaborwa ore is very much more easily ground. Albertin [27] also studied the effect of different abrasives/ores such as iron ore, phosphate rock and quartz sand on high chromium white cast iron and found that silica is more abrasive than the other two ores [27].

2.5. General Metallurgy of Grinding Ball Alloys

This section gives a brief overview of the requirements of a good grinding ball, type of alloys used for production of grinding media and conventional casting processes.

Grinding media are one of the critical consumables in comminution processing and ideally, each ball mill or semi autogenous (SAG) mill should have its own customized design (which includes ball sizes charged, chemistry, hardness and toughness), shown in Figure 2.14 [28]. The following factors may affect the design of grinding media for a particular ball mill:

- Hardness of ore and its range
- Top size and median size of particles in the mill charge
- Sand return ratio – oversize ore to regrind
- Specification of ball mill
- Specification of liners
- pH value of ore and concentrate
- Corrosive nature of grinding environment and milling process.

To optimize the design of grinding media for a particular ball mill, the following pre-conditions should be met [28]:

- Variation of grinding media should be precisely controlled, which requires that all variables during the manufacturing process should be under control;
- The communication between the manufacturer and end users should be transparent with cost, technology, and performance data being freely exchanged;
- All necessary information relating to performance of grinding media should be well recorded so that the manufacturer could implement an analysis periodically:
- Metallurgical support is critical to the design of grinding media. The manufacture must have strong support from a R&D an internal or external supporter.

Details on the developed and designed high chrome grinding media, with demand coming primarily from the platinum, copper, cement and power generation industries, is readily available. Demand for forged alloyed and non-alloyed steel grinding media comes predominantly from the gold and other industries [28].

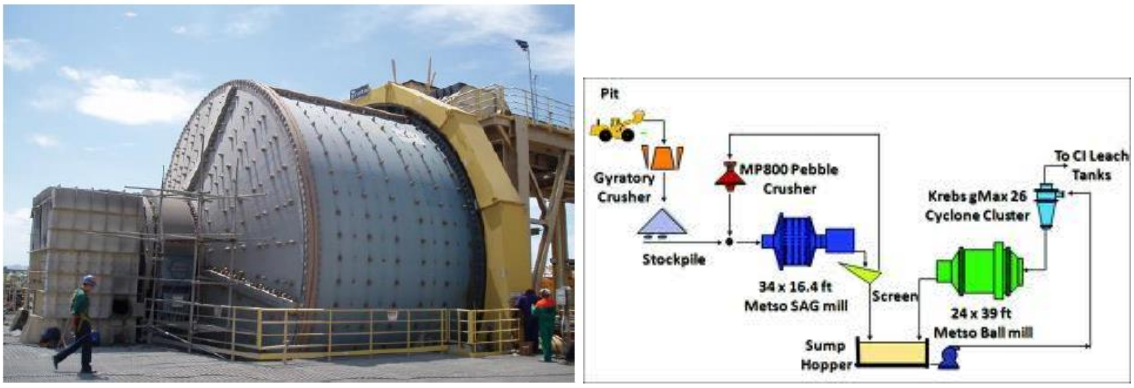

Figure 2.14. Typical industrial SAG grinding ball mill used in the mining industry [28].

2.5.1. High Chromium White Cast Iron (HCWCI)

High chromium white cast irons are based on the Fe-Cr-C ternary system often with the addition of alloying elements such as molybdenum, nickel, copper and manganese [29]. The iron-rich corner of the metastable C-Cr-Fe liquidus surface is shown in Figure 2.15. This shows that the majority of commercial high chrome white cast iron alloys with 11-30wt% chromium and 2-3.3wt% carbon, solidify within the primary austenite (γ) field [29]. In hypoeutectic irons, the austenite dendrites form in the liquid first, and are then followed by an eutectic reaction in which eutectic austenite nucleates in the eutectic liquid. The eutectic austenite is believed to nucleate independently of the primary austenite dendrites, and is said to grow with a cellular interface [29].

The remaining liquid becomes enriched in C and Cr and its composition moves towards the eutectic valley, given by the line $U_1 - U_2$ in Figure 2.15, until the temperature decreases to a level where the eutectic reaction ($L \rightarrow \gamma + M_7C_3$) occurs to form eutectic colonies with constrain to growth of the M_7C_3 phase. The solidification is completed before the invariant reactions can take place.

Hypereutectic grades are only used for a few applications where impact forces are small, such as shot blast blades and certain slurry pumps. The solidification in these irons starts by the formation of hexagonal needles of primary M_7C_3 carbide from the melt, the remaining liquid being rapidly depleted in C and Cr as it crosses the decreasing temperature contours towards the eutectic valley. Figure 2.16 shows the position of high-chromium iron with respect to the chromium-to-carbon (Cr/C) ratio [29].

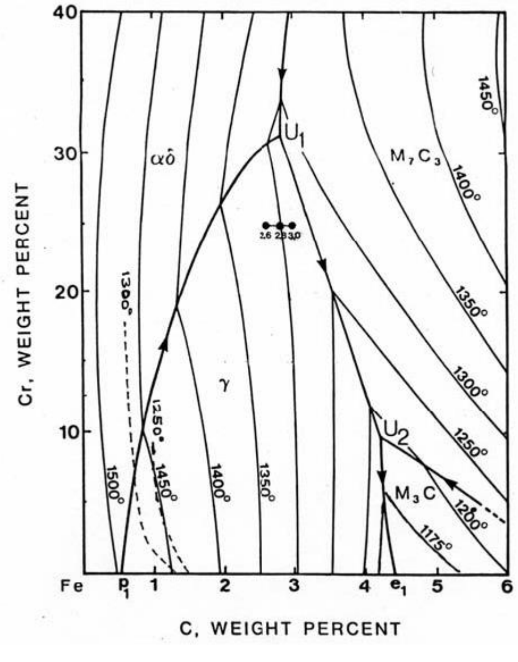

Figure 2.15. Iron-rich corner of the Fe-C-Cr phase diagram showing the liquidus isotherms and two solidus isotherms near the iron corner [29].

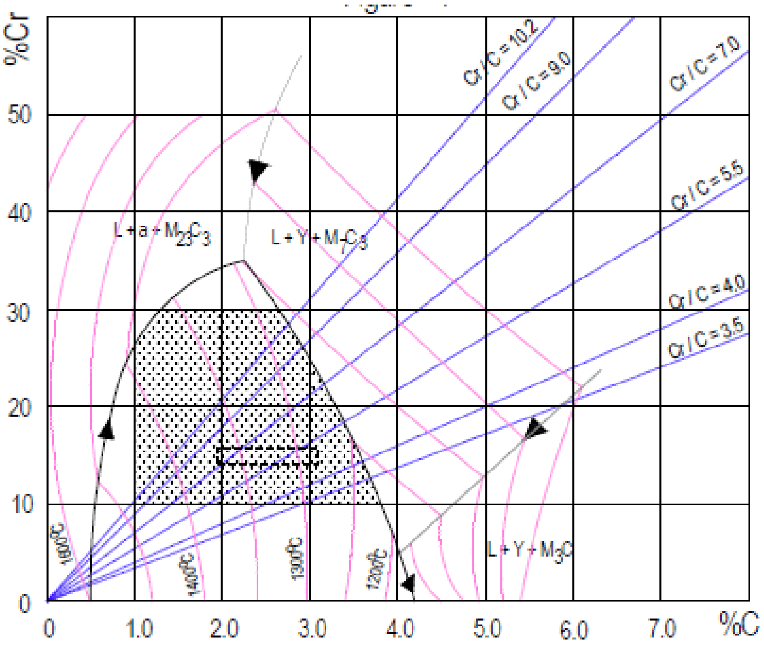

Figure 2.16. Position of the high-chromium iron in the Iron-rich corner of the metastable C-Cr-Fe liquidus surface and chromium-to-carbon ratio [29]

The matrix microstructure of high chromium cast irons can be varied to suit individual application requirements, i.e. from a completely austenitic work-hardenable matrix to a fully heat-treated martensitic product. There are three fundamentally different microstructures that can be obtained in high-chromium cast irons by varying the carbon content. These three possible types are designated as follows and shown in Table 2.2:

- Hypoeutectic alloys,
- Eutectic alloys,
- Hypereutectic alloys.

Table 2.3.Comparison of typical White Iron Classes.

	Hypoeutectic	**Eutectic**	**Hypereutectic**
Example	Ni-hard	27% chrome	Very high chrome (>30%)
Matrix and carbides	Soft primary ferrite dendrites with eutectic carbides	White iron matrix with very fine dispersion of eutectic carbides	White iron austenitic/martensite matrix with coarse, discrete primary carbides
Note on casting	-	-	Solidification during casting must be controlled to avoid cracking

2.5.2. Typical Types of Alloys

High chrome white iron castings based on the ASTM A532 Class III, Type A alloy specification, containing carbon and chromium in the ranges 2.3 - 3.0wt% C and 23 – 28wt% Cr are applied extensively in mining and mineral processing such as ball and slug grinding media and liners for grinding mills [30]. Their very high abrasion and erosion resistance is due mainly to the presence of a significant volume fraction of M_7C_3 type carbides throughout their microstructures. These carbides are significantly harder than quartz which is the main abrasive encountered in most mining operations. Wear-resistance is improved but toughness and spalling resistance decreases with increasing Carbide Volume Fraction (CVF) [31].

High chromium cast irons commercially available are hypoeutectic alloys containing 10-30 wt% Cr and 2 - 3.5wt% C. Typical composition of these alloys are given in Table 2.4 below as per ASTM A532-82 [30].

Table 2.4. Compositions in wt% of commercial high-chromium cast iron as per ASTM A532-82 [30].

Class	**Type**	**Designation**	**Element**								
			C	**Mn**	**Si**	**Ni**	**Cr**	**Mo**	**P**	**S**	**Cu**
I	A	Ni-Cr-HC	2.8-3.6	2.0	0.8	3.3-5.0	1.4-4.0	1.0	3.0	0.15	-
	B	Ni-Cr-LC	2.4-3.0	2.0	0.8	3.3-5.0	1.4-4.0	1.0	3.0	0.15	-
	C	Ni-Cr-GB	2.5-3.7	2.0	0.8	4.0	1.0-1.5	1.0	3.0	0.15	-
	D	Ni-HiCr	2.5-3.6	2.0	2.0	4.5-7.0	7.0-11.0	1.5	1.0	0.15	-
II	A	12%Cr	2.0-3.3	2.0	1.5	2.5	11.0-14.0	3.0	1.0	0.6	1.2
	B	15%Cr-Mo	2.0-3.3	2.0	1.5	2.5	14.0-18.0	3.0	1.0	0.6	1.2
	D	20%Cr-Mo	2.0-3.3	2.0	1-2.2	2.5	18.0-23.0	3.0	1.0	0.6	1.2
III	A	25%Cr-Mo	2.3-3.3	2.0	1.5	2.5	23.0-30.0	3.0	1.0	0.6	1.2

The alloy shown in Table 2.5 is sometimes called 15/3 Chrome/Moly Iron, or 16% chrome. It is a martensitic white iron of moderate erosion resistance. It is used for the casting of pumps for a number of applications such as carbon-in pulp circuits, coal transfer pumps, sewage treatment, and some newspaper recycling pumps [32].

Table 2.5. Compositions in wt% of high chrome abrasion-resistant white iron [32].

	France	Germany	United Kingdom		United States	
Standard	**NF 32-401**	**DIN 1695**	**BS 4844 Pt2:1972**		**ASTM A532 1982**	
Grade	**FB Cr9 Ni5**	**GX 300 CrMo**	**3A**	**3B**	**Class II Type B**	**Class II Type C**
C	2.0–3.6	2.3–3.6	2.4–3.0	3.0–3.6	2.4–2.8	2.8–3.6
S	0.2–0.8	0.2–0.8	1.0 max	1.0 max	1.0 max	1.0 max
Mn	0.5–1.0	0.5–1.0	0.5–1.0	0.5–1.0	0.5–1.0	0.5–1.0
Ni	0.0–2.5	0.7	0.0–1.0	0.0–1.0	0.5 max	0.5 max
Cr	14.0–17.0	14.0–17.0	14.0–17.0	14.0–17.0	14.0–18.0	14.0–18.0
Cu	-	-	0–1.2	0–1.2	1.2 max	1.2 max
Mo	0.5–3.0	1.0–3.0	0.0–2.5	1.0–3.0	1.0–3.0	2.3–3.5
P max	-	-	0.3	0.3	0.1	0.1
S max	-	-	-	0.1	0.06	0.06

Cast iron grinding balls are used in large quantities in grinding mills for crushing coal ores, cement, and many other uses [33]. Grinding balls need to have good resistance to cyclic impact loads in addition to high wear resistance properties as they suffer repeated collisions with other balls, hard liner plates as well as the ore for crushing [33]. Typical chemical compositions of the grinding balls used in the platinum, coal, copper and gold mining industry are shown in Tables 2.6 and 2.7 [34].

Table 2.6. Typical compositions in wt% of commercial high-chromium cast iron balls used in platinum mines.

Ball Diameter (mm)	**Elements**			
	C	**Cr**	**Si**	**Mn**
30	3.06	12.5	0.37	0.50
35	3.01	12.3	0.27	0.44
40	3.06	12.6	0.39	0.55
50	2.64	12.8	0.33	0.39
60	2.59	12.5	0.63	0.44
70	2.25	17.9	0.30	0.39
80	2.18	18.1	0.28	0.31
90	2.13	18.3	0.37	0.58

Table 2.7. Typical compositions of commercial forged steel balls used in gold mines.

	Elements (wt%)							
Ball Diameter (mm)	**C**	**Si**	**Mn**	**P**	**S**	**Cr**	**Cu**	**Mo**
50	0.75	0.15	0.49	0.013	0.046	0.01	0.01	0.01
60	0.54	0.50	0.54	0.018	0.028	0.45	0.07	0.02
80	0.63	1.75	0.51	0.007	0.002	0.86	0.13	0.02
100	0.78	0.34	1.03	0.017	0.011	0.48	0.08	0.19
125	0.80	0.67	0.82	0.016	0.021	0.01	0.03	0.01

High quality grinding media are produced to suit all milling applications including gold, platinum, zinc and other ores, see Table 2.8 [35]. Steel balls are unquestionably providing an improved grinding operation than any of the other commercially available media is shown for a typical application in Figure 2.17 [35. They have proven especially valuable in the paint industry [36]. This has not always been the case, however. In the early days mill operators were insistent on large steel balls, comparable in size to the flint pebbles or porcelain balls in use at the time. Contamination was excessive and they did not appear to grind much faster than the other grinding media. It was not until much smaller sizes were put into use and correct operating techniques were developed that such outstanding results were obtained, in some cases reducing grinding times to one-third of that required for other grinding media.

Table 2.8. Metals that are commonly used as materials for grinding in ball alloys [35].

Alloys	Description
High carbon (C)-high manganese (Mn)	Steel with alloying elements such as molybdenum (Mo), chromium (Cr) or nickel (Ni). These balls are especially made for ball mills and are uniformly through-hardened to 60-65 Rockwell C. They represent the highest quality of all metal balls and most operators insist on using them as shown in Figure 2.17
Cast Nickel Alloy and High chromium white cast iron	This is also very popular and, as it is basically a white metal ball, it causes less metallic staining than other types. The principal objection is its rough outer surface and projecting nubs typical of cast balls. It requires long conditioning periods before being placed into general use. Typical chemical compositions of the alloys are shown in Table 2.6
Stainless Steel	Because of its high cost, austenitic stainless steel is only used for special work that requires an acid resistant and non- magnetic ball.
Forged Low Carbon Steel	The chill iron and low carbon steel are the cheapest metal balls obtainable. They are recommended for rough grinding only, where metallic contamination is not objectionable, a typical composition is shown in Table 2.7.

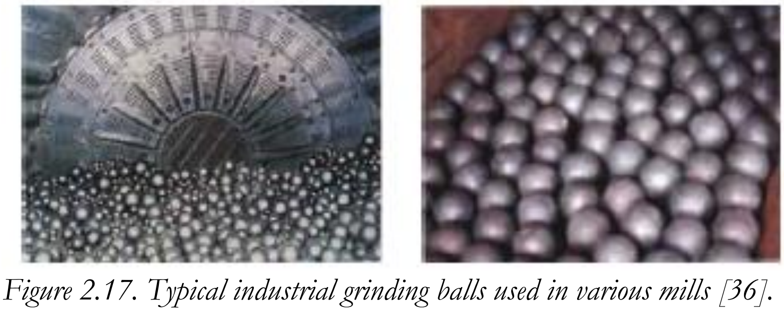

Figure 2.17. Typical industrial grinding balls used in various mills [36].

Wear of grinding media has a great impact on the operational cost and results in huge consumption of liner and grinding media [37]. In one school of thought, it has been argued that low carbon martensite free from retained austenite has the optimum properties and is the most suitable structure of a grinding ball. Retained austenite is argued to be harmful to both abrasion and impact fatigue resistances and is a dangerous factor in grinding balls [37].

2.5.3. The Magotteaux^{TM} Process

A Belgian company/foundry called *Magotteaux* has patented a process in manufacturing high chrome grinding balls of *superior quality* with minimum wear rate without any risk of breakage as described in United States Patent Number US4043842 A (or Patent Number GB1315203 - 1973) [38].

The current invention of the alloys is well suited for use in grinding members for grinding mills, and other environments and/or uses where superior resistance to wear when subjected to abrasion and to repeated impacts is required. The alloy is comprises high chromium content cast steel having a metallographic structure characterized by a martensitic solid solution without pearlite, containing less than 3% residual austenite, and containing eutectic and pro-eutectoid carbides [38]. The alloys, balls and lining plates fabricated therefrom are furthermore characterized by a hardness that is equal to or above 59 HRC. The present invention with its numerous objects and advantages is better understood by reference to the following drawings, Figures 2.18 to 2.20.

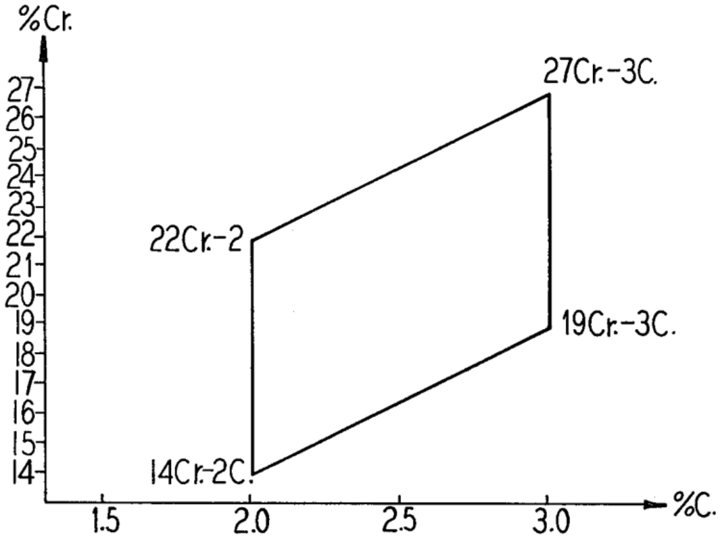

Figure 2.18. A diagram showing the composition range of the chromium and carbon content of steel alloys in accordance with the preferred embodiment of the invention [38].

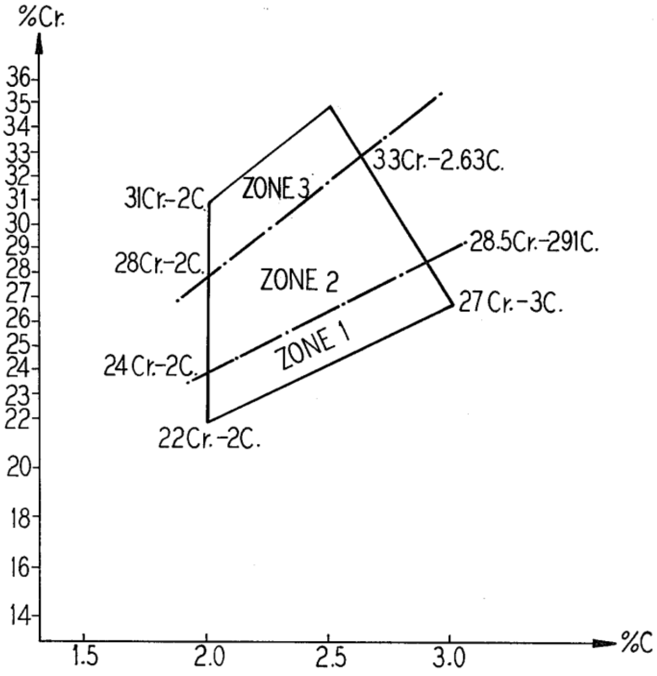

Figure 2.19. A diagram showing the composition range of the chromium and carbon content of alloys in accordance with a second embodiment of the invention, the alloys of the second embodiment having slightly higher chromium content than the alloys represented in Figure 2.18 [38].

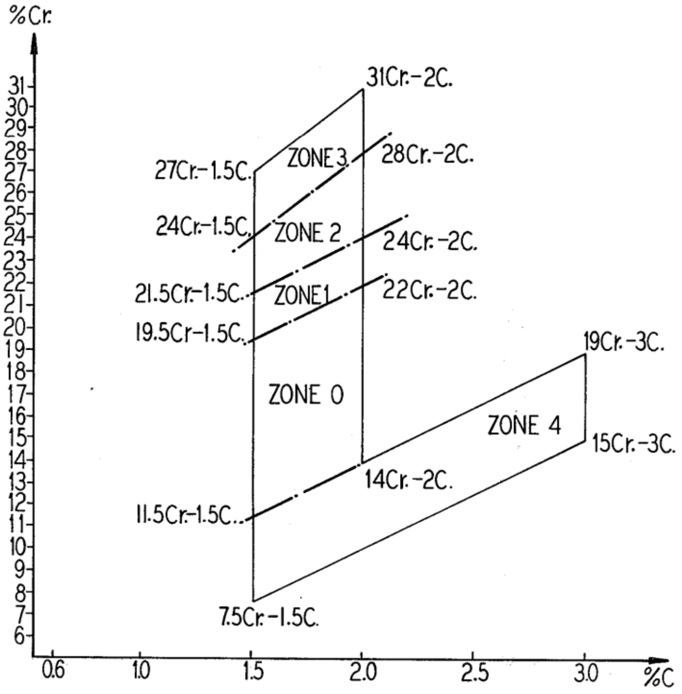

Figure 2.20. A diagram showing the composition range of the chromium and carbon content of alloys in accordance with a third embodiment of the invention, the alloys of the third embodiment having generally smaller percentages of carbon or chromium than in the alloys represented in Figures 2.18 and 2.19 [38].

Magotteaux offers a unique variety of grinding media which combines the following characteristics:

- Size: from 13 to 125mm (1/2" to 5")
- Chromium percentage: from 0.5 to 35%
- Heat treatment cycles.

The choice of media depends upon:

- Material to be ground and its granularity properties
- Grinding process
- Importance of wear mechanisms involved (abrasion, corrosion, impact)
- Factors influencing these mechanisms.

The heat treating process for the alloys consists generally of a hardening operation in still or blast air during which the material is heated to a temperature ranging between 950 °C up to a maximum of approximately 1200 °C. The preferred hardening temperature varies according to specific percentages of chromium and carbon in the alloy. The hardening step is followed by a tempering step in which the temperature ranges between 440 °C to a maximum of approximately 570°C. As in the hardening step, the preferred tempering temperature also varies according to the carbon and chromium content [38].

For Zones 0, 1, 2, and 3 of these alloys in Figure 2.20, the most suitable hardening and tempering temperature are identical with those of the corresponding zones in the more expensive type of alloys [38]. For zone 4 of the type III alloys, the hardening temperature must be within the range of 960 °C to 1000 °C and the tempering temperature must be fixed at 450 ±10 °C (Table 2.9). The characteristics obtained after this heat treatment are a hardness of HRC 57–61 (HV660-750) and <5% retained austenite [38].

Table 2.9. Heat treatment used in Type III alloys [38].

Zone	Hardening Temperature	Tempering Temperature
Zone 0	950 °C + (%Cr – 5 x %C – 4) 18.75	460 °C + (%Cr – 5 x %C – 4) 11.25
Zone 1	950 °C + (%Cr – 5 x %C – 4) 18.75	550 – 570 °C
Zone 2	1137 °C	550 – 570 °C
Zone 3	950 °C + (%Cr – 8 x %C – 1.5) 18.75	950 – 570 °C
Zone 4	950 – 1000 °C	450 ±10 °C

2.6. Ductile Iron (DI)

This section gives a brief overview of ductile iron (DI), typical compositions for ductile iron alloys, type of alloys used for production of wear resistant components, better properties, conventional casting process, and forms of austempering processes.

Austempering is heat treatment that is applied to ferrous metals, most notably steel and ductile iron. In steel it produces a bainite microstructure whereas in cast irons it produces a structure of acicular ferrite and high carbon, stabilized austenite known as ausferrite.

A typical cast iron is an alloy of iron, carbon, silicon, and manganese. Carbon is in the range of 2 to 4%. The cooling rate after casting of cast iron and subsequent heat treatment determine its mechanical properties. The carbon content is very important for the properties of cast iron. The addition of magnesium as an alloying element precipitates excess carbon in the form of small nodules. Nodularisation by magnesium (Mg) or zirconium (Zr) affect the nucleation of graphite directly into spherical nodules. These nodules do not affect the structure of cast iron, as is the case with the graphite flakes. Graphite flakes give sharp stress concentrations at their edges and have a high surface area/volume ratio. The graphite is very loosely bound to the matrix and round graphite nodules with a smaller surface/volume ratio are simply less negative on the mechanical properties [39].

Ductile iron is not a single material, but a family of materials offering a wide range of properties obtained through microstructure control. The common feature that all ductile irons share is the roughly spherical shape of the graphite nodules. These nodules act as crack-arresters and make Ductile Iron "ductile". The importance of the matrix in controlling its mechanical properties is emphasized by the use of matrix names to designate the following types of Ductile Iron [39].

- Ferritic Ductile Iron
- Ferritic Pearlitic Ductile Iron
- Pearlitic Ductile Iron
- Martensitic Ductile Iron
- Bainitic Ductile Iron
- Austenitic Ductile Iron
- Austempered Ductile Iron (ADI).

High percentage of graphite nodules present in the microstructure, mechanical properties are determined by the ductile iron matrix. Figure 2.21 shows a good relationship between microstructure and tensile strength over a wide range of properties.

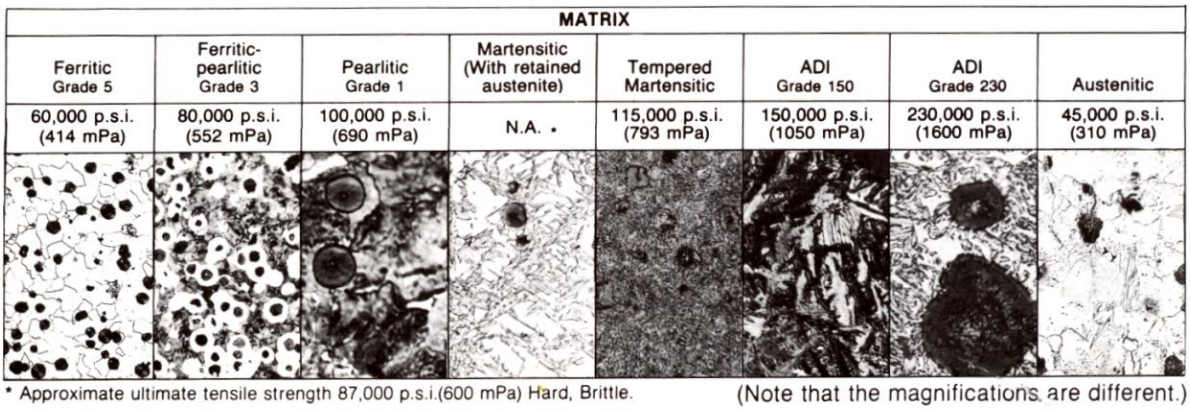

MATRIX							
Ferritic Grade 5	Ferritic-pearlitic Grade 3	Pearlitic Grade 1	Martensitic (With retained austenite)	Tempered Martensitic	ADI Grade 150	ADI Grade 230	Austenitic
60,000 p.s.i. (414 mPa)	80,000 p.s.i. (552 mPa)	100,000 p.s.i. (690 mPa)	N.A. *	115,000 p.s.i. (793 mPa)	150,000 p.s.i. (1050 mPa)	230,000 p.s.i. (1600 mPa)	45,000 p.s.i. (310 mPa)

* Approximate ultimate tensile strength 87,000 p.s.i.(600 mPa) Hard, Brittle.

(Note that the magnifications are different.)

Figure 2.21. Microstructures and tensile strengths for various types of Ductile Iron [39].

The term cast iron refers not to a single material, but to a family of materials whose major constituent is iron, with important amounts of carbon and silicon as shown in Figure 2.22.

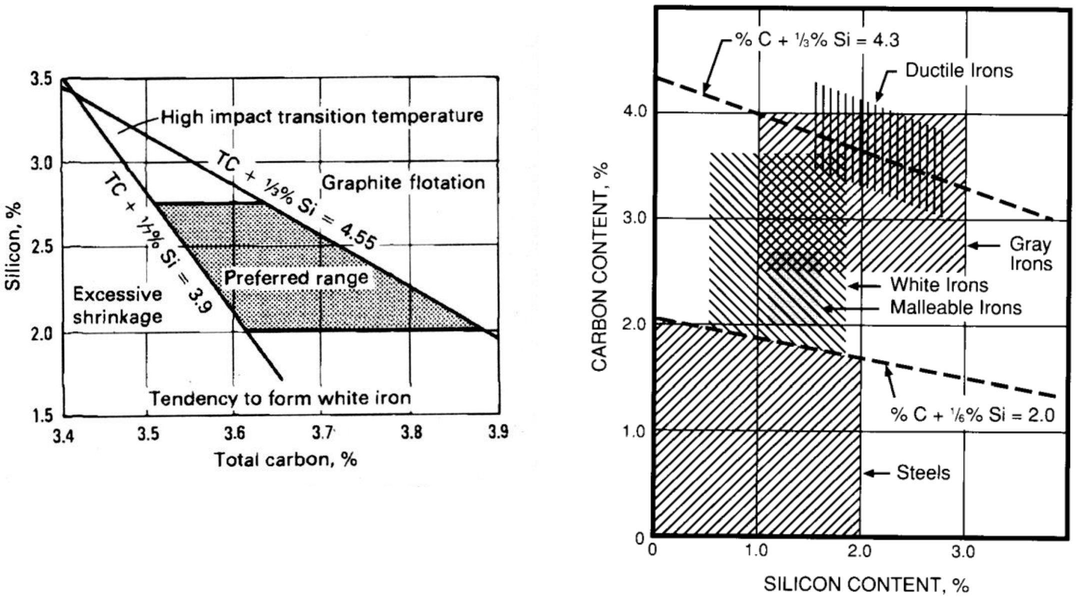

Figure 2.22. Typical ranges of carbon and silicon for steel and various cast irons [39]

2.6.1. *Carbidic Austempered Ductile Iron (CADI)*

Austempered ductile iron offers the design engineer abrasion resistance which is superior to competitive materials over a wide range of hardness. Since the early 1990s several manufacturers have been using various techniques to exploit the advantages of the wear resistance of carbides and the toughness of the ausferrite matrix produced by the austempering process [40].

Carbidic austempered ductile iron (CADI) describes a family of ductile cast irons, with given amounts of carbides that are subsequently austempered to exhibit adequate toughness and excellent wear resistance. The abrasion resistance of this new material is improved over that of ADI and increases with increasing carbide content [41].

The risks/disadvantages of CADI are [40]

- CADI exhibits only limited machinability (possibly grinding only)
- If alloying is used the returns must be segregated
- Additional operations and costs may be incurred if carbides are welded on or cast-in.

The advantages of CADI are:

- CADI is more wear resistant than Grade 5 ADI with acceptable toughness.
- CADI is less expensive and tougher than 18% chrome white iron.
- No capital investment is required for the metal caster to add this new product line.

The market opportunities that CADI present to the ductile iron producer are:

- Replaces Mn steel at equal or lower cost
- Replaces 18% Cr white iron at lower cost
- Cost at a premium, engineered iron with longer life
- Creates new markets for ductile iron.

2.6.2. Composition

Molybdenum (Mo) and chromium (Cr) carbides are used in CADI since they are very stable and tend to retain their as-cast volume fractions after austenitising, thus minimizing the number of iterations for heat treat cycle [42]. Typical chemical compositions of the materials used in different studies are listed in Table 2.10 showing in all cases an approximately eutectic composition (equivalent carbon, EC **~4.3**) [43]. The main alloying element is Cr, introduced in different amounts to promote carbide precipitation. Copper (Cu) and nickel (Ni) are added in small quantities in order to increase the austemperability [42 43].

Table 2.10. Chemical compositions of Carbidic Ductile Iron used in different studies [42, 43].

Alloy	**Elememts (wt%)**								
	C	**S**	**P**	**Si**	**Mn**	**Cr**	**Ni**	**Mo**	**Cu**
Low Carbide[41]	3.68	0.014	0.012	2.24	0.23	0.50	0.03	0.42	0.13
High Carbide	3.85	0.016	<0.005	2.09	0.23	1.04	0.03	0.47	0.13
C1[42]	3.35	0.039	0.042	3.09	0.18	2.59	0.58	-	0.67
C2	3.40	0.015	0.039	3.00	0.13	2.04	0.56	-	0.65
C3	3.29	0.019	0.035	3.28	0.15	1.45	0.59	-	0.60
C4	3.18	0.016	0.037	3.38	0.13	0.84	0.61	-	0.63
C5	3.40	0.019	0.035	3.34	0.17	0	0.63	-	0.62

The resulting microstructure consists of a given volume of carbides within an ausferrite matrix, shown in Figures 2.23 and 2.24 [42]. The microstructures of samples show fewer amount of carbides with larger sizes, and lower nodule count with higher graphite nodule size. The matrix is fully ausferritic in all cases, showing the good austemperability of the different alloys. The carbides are of the type M_3C, with chromium partially substituting iron. Addition of more % chromium would give better M_7C_3 carbides since hardness of M_3C is less than that of M_7C_3.

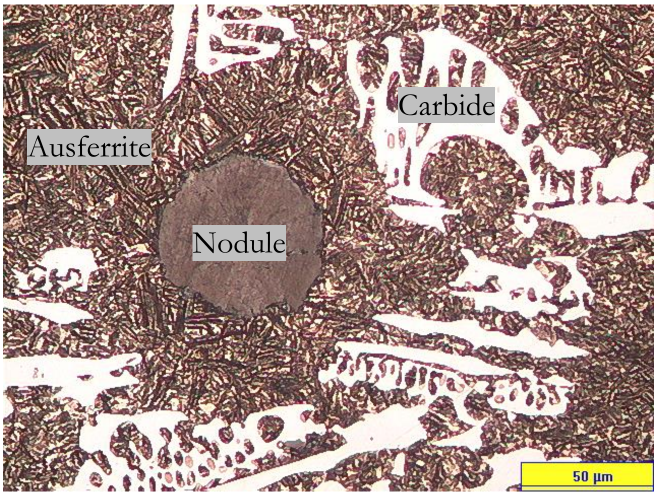

Figure 2.23. CADI with as-cast carbides austempered at 371°C and etched with 8% Nital [42].

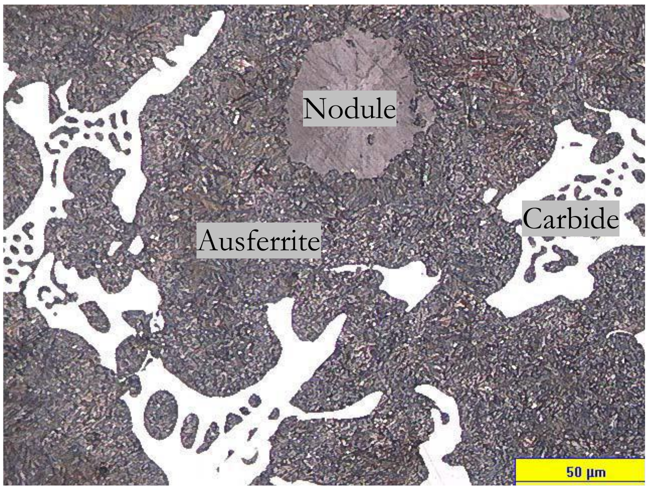

Figure 2.24. CANI austempered at 260 °C showing carbides and fine ausferrite matrix, etched with 8% Nital [42].

Ductile iron is alloyed to produce a carbidic microstructure by alloying with carbide stabilizers (i.e. chromium, molybdenum, titanium), by controlled cooling during shakeout or by adjusting the carbon equivalent to produce a hypoeutectoid iron chemistry. The CADI exhibits improved high stress abrasion resistance compared to ADI [44]. This would be expected due to the presence of carbides in the ausferrite. Figure 2.25 shows a summary of pin abrasion results for cast irons and competitive steels. The cast iron alternatives (ADI, CADI, Ni-Hard, abrasion resistant (AR) irons and quenched and tempered (Q&T) ductile iron) offer better performance in high stress applications than the conventional austempered and Q&T steel [42].

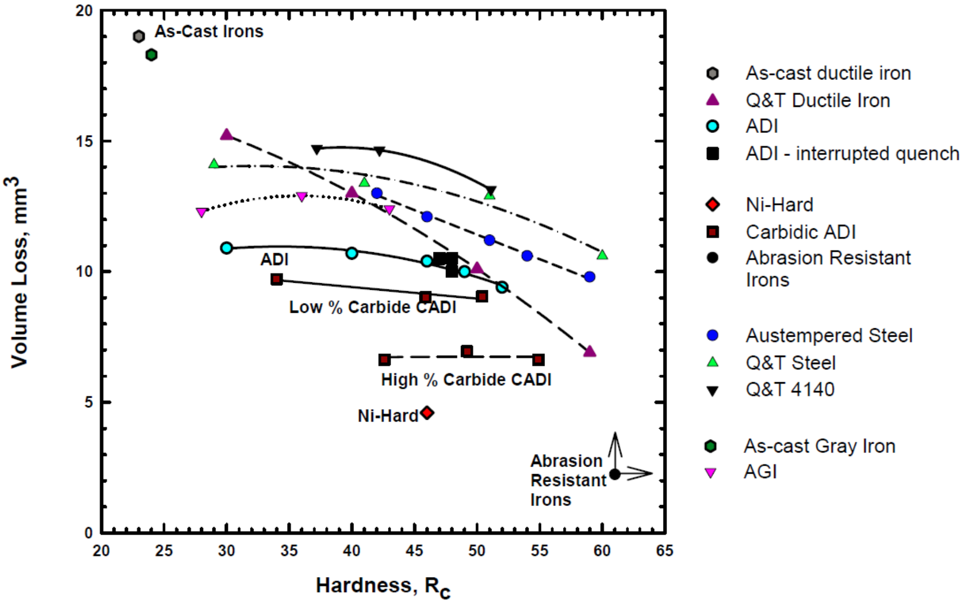

Figure 2.25. Pin abrasion test results for various cast irons and competitive steel alloys. The data point for abrasion resistant irons represents 1 test for a 27% Cr AR iron [42].

2.7. Types of Wear Tests of Grinding Balls

This subsection discusses the different types of wear tests that are used for the grinding balls and reasons why different tests are used. It also discusses how these test methods are compared. Total media wear in a given ball mill or grinding process is a product of three recognised wear mechanisms: abrasion, corrosion and impact.

2.7.1. Abrasion Wear and Test Machine

The abrasion test checks only abrasion wear in conditions typical of cascade type mills. Three classifications of abrasive wear have been suggested; grinding, scratching and gouging abrasion [45, 46]. Abrasive wear is classified in the following three types:

- **Gouging abrasion**, typified by the macroscopic penetration of the working surface by coarse abrasive particles
- **High stress grinding abrasion**, in which abrasive particles are crushed under the grinding influence of moving metal surfaces (two-body abrasion)
- **Low stress scratching abrasion**, in which the stresses are sufficient to cause only microscopic penetration of the working surface and no crushing of the abrasive occurs (three body abrasion).

The commonly used definition for an abrasive wear mechanism is that of two- and three-body abrasion. Two-body abrasion represents the case where a loose abrasive moves over a single, wearing surface, or where an asperity from the counter body abrades the wear surface shown in Figures 2.26 and 2.27. Three-body abrasion represents the case where abrasive particles are trapped between the wearing surface and a counter body, and move relative to both as shown in Figures 2.28 and 2.29.

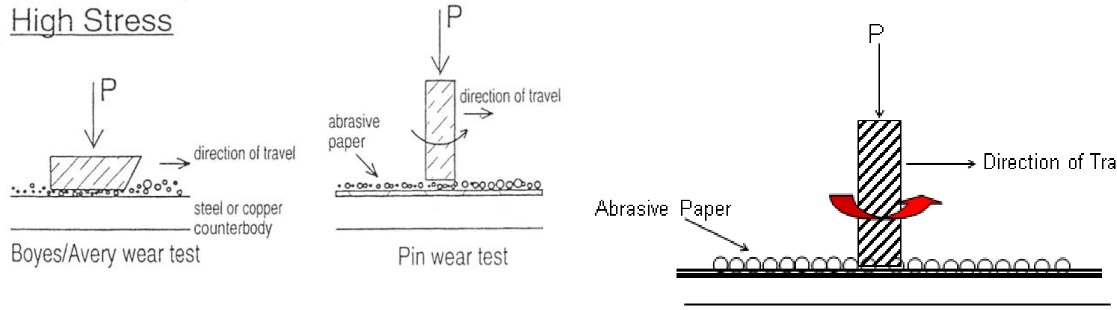

Figure 2.26. Schematic representation of laboratory abrasive wear tests commonly used in the study of wear performance of high chromium white irons [45].

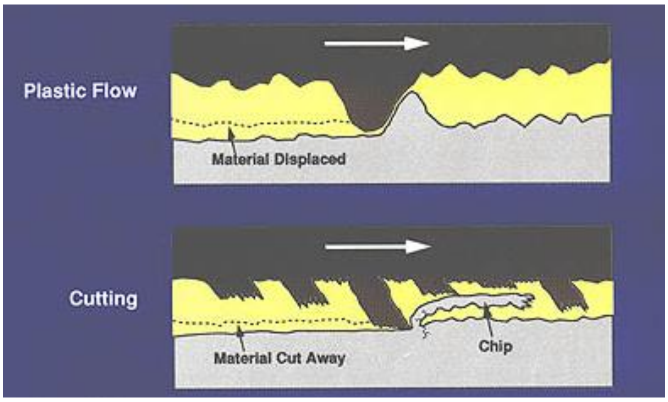

Figure 2.27. Schematic representation showing a two-body abrasive wear mechanism [46].

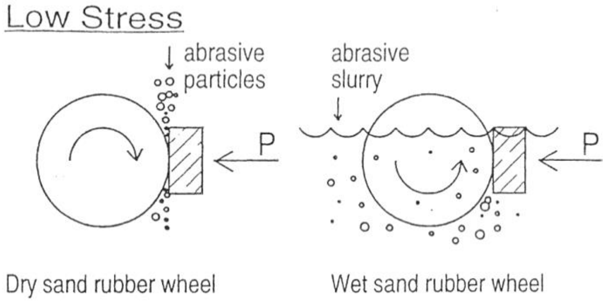

Figure 2.28. Schematic representation of laboratory abrasive wear tests commonly used in the study of wear performance of high chromium white irons [45]

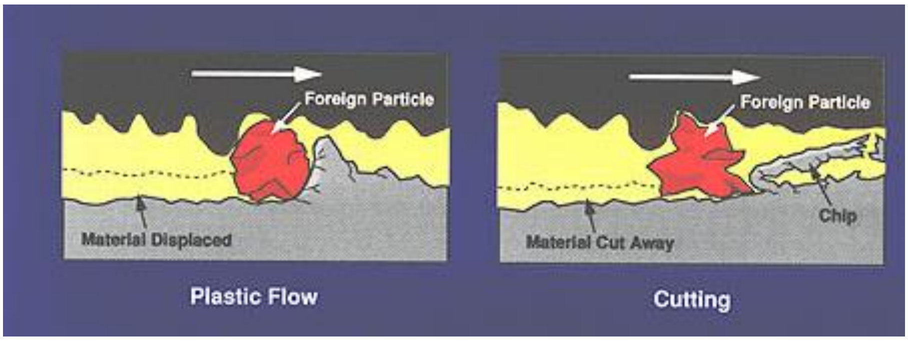

Figure 2.29. Schematic representation showing a three-body abrasive wear mechanism [46].

It is believed that three-body abrasion produces lower wear than two-body abrasion. When abrasive wear is the result of loose wear particles and contaminants, it is called three-body abrasive wear. Various mechanisms of material removal occur during abrasive wear and these mechanisms may be summarised as follows [47, 48].

- **Ploughing** — the relative movement of the abrasive causes material to be displaced either side of the wear groove (see Figures 2.30 and 2.31).

- No direct material removal occurs during ploughing in grinding balls, as the area of the wear groove equals that of the plastically displaced material. However, the displaced material may be subsequently removed via another mechanism. Ploughing has also been described as hummock forming [47, 48].
- **Cutting** — the worn material is removed as primary debris of microchips with little or no displacement, so that the volume of the wear groove equals the volume of material removed. This mechanism is akin to metal machining, and is therefore sometimes referred to as micromachining or chip forming, see Figures 2.30 and 2.31.
- **Fragmentation** — cracks form around and at the base of a wear groove produced by either ploughing or cutting (see Figures 2.30 and 2.31). These cracks may lead to spall formation and hence material removal. The volume loss due to wear may exceed the volume of the wear groove [47].

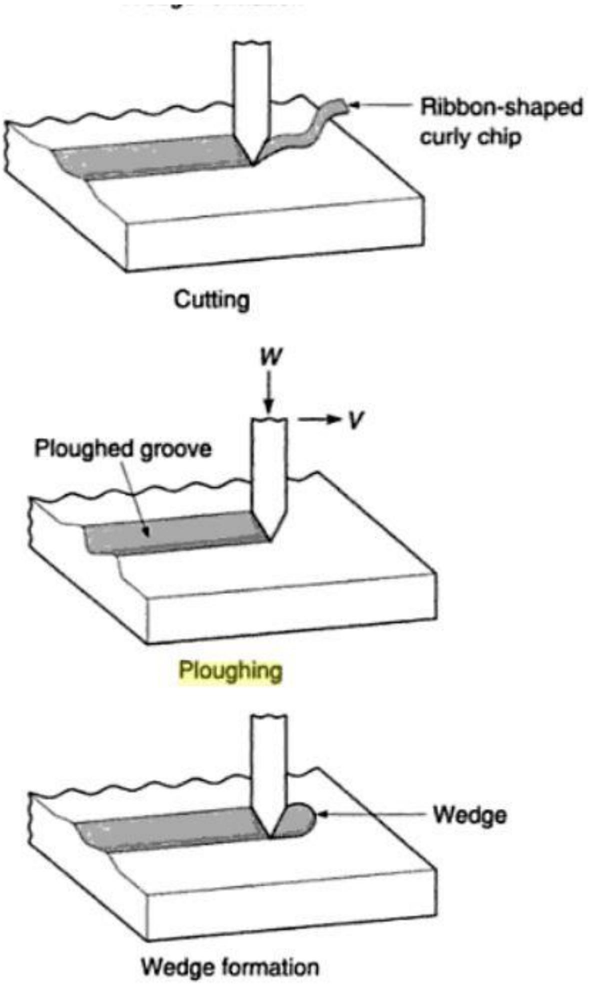

Figure 2.30. Schematic representation showing three different modes of abrasion: cutting, ploughing and wedge-forming mode [47].

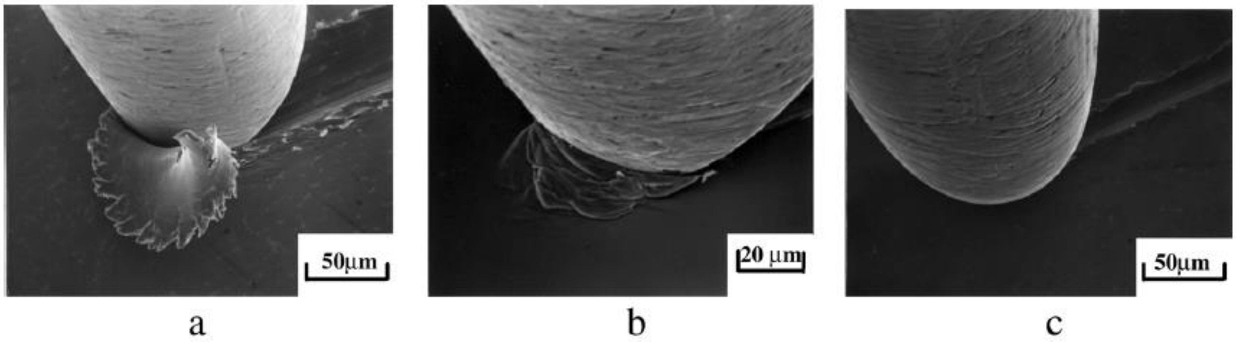

*Figure 2.31. Three different modes of abrasive wear observed by SEM (secondary mode): (**a**) cutting mode, (**b**) wedge-forming mode and (**c**) ploughing mode [48].*

Factors such as the relative movement during abrasion, or the properties of the worn material can affect the wear mechanism that takes place [48]. The relative shearing movement between the abrasive and the wearing material is associated with the cutting and ploughing mechanisms, while relative vertical motion is more likely to lead to fragmentation. Furthermore, the plastic deformation characteristics of a material are thought to determine the extent of ploughing and cutting in a given system, see Figure 2.31 (a) and (c), while the fracture properties influence the extent of fragmentation and cracking.

Kato and Hokkirigawa [49] have used the degree of penetration of the abrasive into the metal surface (which determines the effective attack angle) as a method of constructing a wear mode diagram, as shown in Figures 2.32 and 2.33. The boundary conditions between various abrasive wear mechanisms can then be defined in terms of a critical degree of penetration [49].

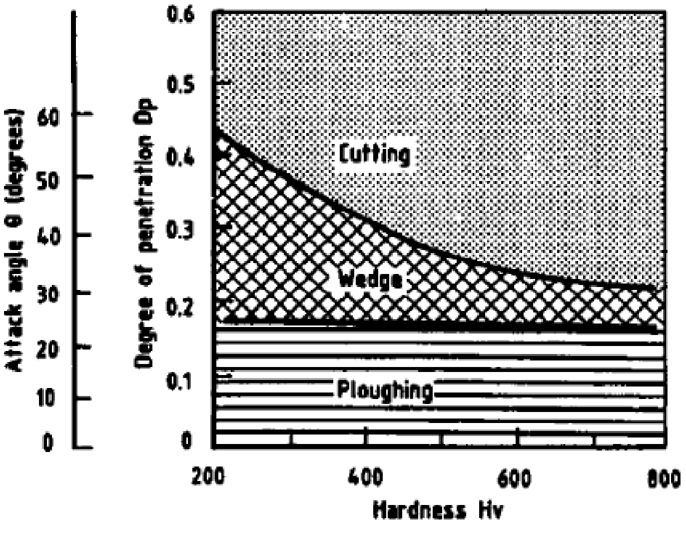

Figure 2.32. Wear mode diagram [49].

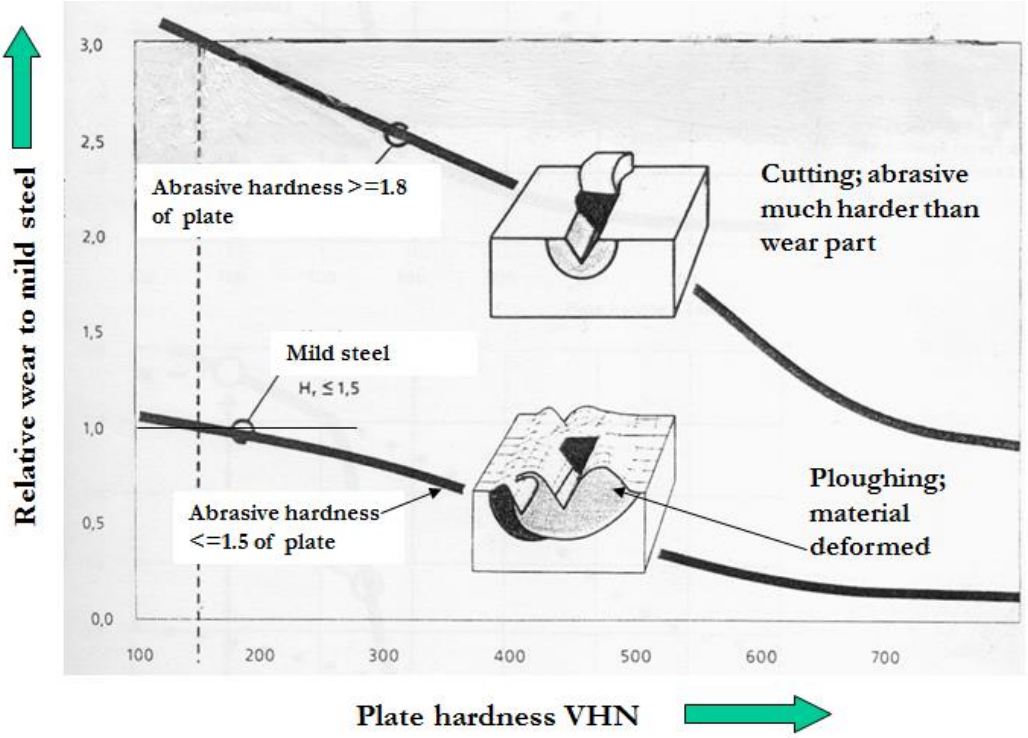

Figure 2.33. Relative wear rates for cutting and ploughing mechanisms [49].

Most of the high chromium white cast irons are resistant to abrasive wear due to the following:

- Result of hard particles (abrasive ore particles) cutting or ploughing out material
- The abrasive is harder than the wearing part
- Reducing the differential between the wearing part and the abrasive part will reduce wear
- If the abrasive index is >1.8 x (the hardness of the wearing part), cutting wear takes place
- If the abrasive index is <1.5 x (the hardness of the wearing part), ploughing wear takes place.

A variety of laboratory tests have been used by researchers in the study of the wear behaviour of white irons. This reflects the wide range of applications, and the varying abrasive conditions encountered, where these high chromium white irons are used.

2.7.2. Pin Abrasion Testing Machine (high stress)

The Standard Test Method for Pin Abrasion Testing according to ASTM G132-96, covers a laboratory procedure for determining the wear resistance of a material when relative motion is caused between an abrasive cloth, paper, or plastic film and a contacting pin of the test material [50].

The amount of wear is determined by weighing specimens both before and after testing. Mass loss values should be converted to volume losses using the best available values of specimen densities [50].

Wear results are reported as a volume loss and as the wear volume normalized with respect to the applied normal load. Schematic drawings of typical pin-on-disk, pin-on-table, pin-on-belt, and pin-on-drum wear testing systems are shown in Figures 2.34 and 2.35.

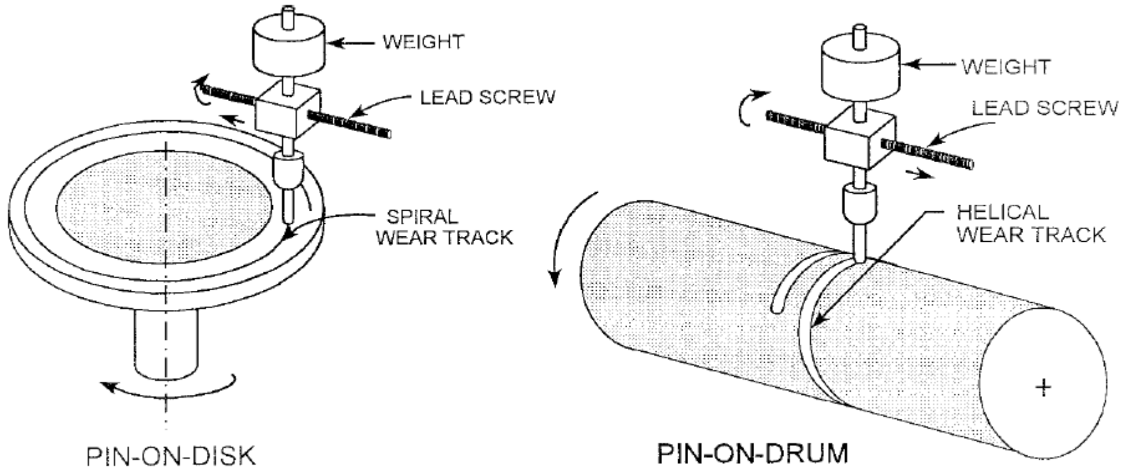

Figure 2.34. Configurations of Pin Abrasion Testing Machines [50].

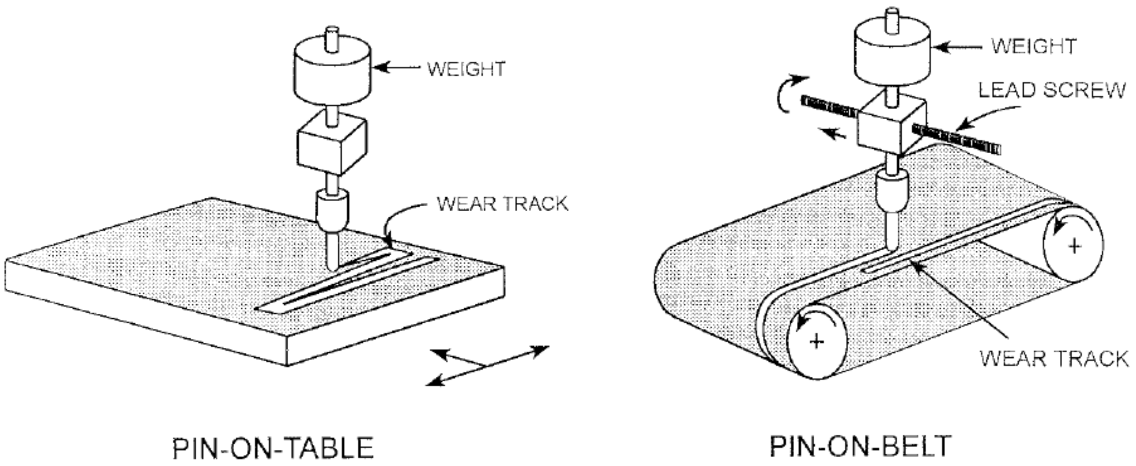

Figure 2.35. Configurations of Pin Abrasion Testing Machines [50].

Various sizes and types of abrasives are used and these include silicon carbide, alumina, emery, garnet, flint, or other silica compounds, and synthetic compounds, but wear results normally will differ with different types of abrasive, see Table 2.11.

Table 2.11 Various sizes and types of abrasive used in Pin-on-belt tests [50].

Abrasive Type	**Particle size of the abrasive material**	
	Grit	**Size (μm)**
Garnet	220	65
Garnet	150	105
Garnet	120	125
Garnet	60	250
Silicon carbide (SiC)	150	105
Silicon carbide SiC	120	125
Corundum (Al_2O_3)	150	125

Other designs of pin-on-belt abrasive wear test machines are illustrated in Figures 2.36 and 2.37 and described more fully by Blickensderfer [51, 52] and Izcilera [53]. In this test, one end of a cylindrical pin specimen is moved over an abrasive paper with sufficient load to abrade material from the specimen and crush the fixed abrasive grains. It has been shown that this test simulates the wear that occurs during crushing and grinding of ore in which the ore (the abrasive) is crushed. The pin-on-drum abrasive wear testing machines represent an improved variation of the more commonly used pin-on-disk machines that others have used to produce high-load abrasive wear. Norman et al. [54] have noticed that unlike the pin-on-disk machines, the pin-on-drum machines provide constant surface speed and rotate the specimen [54].

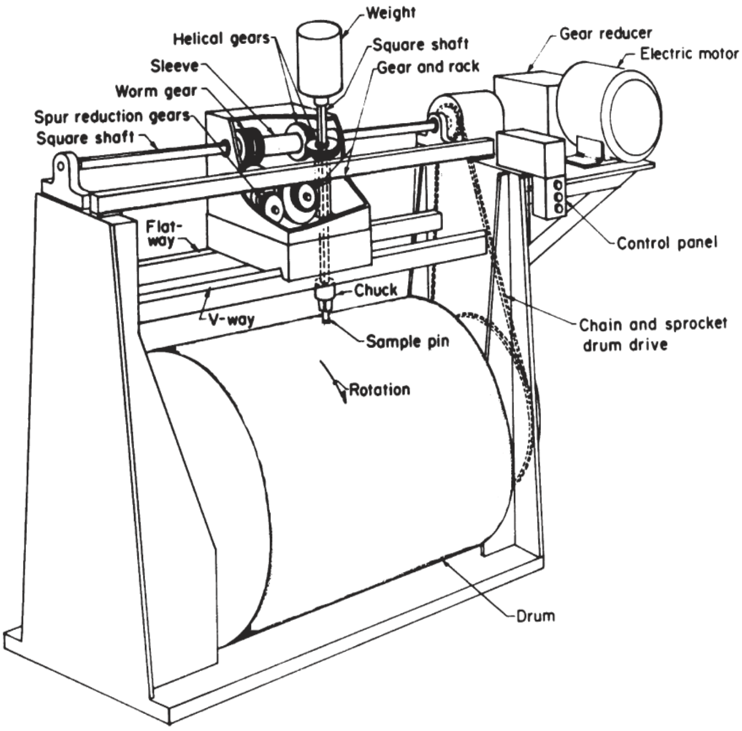

Figure 2.36. Schematic representation of a laboratory pin-on-drum abrasion testing machine [51, 52].

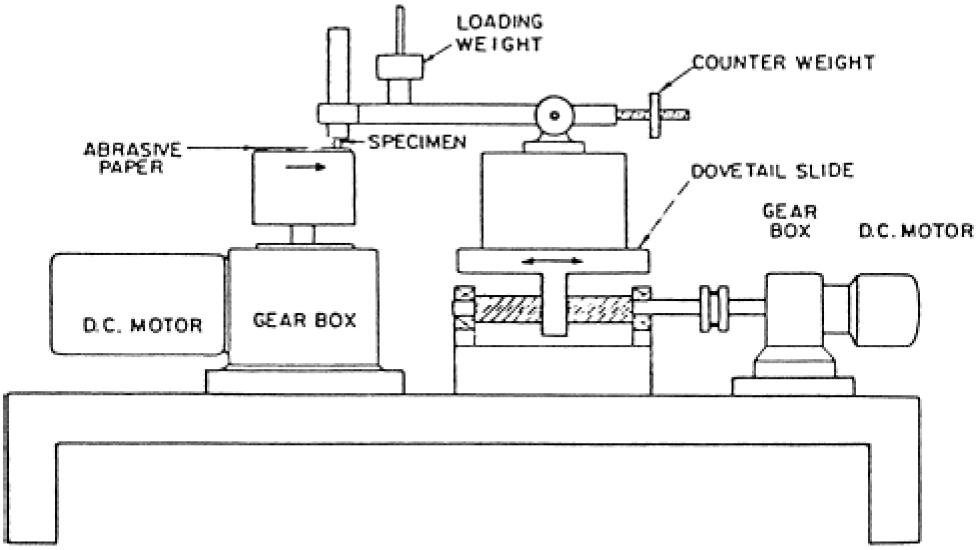

Figure 2.37. Pin-on-disc wear test apparatus [53].

2.7.3. Rubber Wheel Abrasive Tests (Low Stress)

In ASTM G65-04, abrasive wear is defined as "wear due to hard particles or hard protuberances forced against and moving along a solid surface". This definition encompasses several different mechanisms by which material removal occurs [55. These include ploughing, wedge formation, cutting, gouging and delamination. The abrasive wear process has also been classified in terms of high-stress and low-stress abrasion, the transition between the two often being defined as the point at which fragmentation of the abrasive occurs [55, 56]. This type of wear occurs in the mining industry in linkages, pivot pins and wire ropes, which suffer slow wear from the sliding and rolling action of abrasive fragments of rock and ore trapped between metal surfaces [57].

Although several different mechanisms have been identified and discussed in the literature, they may all be considered in terms of local plastic damage resulting from the abrasive particle/metal surface interaction and eventual fracture to generate wear debris, see Figures 2.38 to 2.40 [55, 56, 57]. The ploughing and cutting modes of material removal have received considerable attention. The transition from ploughing to cutting occurs at a critical attack angle which lies between 30° and 90° for most metals. ASTM G65-04 has proved to be a reliable low stress abrasive wear test to assess the performance of a wide range of materials. In all cases, the wear rate increased with load, and material loss was proportional to the quantity of abrasive [55].

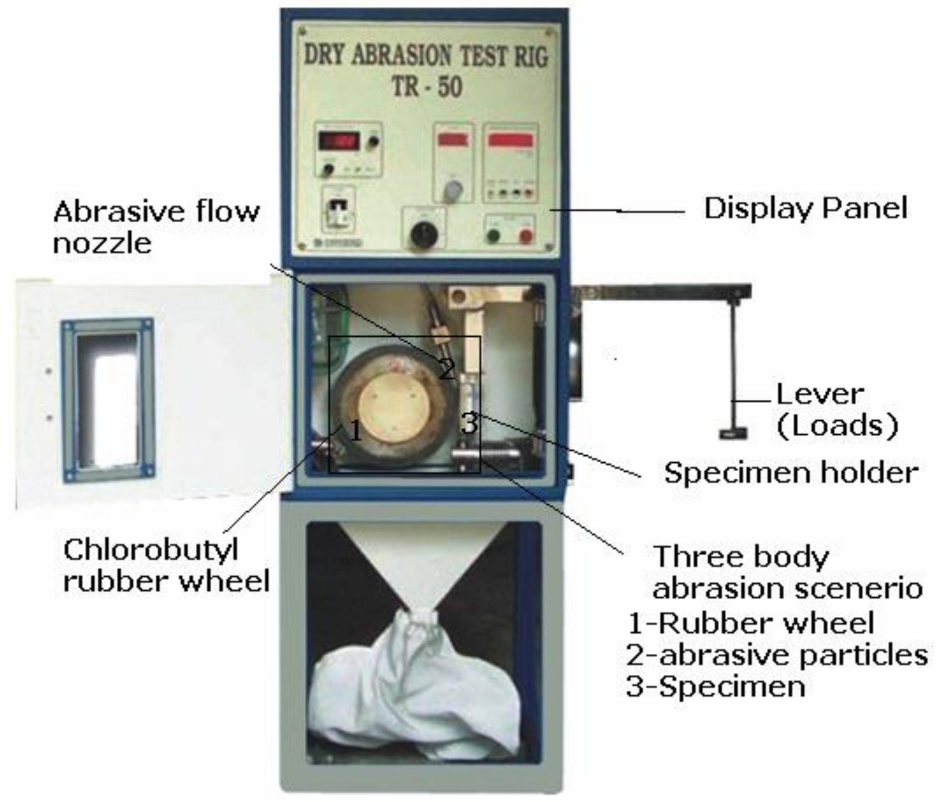

Figure 2.38. Three-body abrasive wear testing machine [56].

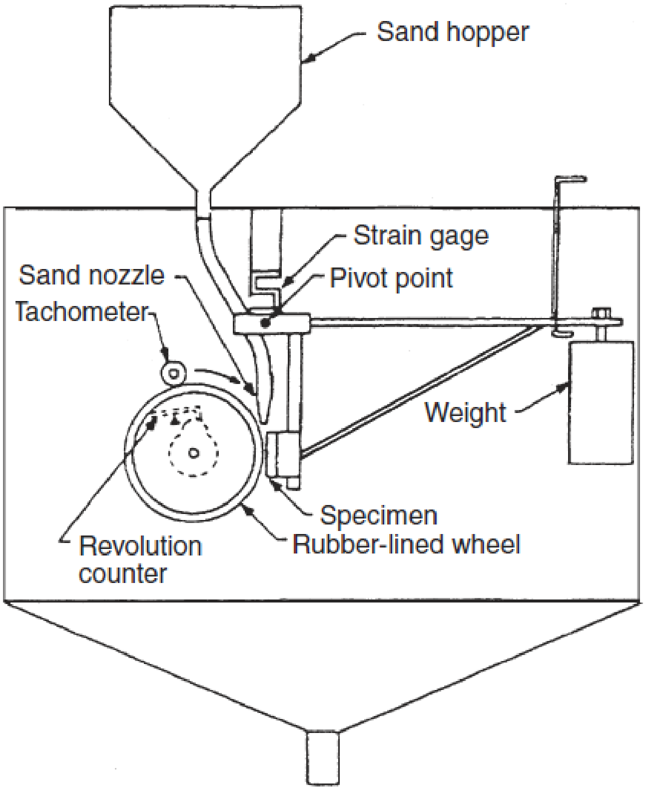

Figure 2.39. Schematic diagram of the dry sand, rubber wheel wear apparatus [55].

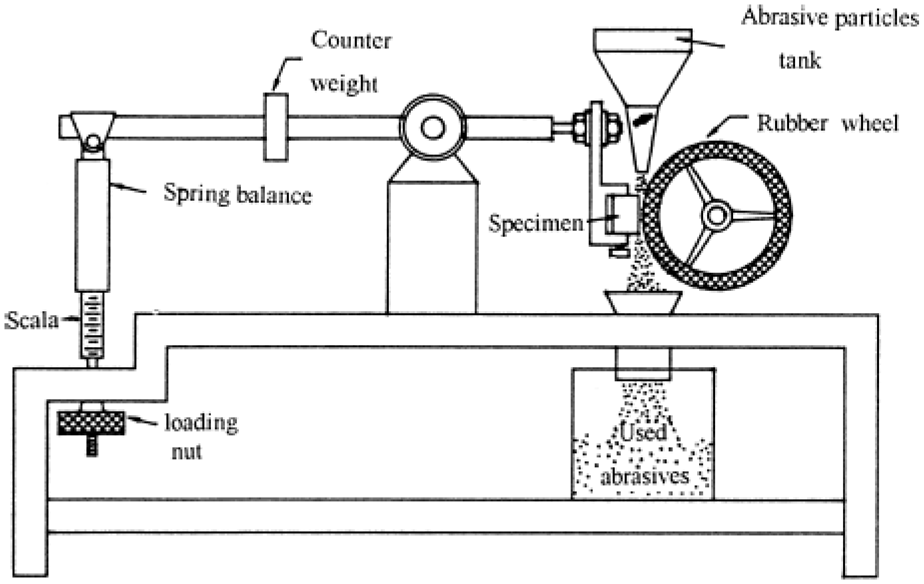

Figure 2.40 Schematic diagram of the rubber wheel abrasive tester [57].

In the above two test facilities, the corrosion effect is neglected and in another study, an improved version of this laboratory wear test machine is presented see Figure 2.41, ASTM G105 [58]. In addition to its capability of producing impact of a magnitude comparable to those encountered in actual grinders, this apparatus now uses an abrasive cup filled with real ore particulate slurry producing three-body abrasion according to ASTM G105 [58]. Tests may also be carried out in dry or humid conditions in order to better follow the effect of corrosion from the grinding media into account. The test specimen is abraded in a slurry of water and ore particles but also containing abrasive grit of controlled size and composition.

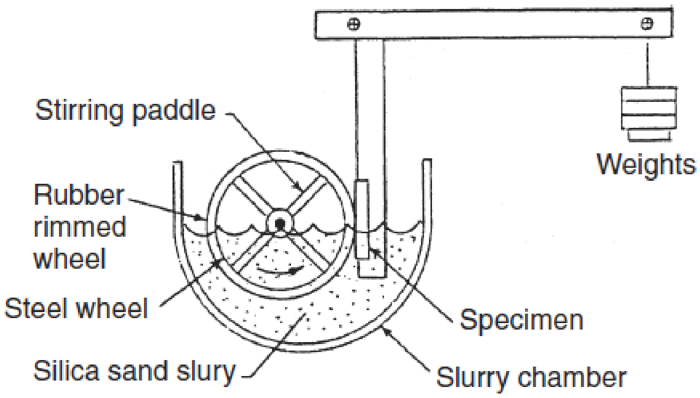

Figure 2.41. Schematic diagram of the wet sand, rubber wheel wear apparatus [58].

In research on wear of materials, the problem of reproducing real-life conditions is always present when one intends to measure or rank wear resistance values. Therefore, a modified three-body impact-abrasion laboratory testing for grinding ball materials was developed, Fiset [59]. An impact-abrasion test consists of a series of wear cycles, each cycle involving an impact between the specimen and the abrasive media followed by a rotation of the specimen in contact with the abrasive. In this test, impacts are direct impacts, i.e. the specimen itself is used as a hammer to impact the abrasive media. A schematic diagram of the test apparatus is shown in Figure 2.42.

It has been shown that the use of a humid abrasive mixture leads to better correlations with the marked-ball test in a real-life ball mill. Such a test could successfully replace the expensive marked-ball tests in order to rank the wear resistance of experimental grinding ball materials [59].

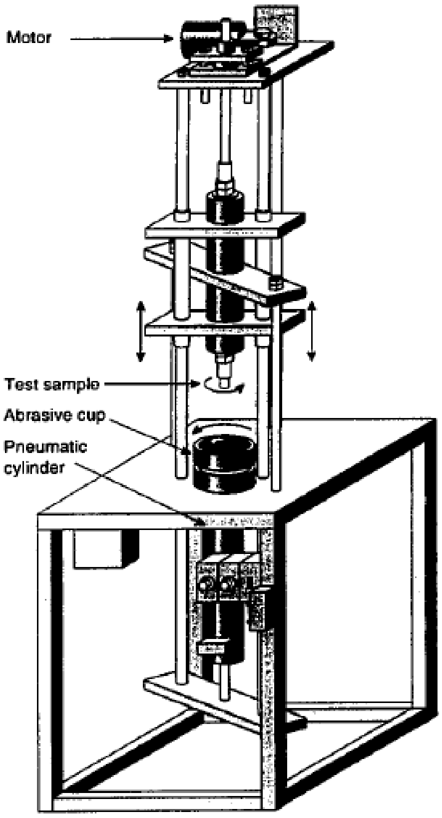

Figure 2.42. Schematic diagram of the laboratory wear test apparatus [59].

2.7.4. Impact Wear

According to Morrison et al. [60] impact breakage in AG/SAG mills is caused by steel balls or bigger particles that break smaller particles against the mill liner or charge, or when a falling particle breaks itself against the liner or the charge [60]. Impact breakage is the dominant mode of breakage in crushers and many ore characterisation devices and is one of the major modes in SAG mills. The progeny size distributions of impact breakage generally consist of some medium sized particles (smaller than the mother particles) and fines.

Cast iron grinding balls are used in large quantities in grinding mills for crushing coal, ores, cement. Grinding balls need to have good resistance to cyclic impact loads in addition to high wear resistance as they suffer repeated impact collisions with other balls, hard liner plates as well as the objects for crushing [60].

2.7.4.1. Impact/Drop Test Machine

Some research was undertaken in the past for ascertaining the effects of pure impact on alloy steels and cast irons. Equipment described by Blickensderfer and Tylczak [61] involved balls made from alloys being dropped 3.4m on to a column of balls, with each successive ball receiving an impact on each side, Figure 2.43. The first ball receives maximum impact while the last one receives the least. This impact tester does not take into account the longitudinal or parallel directions of the samples used which can be up to 50mm in diameter.

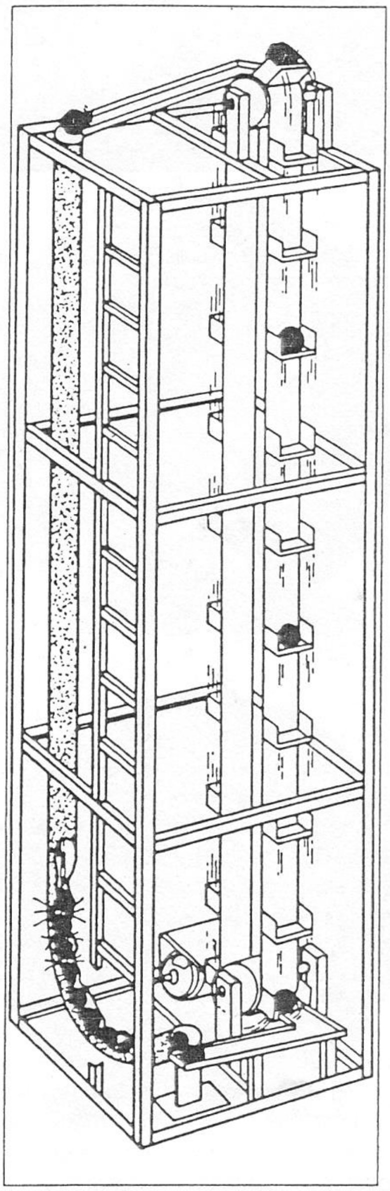

Figure 2.43. Ball-on-ball impact-spalling testing machine [61].

Impact fatigue resistance is determined on a ball-on-ball test machine (see Figure 2.44). The balls tested were 60 mm in diameter and every group contains 22 balls. The drop height was 3.5m and total drops for each group of balls were 50 000 times. The ball mass before and after the test was measured [62].

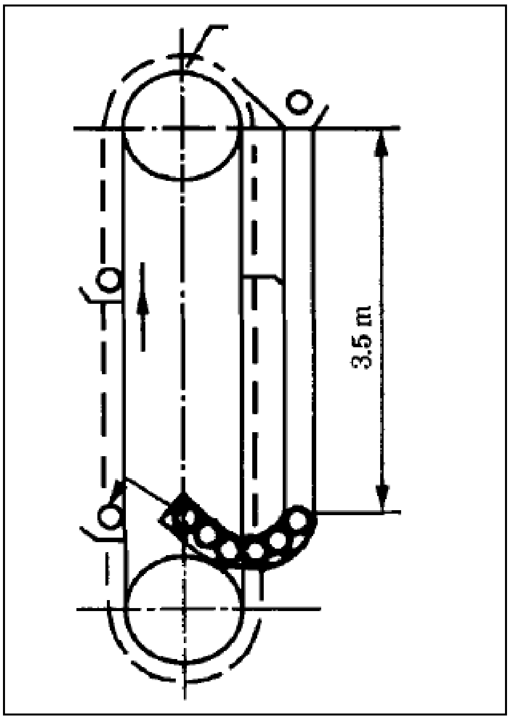

Figure 2.44. Ball-on-ball impact-spalling testing machine [62].

2.7.4.2. *Repetitive Drop Tester*

An automatic repetitive drop tester was developed by Noguchi et al. [63] as shown in Figure 2.45. In this test a ball is carried by a bucket chain system to a predetermined height, is released and drops in a 100mm diameter plastic pipe to collide with an anvil. The anvil is made of Ni-hard cast iron, 250mm x 250mm cross-section and 500mm deep, of HS 95 hardness and weighing 250kg [64]. Resistance to repeated impact is measured as the weight loss per number of impacts or as the number of impacts before cracking is observed.

Test pieces [64] for impact and fatigue tests are inclined by about 58° from the horizontal, and the ball rebounds forward, bumps into a cushion filled with styrene balls to absorb the kinetic energy, and rolls down to the original waiting spot. The impact and rebound velocities of each drop are measured by a light source and photo-transistor system and recorded in a computer. Failure of the ball is detected by it not arriving at the waiting spot within a certain time, then the machine stops automatically [63, 64].

Ball-on-block test rigs [64] have been used for some years. These generally consist of grinding balls between 40mm and 75mm in diameter, being raised to a height of 3m to 6m, and falling down a vertical chute where they impact an anvil or block (Figure 2.46). The tests commonly measure weight loss against the number of impacts to give an impact wear rate [51].

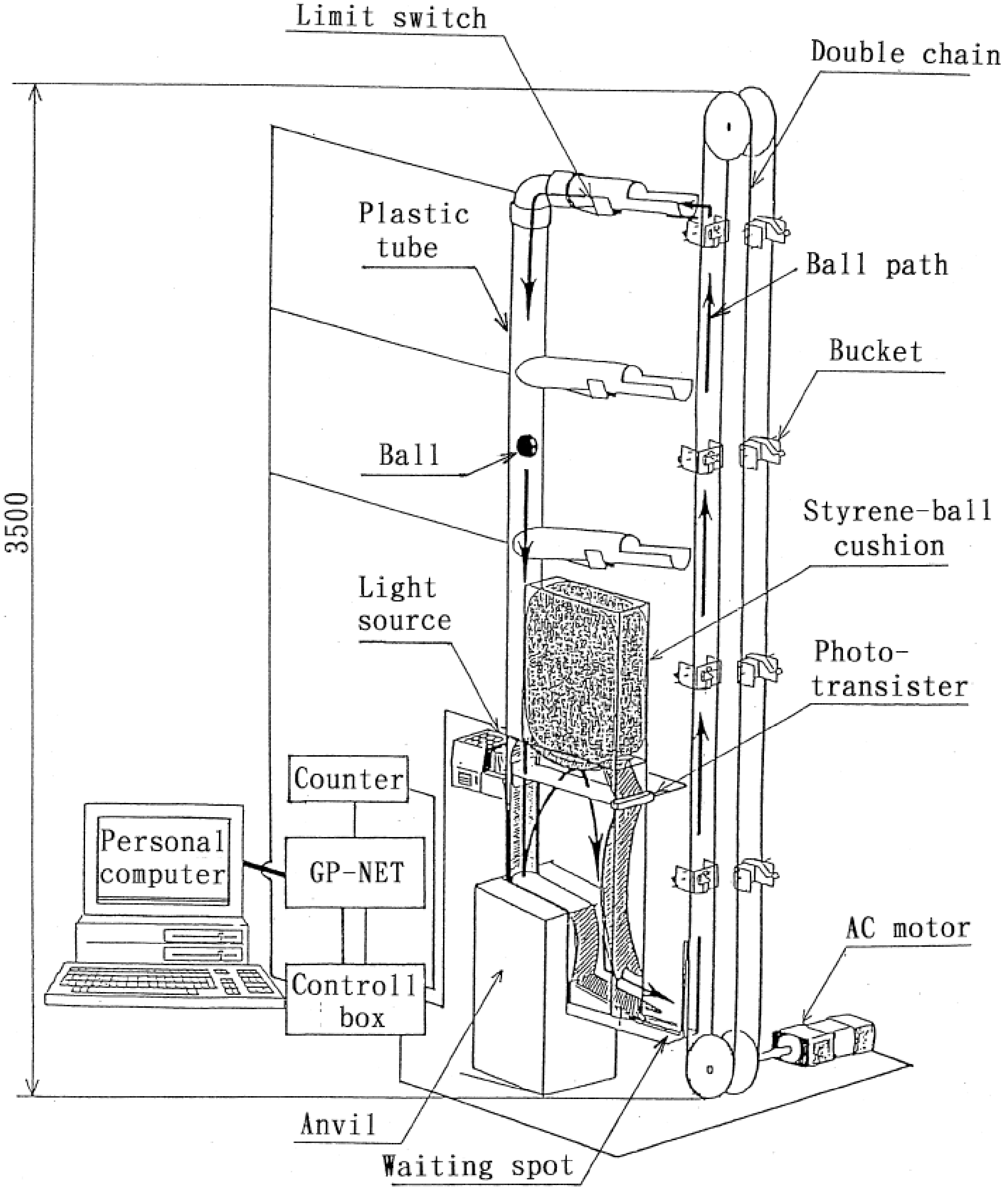

Figure 2.45. Automatic repetitive ball drop test system [63, 64].

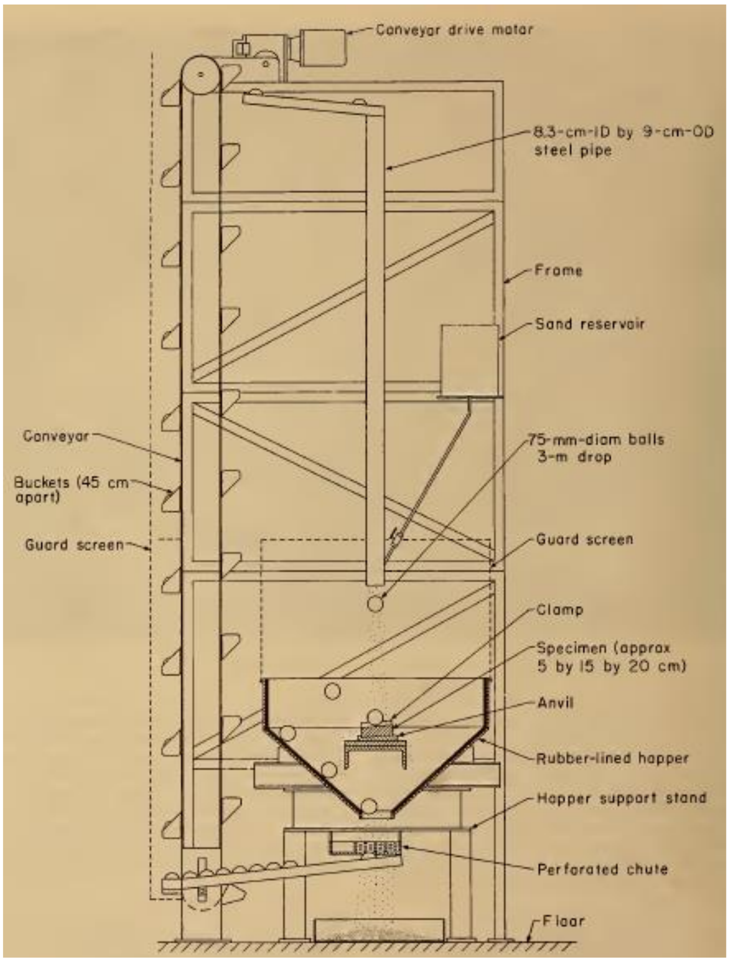

Figure 2.46. Schematic diagram of a Ball-on-block impact-spalling test machine [51].

2.7.5. Marked Ball Wear Test (MBWT)

The marked ball wear test (MBWT) is an excellent tool for comparing wear rates of different materials under identical production milling conditions. Direct comparisons can be made, eliminating the need to compensate for differences in *ore hardness, feed rate, mill volume*, etc., factors which have been associated with historical comparison testing and parallel production testing, see Table 2.15 and Figure 2.47 [65] and [66].

Plant tests involving the gradual introduction of a full charge of balls of a new type are long and expensive. An attractive alternative is a test in which several types of balls carrying distinguishing marks (e.g., fine holes) are introduced simultaneously into a mill and are removed for examination at intervals [65, 67]. The MBWT method also avoids the time necessary to convert a mill charge from one type of ball to another to conduct a full production test. A final feature is that production wear rates can be accurately predicted directly from MBWT results.

In preparation for testing, selected groups of balls are identified by some means to allow decoding of recovered balls at the conclusion of each recovery period. There are two popular means to identify balls for MBWT [68].

- One method is to drill each ball with an identical hole, place an identification tag in the bottom of the hole, and then fill the hole with a low melting point metal alloy plug to secure the tag. At recovery, the plug is melted and the identification tag is recovered.
- A second method of marking balls is to use different combinations of holes, hole diameters, and hole orientations to differentiate between test groups.

Typically, two holes of equal or different sizes are drilled at 90° or 180° orientations [68]. With this method, the initial weight of all balls within a test group must be essentially the same since wear rate calculations are based on average initial and final weights. Marking of the balls must be done carefully or excessive localized heating in the drilled region may occur, causing transformation products in the microstructure of some alloys. An electrical discharge machining (EDM) is the preferred method of creating the identifying holes.

When making comparisons between two types of balls under these conditions, it is important that both ball types have the same size [68]. The coded groups of balls are individually weighed prior to placing them into an operating production mill. Periodically, when the mill is down for scheduled maintenance, the test balls are recovered, decoded, and reweighed. Assuming the balls remain as perfect spheres, the ball weights are converted to ball diameters and a plot of ball diameter vs. time is generated. The wear speed and wear speed exponent are determined from interpretation of the plot [68]. Table 2.15 summarises the effect of various milling parameters on wear rate.

Table 2.12 The effect of various milling parameters on wear rate [68].

	Factors	Trends	Effect
A	**Grinding charge**		
	1. grinding media size	> size	< wear rate
	2. grinding media distribution	> small size	> wear rate
	3. charge weight	> charge weight	> wear rate
B	**Ore**		
	1. work index	> work index	> wear rate
	2. hardness	> hardness	> wear rate
	3. density	> density	> wear rate
	4, concentration/grade	> concentration/grade	> wear rate
	5. abrasion/nature of gangue	> silica content	> wear rate
C	**Particles**		
	1, feed size	> size	> wear rate
	2. product site	> size	< wear rate
	3. shape	sharp corners	> wear rate
D	**Slurry**		
	1. corrosion	> pH	> wear rate
	2. viscosity	> viscosity	< wear rate
	3. % solids	< % solids	> wear rate
E	**Nature of contact**		
	1. impact velocity	> velocity	> wear rate
	2. impact angle	> angle	< wear rate
F	**Mill**		
	1. discharge type	overflow → grate	> wear rate
	2. diameter	> diameter	> wear rate
	3. speed	> speed	> wear rate
G	**Circuit**		
	1. throughput	> throughput	< wear rate
	2. circulating load	> circ. load	> wear rate
H	**Grinding media quality**		
	1. hardness:- surface or avg. volumetric	> hardness	< wear rate
	2. grain size	> grain size	> wear rate
	3. C content	> content	< wear rate
	4. alloy content	> alloy content	< wear rate
	5. shape	sphere	min. wear

With (>, <) "Trends": > = increasing, < = decreasing, the "Effect" (<, >): > = increases, < = decreases.

for instance a trend of "> small size" means increasing amount of small sizes of grinding media distribution the wear rate increases

Certain difficulties are associated with the interpretation of the results of marked-ball tests. These difficulties are as follows [66]:

(i) Ball consumption decreases systematically with time (or mass of material milled) in a manner suggesting that equilibrium has not been reached, and

(ii) Marked balls that are of the same type as the 'background' of balls within the mill appear to be more durable than the background balls – an effect referred to as the "marked-ball anomaly".

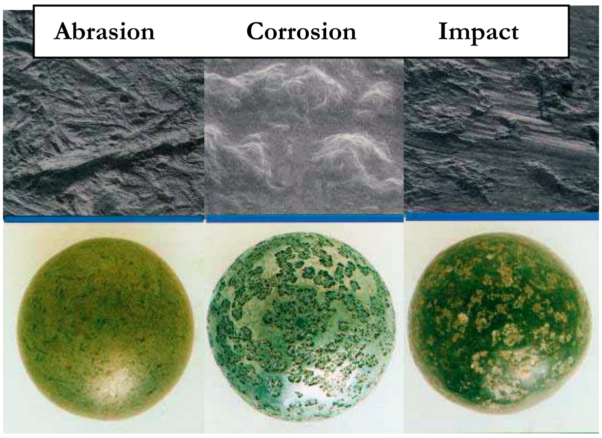

Figure 2.47. A diagram showing the wear mechanisms in a ball mill (abrasion, corrosion and impact) [66].

2.8. Theory of carbon partitioning and deformation induced martensite transformation

Quenching and partitioning (Q&P) processing was originally proposed by Speer et al. [69] as a new approach to produce steel microstructures consisting of a martensitic matrix containing considerable amounts of retained austenite. A schematic diagram heat treatment cycle for Q&P processing is given in Figure 2.48. The austenitized steel is initially quenched to a quench temperature (T_Q) in the M_s to M_f temperature range, and the microstructure is partially transformed to primary martensite (α'_p). It is then partitioned at the partitioning temperature (T_P). During the partitioning stage, carbon diffuses from the supersaturated α'_p into the untransformed austenite. If not enough carbon partitions to austenite, some of the austenite will transform to secondary martensite (α'_s) in the final quenching stage.

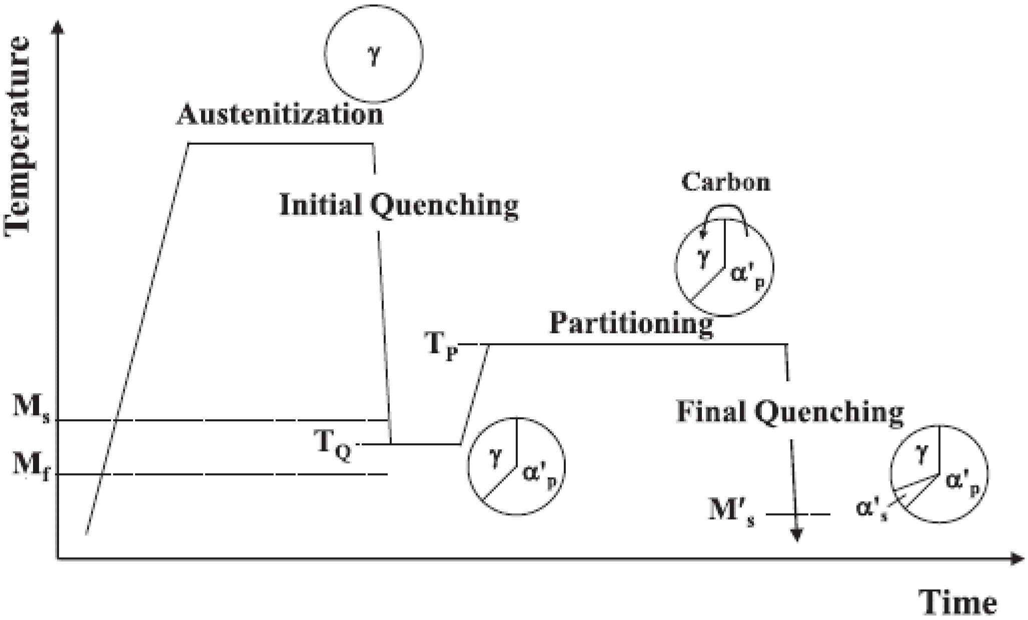

Figure 2.48. Schematic diagram of the heat treatment cycle for the Q&P processing. γ, α'ₚ and α'ₛ are retained austenite, primary martensite, and secondary martensite, respectively [69].

The Quenching and Partitioning (Q&P) heat treatment cycle is an alternative route for obtaining multi-phase steel, in which the volumetric fraction of retained austenite is controlled by carbon partitioning from supersaturated martensite into austenite, allowing the stabilization of austenite [69]. Speer et al. [70], further emphasised that T_q is usually much higher than room temperature for low and medium carbon steels; partitioned at or above T_q to accomplish the partitioning (diffusion) of carbon from supersaturated martensite into retained austenite so as to keep carbon-enriched retained austenite stable during subsequent cooling to room temperature.

Xiaoshuai et al. [71] studied the partitioning of carbon from martensite to retained austenite during a multicycle quenching and sub-critical treatment (De-MQ-Sct) process (see Figure 2.49) of the high chromium white cast iron (HCWCI) material, compared to that of steel and found that it promotes the interaction between carbide precipitation and martensitic transformation. This interaction is a unique effect only produced by multicycle quenching linking destabilizing and sub-critical treatments, which lead to more and finer secondary carbides and more carbon-enriched austenite in a De-MQ-Sct sample than those in conventional normalization (NOR) or an oil-quenching samples.

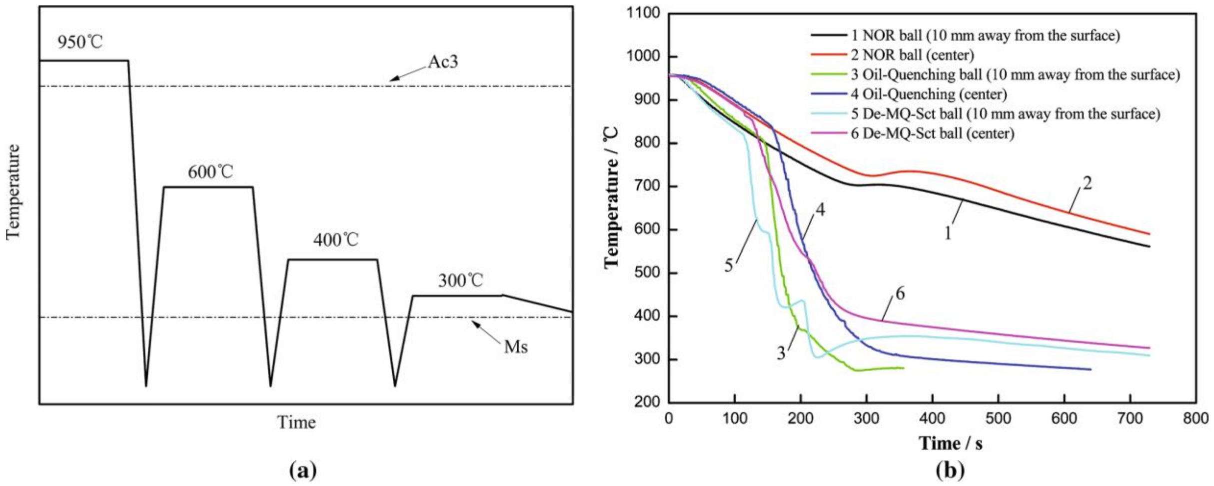

Figure 2.49. (a) Schematic illustration of the De-MQ-Sct process; (b) Cooling curves measured at different positions of white cast iron balls treated, by three processes [71].

Xiaoshuai et al. [71] also found that martensitic transformation increases the carbon content in austenite by the partitioning of carbon from supersaturated martensite into austenite, which then accelerates the precipitation of secondary carbides from supersaturated austenite [71]. The retained austenite has a high intrinsic fracture toughness and transformation-induced plasticity (TRIP) by strain-induced martensitic transformation, such as wear-induced martensitic transformation. During the abrasive wear of the cast material, the TRIP effect can enhances ductility by the martensitic transformation from retained austenite, see Figure 2.50 [71]. It was concluded that high wear resistance in high chromium white cast iron is mainly attributed to considerable fine secondary carbides and stable carbon-enriched retained austenite.

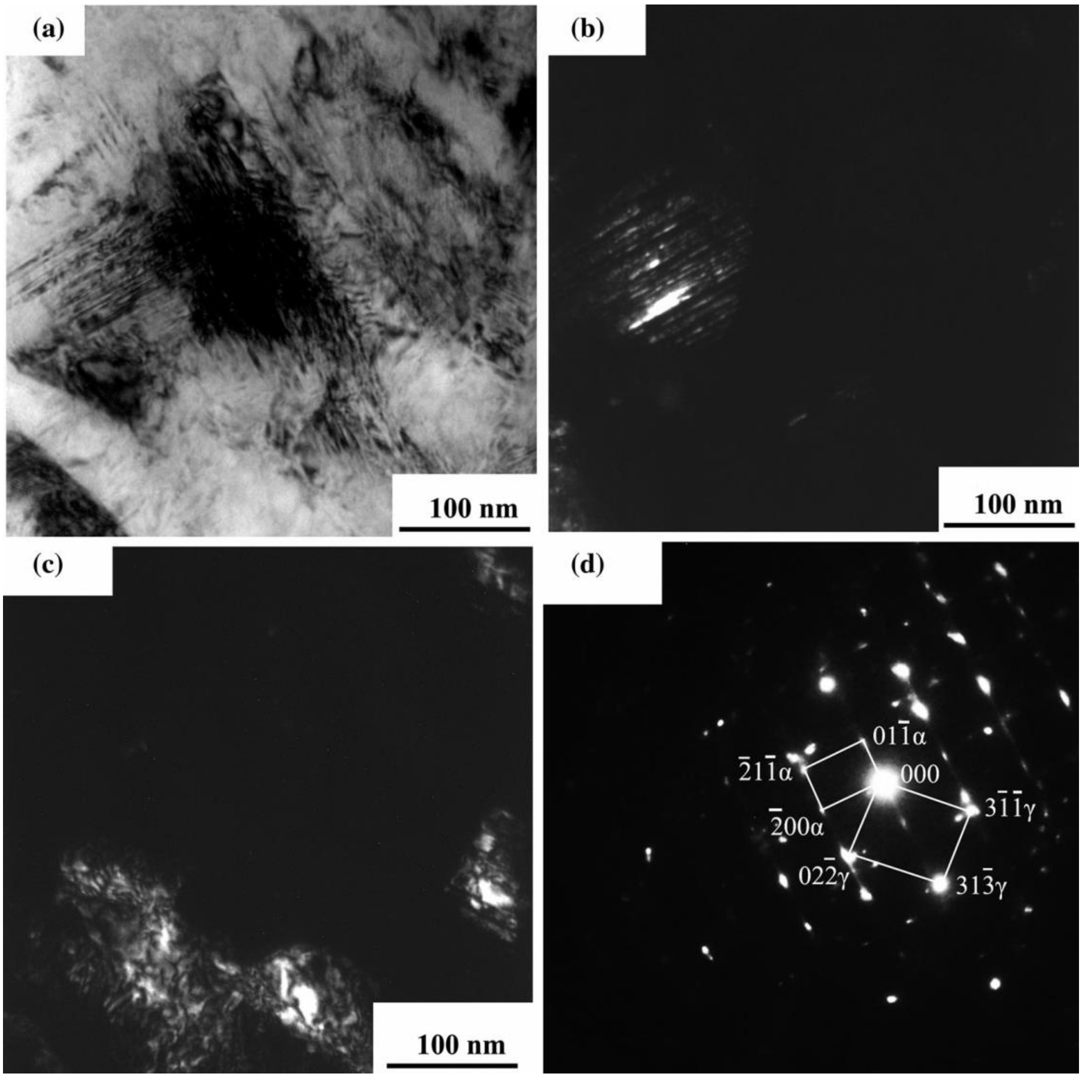

Figure 2.50. The characterization microstructures in the worn surface of an Oil-quenched sample. (a) BF image of twin-type martensite and retained austenite, (b) DF of twin-type martensite, (c) DF image of retained austenite, and (d) SAED pattern.

Speer et al. [69] and Ooi et al. [72] pointed out that the carbon concentration $\boldsymbol{x}_\gamma$ of the austenite in the material can be estimated from the lattice parameter $\boldsymbol{a}_\gamma$ using the equation:

$$x_\gamma = \left(a_\gamma - 0.3570\ \text{nm}\right)3.8\times10^{-3}\ \text{wt\%} \qquad \text{Equation 2.7}$$

The authors [69, 72] confirmed that there is a competition between the processes of carbon partitioning from the martensite into the residual austenite, and the precipitation of excess carbon in the martensite, e.g. the highest martensite-start temperature (which facilitates partitioning) and the lowest carbon concentration (which reduces the driving force for precipitation).

Yuki at al [73], investigated the carbon partitioning behaviour from martensite into austenite during a partitioning step accompanied by the carbide precipitation inside the martensite for the low (0.59%) and high (1.07%) carbon steel. They found that the austenite carbon concentration after the partitioning step was not influenced by either the martensite volume fraction or the bulk carbon content [73].

2.9. The Quenching and Partitioning (Q&P) process of commercial ductile iron alloy

Da Silva et al. [74] investigated the Q&P process in ductile cast iron and found that it is suitable to achieve large fractions of retained austenite in ductile cast irons. Their investigation was on a commercial ductile iron alloy (ADI), used in components for the automotive industry. The microstructural analysis from this work showed that the microstructure resulting from quenching and partition heat treatments was composed of a mixture of partitioned martensite (low carbon) + fresh martensite + ausferrite (bainitic ferrite free of carbides + retained austenite), see Figure 2.51.

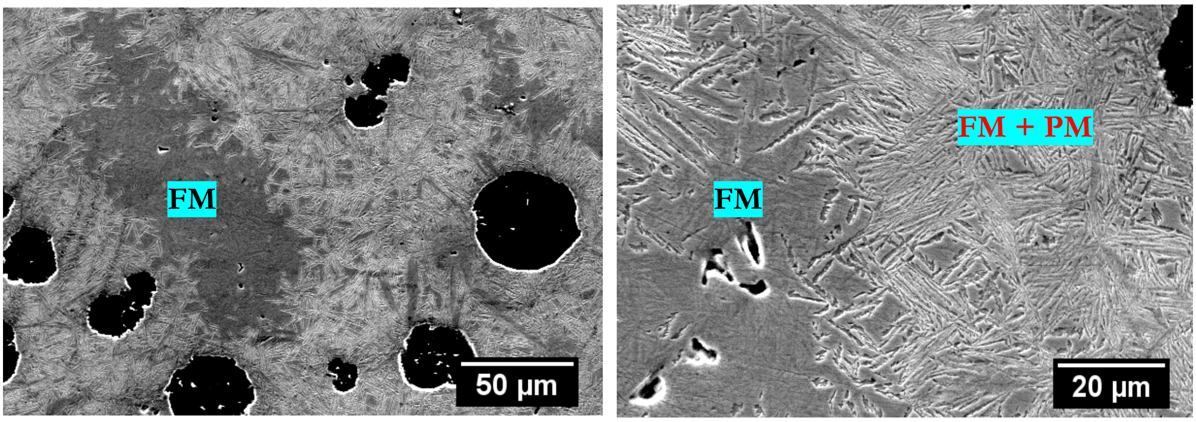

Figure 2.51. SEM microstructure of the sample partitioned at 300°C during 2 minutes, showing the differences of microstructures around the nodules (PM = partitioned martensite, AF = ausferrite) and around the eutectic cells (FM = fresh martensite) [74].

The amount of carbon dissolved in the austenite was obtained using the method developed by Dyson and Holmes [75] through an empirical **Equation 2.8** which considers the volumetric changes of crystalline structure with the percentage of alloying elements in solid solution using the change in lattice parameter (**a_γ**):

$$\mathbf{a_\gamma = 3.5780 + 0.033\ at.\%C + 0.00095\ at.\%Mn + 0.002\ at.\%Ni + 0.0006\ at.\%Cr + 0.0031\ at.\%Mo + 0.0018\ at.\%V} \qquad \text{Equation 2.8}$$

In the areas surrounding the nodules of the ADI, Da Silva et al. [74] observed the presence of partitioned martensite (i.e., martensite formed during the quenching step and tempered during the partitioning step) and ausferrite (bainitic ferrite + retained austenite). According to Da Silva et al. [74], the areas around the nodules and intercellular areas behaved almost as two different alloys, with different compositions and the kinetic of transformations resulting from the heat treatment will differ on both areas.

The austenite is stabilized by carbon in areas close to the graphite nodules whereas in the intercellular areas there is still austenite with low carbon content, which will transform to fresh martensite during final cooling. The final microstructure obtained through quenching and partitioning in ductile cast irons is composed of graphite nodules formed during solidification and a mixture of ausferrite (bainitic ferrite free of carbides and retained austenite) with high and low carbon (carbon depleted) martensite as shown in Figure 2.51 [74].

According to work conducted by Bhople et al. [76], during the austempering process ADI undergoes two-stage transformation, the austenite (γ) is transformed into bainitic ferrite (α) and carbon enriched austenite (γ_{hc}), a product known as ausferrite i.e.:

$$\gamma \rightarrow \alpha + \gamma_{hc} \text{ ....Equation 2.9}$$

If the material is held for a longer time during austempering, carbon enriched austenite (γ_{hc}) converts into ferrite (α) and carbide [77, 78]:

$$\gamma_{hc} \rightarrow \alpha + \text{carbide ....Equation 2.10}$$

The austenitizing temperatures play a vital role in the control of the carbon content of austenite and this affects the structure and properties of an austempered castings. The austempering temperature is one of the significant parameters on which properties of ADI components depend. It has been found that the temperature range 350 – 400 °C will give an ADI with lower strength and hardness but higher elongation and fracture toughness (coarse ausferrite matrix). While austempering below 350 °C will produce an ADI with higher strength and greater wear resistance. It has been found that the temperature 350 °C is the threshold temperature for various mechanical properties of ADI components [76, 77, 78]. Figure 2.52 shows a schematic presentation of the effects of austempering temperature on the mechanical properties of ADI.

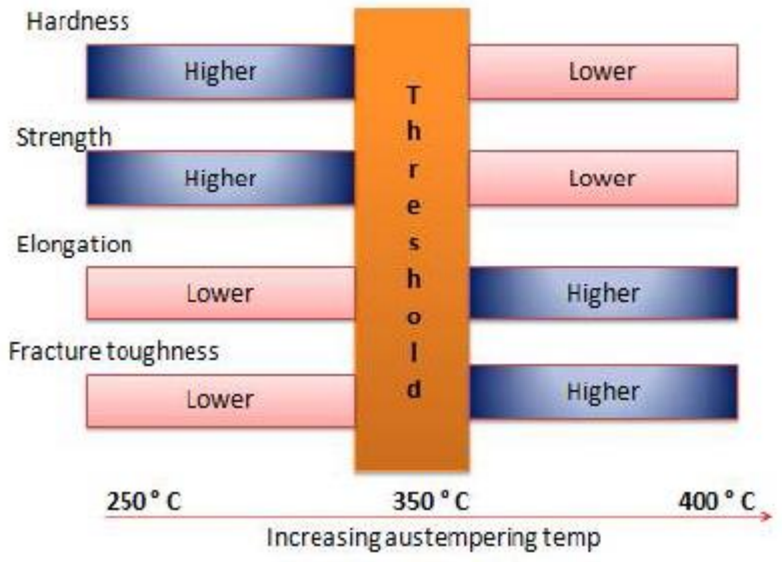

Figure 2.52. Effects of austempering temperature on the mechanical properties of ADI [76].

The phenomena for the ADI shown in Figure 2.52 was also illustrated by Zhang et al. [79], on the carbidic austempered ductile iron (CANI). They showed that when autempering at 280 °C, the fracture mechanism is mainly brittle fracture, while at 320 °C fracture mechanism was both ductile fracture and brittle fracture, i.e. in the transition region. At 360 °C fracture mechanism was found to be ductile fracture, i.e. the fractography of specimens changed from cleavage facets at 280 ℃ to dimples at 360 °C.

Liu et al. [80] in their study found that the impact toughness of CADI was lower than that of ADI. However the hardness of CADI is equivalent to that of high chromium cast iron (HCWCI), and much higher than that of low chromium cast iron which is widely used as grinding balls in mining. With an increase of austempering temperature, the acicular ferrite becomes thicker and larger, and its proportion gets smaller and the quantity of carbon-enriched austenite rises. When the austenite contains less carbon, it is not stable thermodynamically and can be transformed into martensite when the sample is taken out of the salt bath used as a quenching media. When the carbon of austenite reaches the range of 1.8 to 2.2%, it becomes more stable and when the carbon-enriched austenite cools to room temperature, it does not transform into martensite [80].

The phases from austempered ductile iron were also investigated by Swain et. al. [81]. In their study, the ADI samples were austenitised at 900 °C for one hour in a muffle furnace and then austempered in a salt bath maintaining at three different austempering temperatures (250°C, 300°C and 350°C). The authors found the superior mechanical properties of ADI to be due to acicular ferrite and carbon enriched stabilized austenite present in the matrix.

2.10. Deformation induced martensite transformation in ADI material

Aslantas et al. [82] evaluated the performance of tools when machining ADI material, see Figure 2.53. The ADI samples were austenitised at 900°C for 60 minutes followed by austempering at 250°C and 325°C for 60 minutes. They found that when a high normal force was applied to ADI, a strain-induced phase transformation of martensite (SIM) occurred on the surface of the component. The force exerted by the tool during turning can cause a localized phase change in the material in front of the tool. Austenite on the surface undergoes a transformation to martensite, which is harder and more brittle than the ausferrite structure, see Figure 2.54 [82].

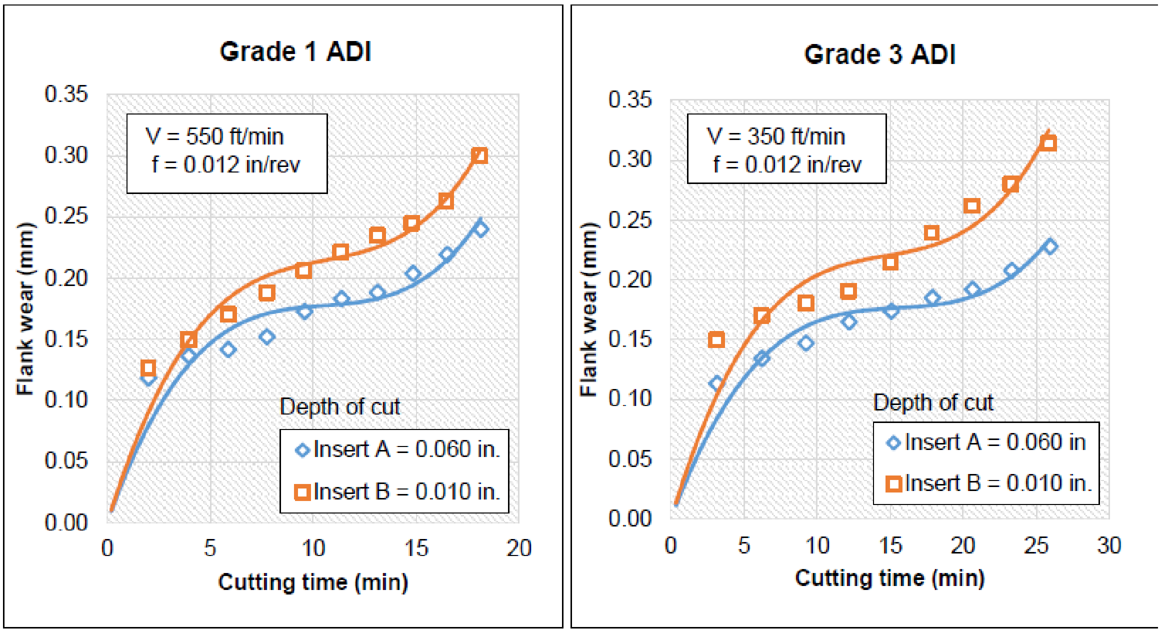

Figure 2.53. The effects of depth of cut on tool wear during turning of Grade 1 ADI and Grade 3 ADI [82].

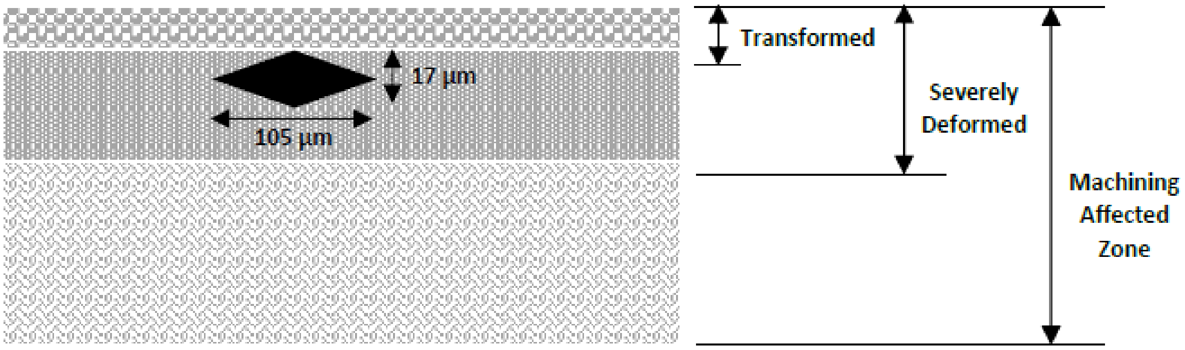

Figure 2.54. Machining affected zone (MAZ) consists of three different layers [82].

Ławrynowicz et al. [83], in their study on the carbon concentration of austenite in austempered ductile iron (ADI), found that it is possible to predict the carbon concentration in the retained austenite at the end of bainite transformation simply from chemical composition if the carbon is distributed evenly in the austenite. If bainite grows in a manner without supersaturation of ferrite, the reaction should be able to proceed until the carbon concentration in the retained austenite reaches the para-equilibrium T_0 phase boundary shown in Figure 2.55 [83].

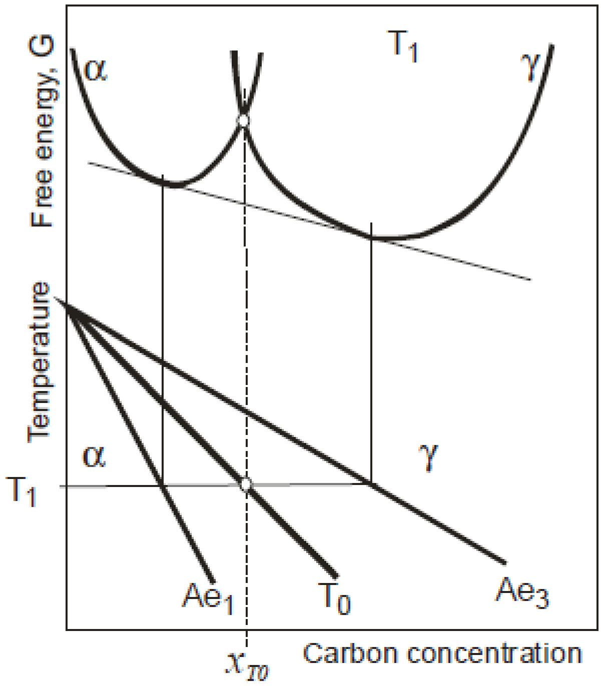

Figure 2.55. Schematic illustration of the origin of the T_0 curve on the phase diagram. α and γ refer to ferrite and austenite, respectively. T_1 is the temperature corresponding to the free energy curves [83].

During isothermal transformation the excess carbon in the bainite partitions into the residual austenite, forcing the next plate to grow from carbon enriched austenite. Ławrynowicz et al. [83] concluded that the carbon concentration of the residual austenite increases during bainitic transformation as a consequence of the increasing volume fraction of bainitic ferrite. The excess carbon in the bainitic ferrite partitions into the residual austenite and partitions inside the sheaves of banitic ferrite [83].

3. CHAPTER 3: EXPERIMENTAL TECHNIQUES

To study the influence of retained austenite on the wear properties of cast iron used in the mining and minerals processing industries for grinding ball applications, two different test alloys were produced. The test materials consisted of high chromium white cast iron (HCWCI) and carbidic nodular cast iron (CNI) [84]. Specimens for the test work were in the form of 70 mm diameter grinding balls and 12 mm x 25 mm by 150 mm rectangular flat test bars. A commercial high chromium white cast iron grinding ball was sourced and used as a reference material [16, 38]. The production and heat treatment of the two experimental alloys is fully discussed in Sections 3.1 to 3.7.

3.1. Pattern preparation

Wooden patterns were designed for casting of the ball and flat test pieces [85]. In the case of balls, special attention was paid to the feeding requirements to avoid formation of shrinkage cavities in the centre of the cast balls – a common problem in some of the commercially produced balls. In this case feeders, with a modulus of 1.25 times that of the balls were incorporated on the pattern. The 25% bigger modulus ensured that the feeders solidified after the balls and therefore were able to act as metal reservoir for the balls. Figure 3.1 shows the balls pattern configurations.

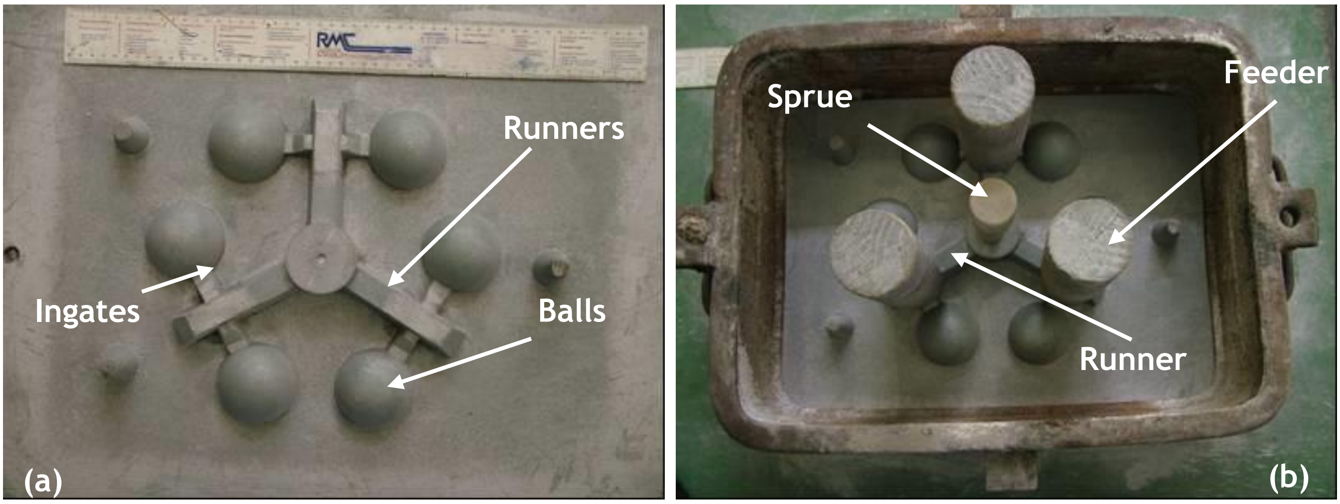

Figure 3.1. Photograph of the pattern used in the mould preparation of grinding balls (a) before modification (b) the pattern after modification.

3.2. Sand preparation

Cast iron mould boxes (0.5 m length, 0.38 m width and 0.14 m depth) were used to accommodate both the drag (bottom) and cope (top) parts of the pattern. Approximately 80kg of silica (SiO_2) sand with a particle size range of 0.075 to 0.65 mm was mixed with 5.5% of sodium silicate (Na_2SiO_3) binding agent [85]. The mould box with the pattern in place was then filled with this sand, rammed until the sand was compact. Gas holes of 3mm diameter were made in the rammed sand throughout the mould, to permit the mould to be gassed with carbon dioxide (CO_2) which was introduced through the holes to harden the mould by reaction with the sodium silicate (Na_2SiO_3). The mould was then lifted from the pattern and loose sand was removed by blowing with compressed air. The mould was coated with an alcohol based ceramic mould coat which helps to prevent sand burn-on during casting, and improves the surface finish. The moulds were ignited to burn off excess alcohol. The drag and cope were clamped tightly together in order to prevent any metal leakages during casting. Photographs of the moulds (cope and drag) and the intended grinding balls and plates given in Figures 3.2 to 3.5.

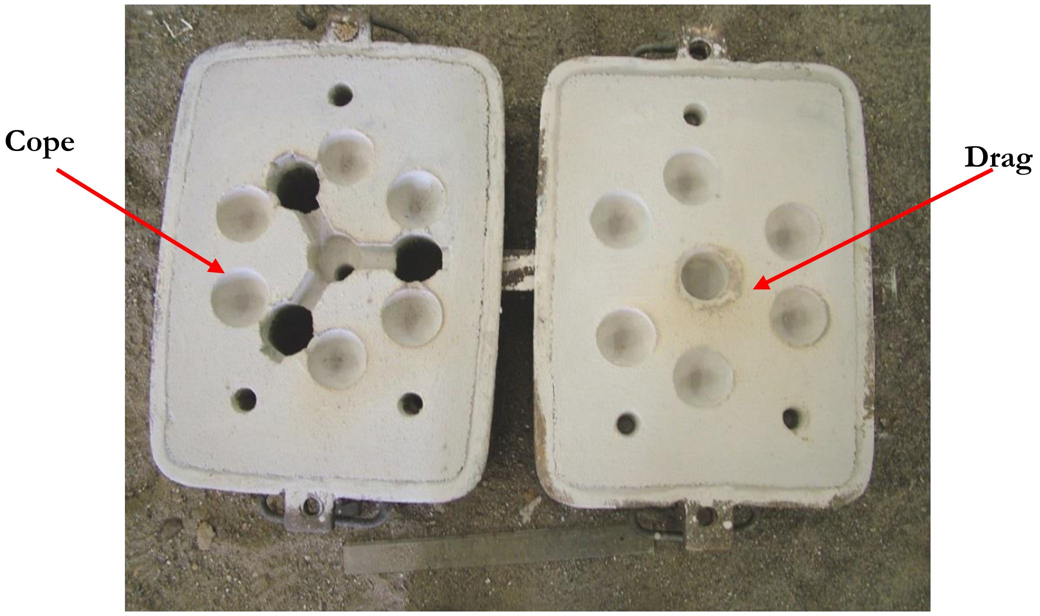

Figure 3.2. Photograph of the cope and drag used for sand casting grinding balls.

Figure 3.3. As-cast grinding ball on a tree.

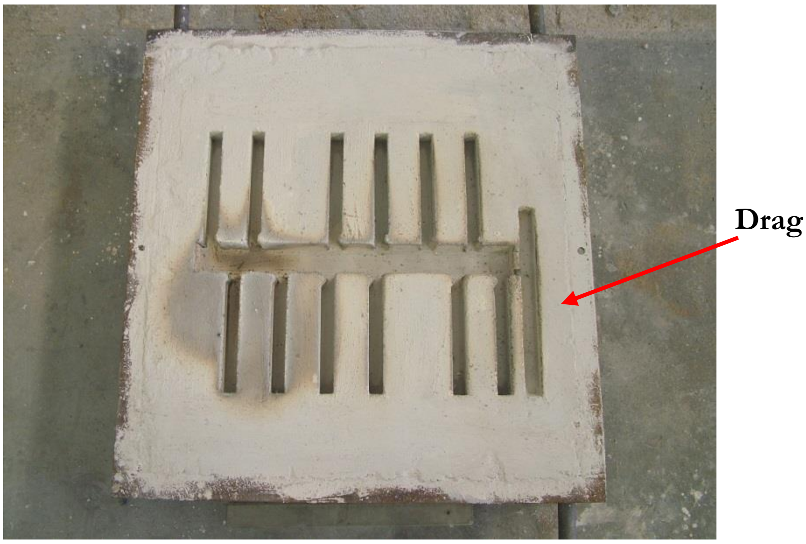

Figure 3.4. Photograph of the drag used for sand casting rectangular shaped wear test bars.

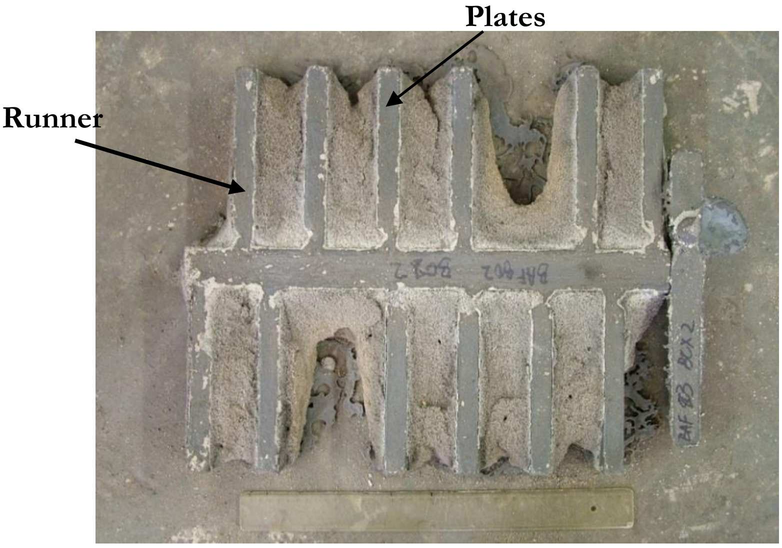

Figure 3.5. Photograph showing a rectangular wear test plates, the runner and risers.

3.3. Raw material used

The raw material requirements of the experimental grinding balls and flat bars were calculated and these were typical of those used for production of alloys in a normal foundry casting these alloys. This spread sheet used for calculational purposes (melt feed program) can be used to determine the melt composition of any alloy (even non-ferrous) to be cast [85]. Table 3.1 below shows the raw materials and their nominal compositions used in the alloy melting and casting.

Table 3.1. Raw materials used for the production of the alloys.

Elements	Raw materials used	Nominal composition (wt%)			Balance
Chromium	FeCr(Low C)	0.104%C	54.89%Cr	1.32%Si	Fe
Copper	Cu, pure	100%Cu	-	-	-
Scrap metal	EN 3B	0.18%C	0.76%Mn	0.23%Si	Fe
Scrap metal	Fe Sorrel F2	3.9%C	0.045%Cr	0.15%Si	Fe
Manganese	FeMn(Med C)	1.8%C	80%Mn	1%Si	Fe
Molybdenum	FeMo(0-50mm)	0.04%C	68.97%Mo	1.02%Si	Fe
Magnesium	MgFeSi	5.8%Mg	47.8%Si	1.03%Ca	Fe
Silicon	FeSi	0.4%C	-	71.2%Si	Fe
Vanadiun	FeV	0.15%C	81.6%V	1.9%Al	-

3.4. Melting and casting

Melting was accomplished in a medium frequency induction furnace open to the atmosphere and with a capacity of about 50kg of iron, lined with a magnesia crucible. The melting procedure was to melt some of the material and add the manganese, silicon and chromium in that order. A sample taken from the melt was analyzed on an emission spectrometer, and any required additions were then made to achieve the target composition. After further analyses, and when the composition was correct, the temperature was measured with a disposable-tip immersion thermocouple, and was then adjusted to about 120 °C above the liquidus of the corresponding C-Cr-Fe alloy, and the melt was tapped into a pre-heated insulated magnesia lined hand ladle and poured into the mould.

The small variation in melting procedure was on the ductile irons, where treatment with the inoculant MgFeSi, to introduce graphite nodularity, was carried out in the ladle before pouring into the mould. In addition, inoculants were also added to the metal stream during pouring from the furnace to the ladle to improve the nodule count. Provisions were made to the base iron chemistry for silicon pick-up due to both inoculation and addition of MgFeSi. Table 3.2 summarises the targeted compositions of the different alloys produced.

Table 3.2. Target compositions for the experimental alloys.

Material	Elements (wt%)									
	C	Si	Mn	Cr	Cu	Mo	Mg	S	P	Fe
Carbidic Nodular Iron	3.0-3.6	1.5-2.3	0.3 max	1.0 max	0.8 max	0.4 max	0.02-0.05	0.03	0.02	Balance
High chrome white cast iron	2 – 3.1	0.8 max	1.0 max	12 - 14	-	0.4 max	-	0.02	0.03	Balance

3.5. Casting knockout and fettling

The castings were removed from the mould after being allowed to cool on their trees on a sand floor. When cool, the runners and risers were removed by nicking with an angle grinder. The remains of the feeding system were merely rounded off, and flash removed by light grinding. Before proceeding with any tests, it was deemed critical to ascertain the integrity of the cast balls. Several balls were sectioned in the middle and visually examined for casting defects, including shrinkage porosity; see Figure 3.6(a). No shrinkage porosity was observed, confirming the adequacy of the feeding system used; see Figure 3.6(b). No non-destructive testing (NDT) such as die penetrant was carried out on the grinding balls.

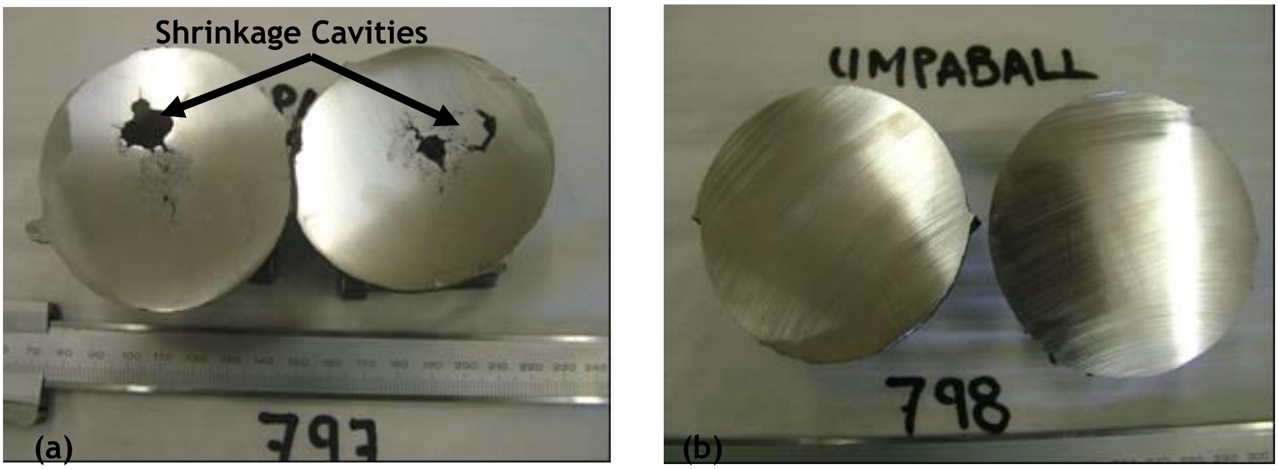

Figure 3.6. ***(a)*** *Cross-section of an as cast ball showing shrinkage cavities* ***(b)*** *cross-section of balls with a modified feeding systems showing no defects.*

3.6. Heat Treatment

The heat treatments of the high chromium white cast iron and carbidic nodular iron balls were carried out separately. The HCWCI balls were heat treated to produce a martensitic matrix whilst the carbidic balls were austempered to produce carbidic austempered nodular iron. The plates were heat treated similar to the grinding balls and used for wear testing. The heat treatment schedule of the alloys is described in Sections 3.6.1 and 3.6.2.

3.6.1. High Chrome White Iron

To achieve a microstructures with different amounts of retained austenite, each cast grinding ball was heat treated at temperatures of 875 °C, 925 °C, 1000 °C, 1050 °C and 1100 °C then air-quenched. To study the effect of tempering temperature on the amount of retained austenite, some of the grinding balls were tempered at temperatures of 350 °C and 450 °C for four hours and air cooled. The heat treatment schedule is shown in Figure 3.7 and Table 3.3.

The conventional heat treatment of high chrome white cast iron balls typically involves a high temperature (~1000 °C to 1100 °C) austenite destabilisation process followed by air quenching and tempering in the region of 350 °C to 550 °C [84]. The high temperature process is meant to destabilise the supersaturated austenite (formed after casting) through secondary carbide precipitation, mainly Cr carbides. This has the net effect of decreasing the amount of carbon dissolved in the austenite and thus rendering it susceptible to transforming to martensite on rapid cooling (through raising its martensite start temperature, M_s) [85].

Unfortunately, in this work no dilatometry tests were performed in order to produce the time temperature transformation (TTT) and a continuous cooling transformation (CCT) phase diagram for the two alloys.

The high chrome white cast iron grinding balls and wear plates were heat treated in an electric resistance furnace (Lenton High) with no protective atmosphere. Fast cooling rates (such as water) were avoided, because the casting can develop cracks due to high thermal or transformation stresses. Therefore, in this work only forced air quenching was applied for cooling. To determine the cooling rate of high chromium white cast iron, one ball was heated to a temperature of 875 °C for 3 hours followed by forced air cooling. The rate of cooling during the forced air quench was determined using a thermocouple inserted in a hole that had been drilled to the centre of one of the balls. This resulted in a cooling rate of approximately 2 °C/s at the centre of the ball. This cooling rate was then assumed to be the same for other alloys subjected to a similarly forced air quench.

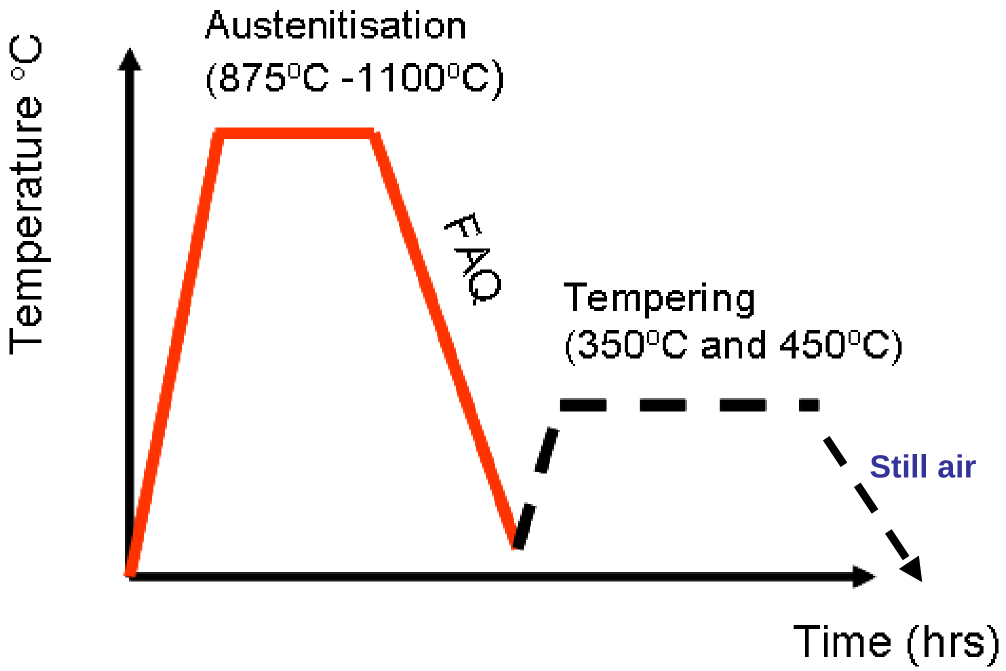

Figure 3.7. Schematic representation of the heat-treatment schedule used for the high chrome white cast iron.

Table 3.3. Heat treatment schedule of the HCWCI grinding balls.

Sample number	Austenitising temperature °C	Cooling	Tempering temperature °C	Cooling
Ball A1	875	**Forced air quench (FAQ)**	none	FAQ
Ball A2	875		350	Still air
Ball A3	875		450	Still air
Ball B1	925		none	FAQ
Ball B2	925		350	Still air
Ball B3	925		450	Still air
Ball C1	1000		none	FAQ
Ball C2	1000		350	Still air
Ball C3	1000		450	Still air
Ball D1	1050		none	FAQ
Ball D2	1050		350	Still air
Ball D3	1050		450	Still air
Ball E1	1100		none	FAQ
Ball E2	1100		350	Still air
Ball E3	1100		450	Still air

3.6.2. Carbidic Nodular Irons

Carbidic nodular iron (CNI) balls and wear plates were scheduled for austempering heat treatments to carbidic austempered nodular iron (CANI). The 70 mm diameter grinding balls and 25 mm x 75 mm wear plates were austenitized for 2 hours at 900 °C prior to austempering at selected temperatures as shown in Figure 3.8, a schematic diagram of the heat treatment cycle used to achieve CANI balls. Austempering was done in a salt bath at temperatures of 275 °C, 320 °C, 350 °C, 375 °C and 400 °C to yield different amounts of retained austenite. The austempered grinding balls were labelled 1 to 6. The austempering salt used was AS140 with working temperature of 150 °C to 550 °C (made of 50% KNO_3 + 40%$NaNO_2$ + 10%$NaNO_3$) [86]. It was sourced from the company Dureferrit. The austempering salt bath is shown in Figure 3.9. This involved austenitising at 900 °C for 2 hours followed directly by austempering in the temperature range 275 °C to 400 °C for 1 hour before cooling in still air. The heat treatment schedule is also shown in Table 3.4.

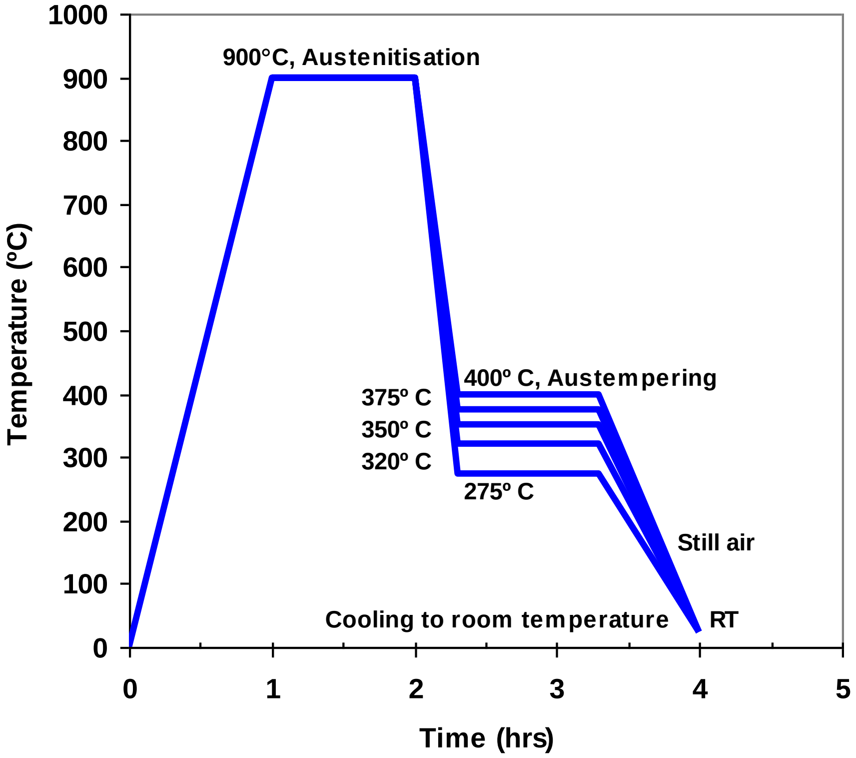

Figure 3.8. A schematic representation showing the austempering heat-treatment cycle for CANI alloys.

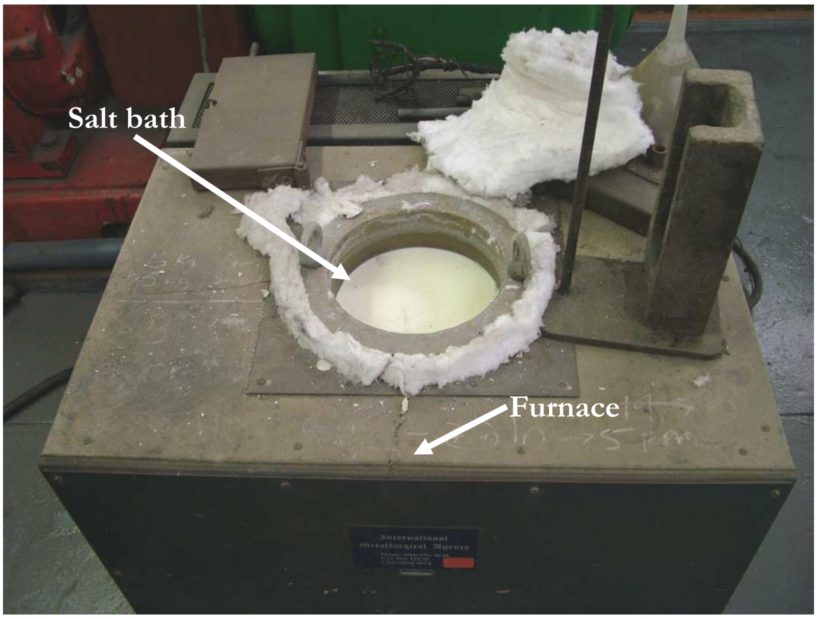

Figure 3.9. The austempering salt bath.

Table 3.4. Heat treatment schedule of the CANI grinding balls.

Sample number	Austenitising temperature °C	Austempering temperature °C
Ball 1	As cast	None
Ball 2	900	275
Ball 3	900	300
Ball 4	900	350
Ball 5	900	375
Ball 6	900	400

3.7. Measurement of Retained Austenite

The traditional heat treatment of high chrome white cast iron can result in a martensitic matrix containing over 20% retained austenite which cannot be distinguished by optical microscopy, hence X-Ray Diffractometry was used. X-ray diffraction analyses were performed on the samples removed from the *surface* and at the *centre* of the grinding balls to determine the volume percentage of retained austenite using a Siemens D500 Diffractometer fitted with a molybdenum tube, using software developed according to the ASTM E915 [87] and SAE J784a standards [88].

The Advanced Materials Division at Mintek obtained a new **LynxEye Detector** for the Bruker D8 X-ray Diffractometer. Samples that were analysed on the **old point detector** were re-analysed on the new LynxEye detector.

The amount of noise in the background was also greatly reduced, which allowed for a much better calculation of phases by Rietveld refinement [89]. Previously, with the scans obtained by the point detector it was not possible to obtain a good Rietveld Refinement and so a calculation was done based on the calculation contained in ASTM Standard E975-03 which details how to calculate the percentage of austenite from the intensity measured in the peaks of the two phases [89]. The standard is directly applicable to scans that are obtained from a molybdenum source, and since the Bruker D8 XRD installed at Mintek has a cobalt source it was not directly applicable and a large amount of mathematical determination were required to get the correct values to be used in the calculations.

The samples which had dimensions of 15 mm long by 8 mm width and 5 mm thick that were analysed on the old Siemens XRD, which was operated with a molybdenum source, and so had retained austenite calculations done according to ASTM Standard E975-00, *were rescanned on the Bruker D8 XRD and the calculations were done by Rietveld Refinement.*

Retained austenite measurement is important for grinding ball evaluations as the amount of retained austenite may vary with cooling rate as one goes deeper into the ball. The samples were cut by a water cooled Secotom-10 cut-off machine from the investigated materials. The samples underwent the usual metallographic polishing in different stages on abrasive papers of progressively finer grits. These were lightly electro-polished in a 20% perchloric acid solution (i.e. 20 ml perchloric acid + 80 ml alcohol), at 18 volts for 2 minutes to remove any material possibly suffering from deformation due to the polishing action. The relative intensities of X-rays diffraction peaks from (200) and (220) planes of ferrite, and those from (220) and (311) planes of austenite were measured. The relative phase amounts (weight %) was estimated using the Rietveld Refinement method. The carbide morphology and quantity data (determined by metallography) were used to ensure accurate retained austenite (RA) peak identification to avoid erroneous overestimation.

Changes in the volume fraction of austenite retained during austempering of carbidic nodular iron at various temperatures were also determined by the X-ray diffraction technique. The Rietveld method is rather practical for quantifying the amounts of each phase and offers the additional advantage of providing information about the crystallographic properties of the phases at the same time. Therefore, in this work this method was preferred to neutron diffraction and EBSD techniques. Special communication with Sir Harry Bhadeshia, (FRS, FREng, FNAE), TATA Steel Professor of Metallurgy at the University of Cambridge confirmed that the best method to measure retained austenite would be the X-ray diffraction technique.

3.8. Hardness Tests

To determine the influence of retained austenite on the hardness, the heat treated grinding balls were sectioned to produce half diameter slabs upon which surface to centre hardness traverses were made using Brinell hardness test equipment. Macro and micro hardness measurements were performed on the as-cast and heat treated materials to study the influence of heat treatment on the resultant microstructures. A Shimadzu micro hardness test machine was used to measure the hardness of the matrix and carbides of the high chromium white cast iron and the carbidic austempered nodular iron.

3.9. Abrasion Wear Tests

3.9.1. Pin-on-belt abrasion test (high stress)

A pin-on-belt (POB) test as shown in Figures 3.10 and 3.11 was carried out to investigate the influence of retained austenite on high stress two-body abrasive wear behaviour of the materials [90]. The test was also used to evaluate the relative performance of the selected experimental alloys when subjected to high-stress two-body abrasion conditions.

Different types of abrasive materials, which include Al_2O_3 and garnet abrasive paper and silicon carbide, are commonly used [50]. However, for this project only silicon carbide of different grit sizes was used. This test includes abrading a dead loaded specimen 10mm by 10mm by 20mm in length against the surface of a bonded abrasive belt. The pins cut from the balls were used in the later POB [90].

The continuous belt ran horizontally at a constant velocity while the specimen was made to transverse normal to the direction of the belt movement. Thus the specimen abraded against unworn particles at all times. Prior to testing, the specimen surfaces were run in by abrading for a distance of 10m on fresh abrasive cloth. The specimens were then reweighed to an accuracy of 0.001g and abraded for a distance of 10m. The actual conditions which were employed for testing are shown in Table 3.5.

The loss in weight was converted to volume loss and the wear resistance was calculated relative to mild steel by using the reciprocal of volume loss, i.e. **wear resistance = volume loss of mild steel/volume loss of specimen**. In this way the relative abrasion resistance (RAR) of the materials could be compared. The density of the material used was sourced from the literature and was not measured [90].

Table 3.5. The actual conditions which were employed for testing are shown below [90].

Load	3.5kg
Stress	0.34 MPa
Length of abrasion path	10m
Type of abrasive	Silicon carbide
Velocity of the belt	0.28 m/s
Environment	Normal laboratory condition
Grit size	120 and 180

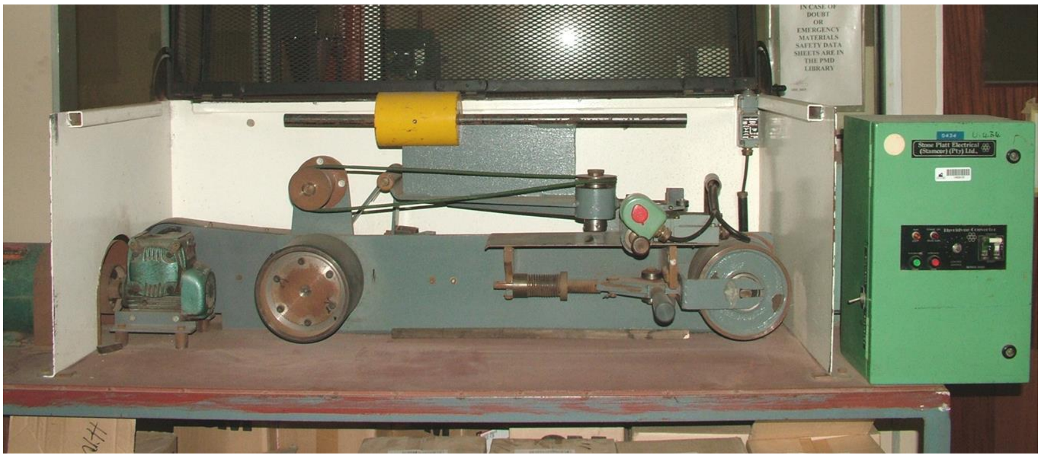

Figure 3.10. The Pin-on-belt (POB) test machine [90].

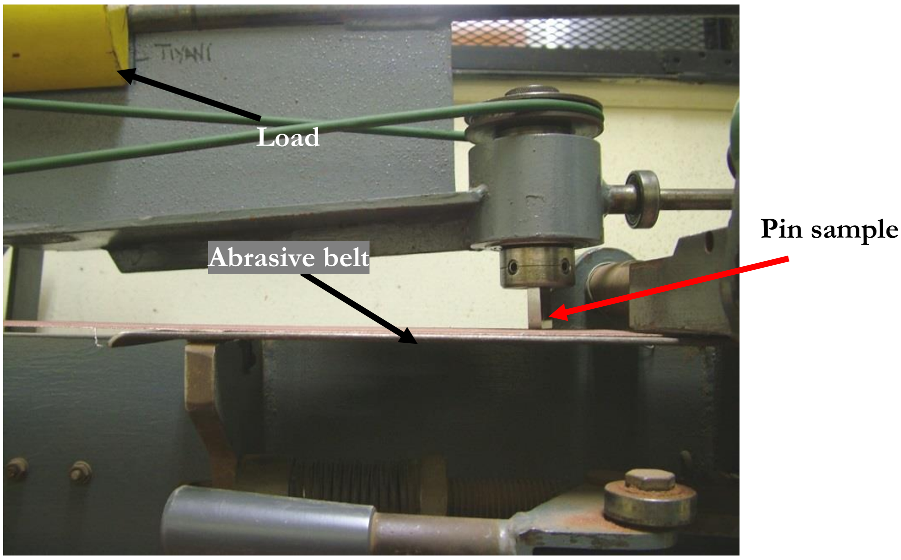

Figure 3.11. A close up view of the pin-on-belt test machine [90].

The 15 mm pins were cut from the balls near the surface and were used in the later POB tests. The %RA were measured on the end taken from the surface of the ball. Following pin abrasion testing of HCWCI and CANI, the worn surfaces were examined by X-ray diffraction again to measure the possibility of retained austenite having transformed to martensite. The worn surfaces were also examined by scanning electron microscopy (SEM) to study the mechanism of wear experienced by the materials.

3.9.2. Rubber wheel abrasion test (low stress)

The dry rubber wheel abrasion test (DRWAT) as described in ASTM Standard G65-85 (see Figures 3.12 and 3.13), Standard Practice for conducting dry sand/rubber wheel abrasion tests, was used to investigate the influence of retained austenite on low stress abrasive wear behaviour of the materials under three-body conditions [91]. This test method covers laboratory procedures for determining the resistance of metallic materials to scratching abrasion by means of the dry sand/rubber wheel test. It is the intent of this test method to produce data that will reproducibly rank materials in their resistance to scratching abrasion under a specified set of conditions.

Abrasion test results are reported as volume loss in cubic millimeters for the particular test procedure specified. Materials of higher abrasion resistance will have a lower volume loss. This test method covers five recommended procedures which are appropriate for specific degrees of wear resistance or thicknesses of the test material. For this project only two procedures were used, A and B.

Procedure A - This is a relatively severe test which ranks metallic materials on a wide volume loss scale from low to extreme abrasion resistance. It is particularly useful in ranking materials of medium to extreme abrasion resistance. ***AISI D2*** *Tool Steel hardened to 58.8 – 60.5 HRC is used as a reference material No. 1 and will give a volume loss range 36 ±5mm*^{3}.

Procedure B - A short-term variation of Procedure A. It is used for highly abrasive resistant materials but is particularly useful in the ranking of medium and low- abrasive-resistant materials. Procedure B should be used when the volume loss values developed by Procedure A exceed 100 mm^3. ***AISI H13*** *Tool Steel hardened to 47 – 48 HRC is used as reference material No. 2 and will give a volume loss range 56 ±4mm*^{3}. ***SAE 4340*** *alloy steel hardened to 31 – 33 HRC is used as a reference material N0. 3 and will give a volume loss range 91 ±4mm*^{3}.

Specimen size - a rectangular shape 25 mm by 76 mm and between 3.2 mm and 12.7 mm thick. The test surface was flat within 0.125 mm maximum and this was measured with a digital caliper. According to the standard the test specimen must be smooth, flat, and free of scale with finely milled or milled surfaces. A ground surface of 0.8μm or less is acceptable. The samples tested in this work had a surface finish of approximately 6μm.

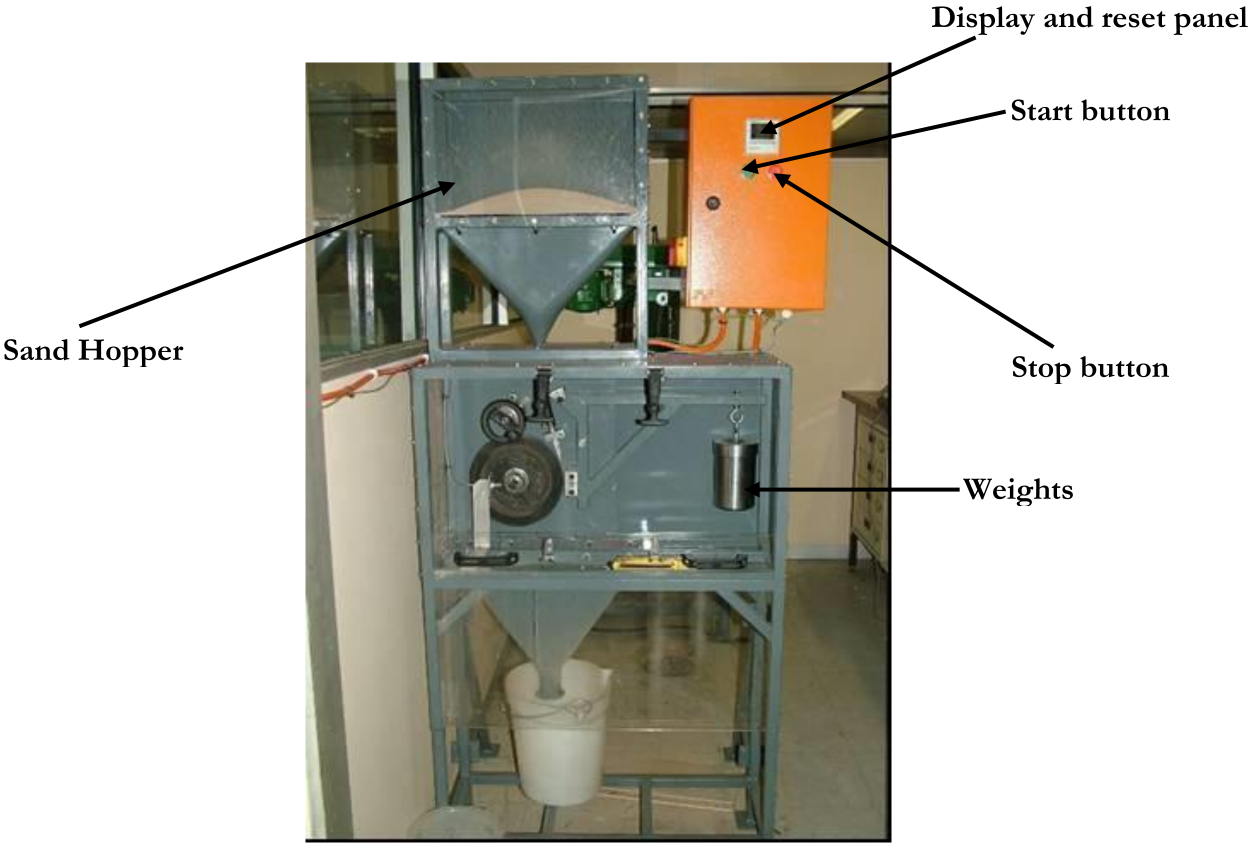

Figure 3.12. The dry rubber wheel abrasion test machine.

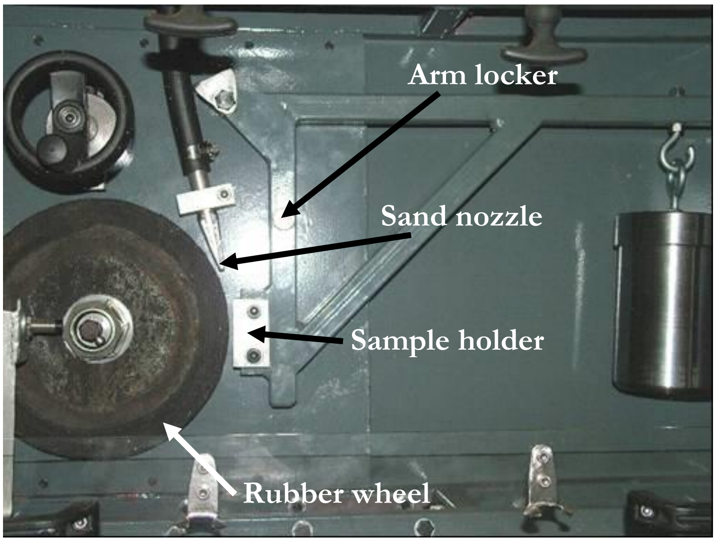

Figure 3.13. A close up view of dry rubber wheel abrasion test machine.

The nozzle was opened so that it produces a sand flow rate of 300 to 400 g/min. According to the ASTM G65 [91] specification the type of abrasive shall be rounded quartz grain sand as typified by AFS 50/70 Test Sand. Unfortunately, due to the shortage of this particular sand, this test was considered to be only comparative. A locally available 212μm to 300μm angular silica sand deemed appropriate, see Figure 3.14.

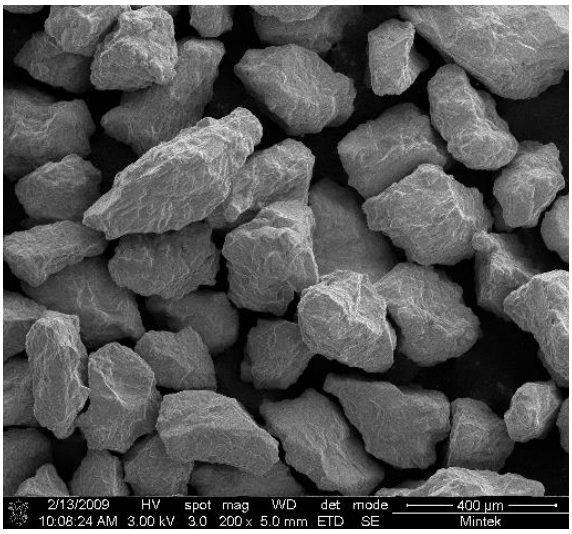

Figure 3.14. A SEM-secondary mode micrograph of the angular silica sand particles used for the wear test.

During use, the nozzle opening was positioned as close to the junction of the test specimen and the chlorobutyl rubber wheel as the design would allow (see Figure 3.13). The time of the test was about 30 minutes for Procedure A and 10 minutes for Procedure B, depending upon the actual wheel speed.

In all cases the number of wheel revolutions and not the time was used as the controlling parameter. Table 3.6 shows all significant test parameters that were taken into consideration when performing dry rubber wheel abrasion test.

Table 3.6. Dry Rubber Wheel Abrasion Test Parameters

Specified procedure	**Force against specimen (N)**	**Wheel revolutions (rev)**	**Sand flow (g/min)**	**Specimen size (mm)**			**Linear distance (m)**
A	130	6000	300 - 400	25 width	76 length	3.2 - 12.7 thick	4309
B	130	2000	300 - 400	25 width	76 length	3.2 - 12.7 thick	1436

The specimens were cleaned, dried and weighed to the nearest 0.001g prior to the testing to find the initial mass. These were then securely seated in the sample holder, weights added to the lever arm to develop a proper contact force (130N) pressing the specimen against the wheel. When the test had run the desired number of wheel revolutions, the specimen was lifted away from the wheel and the rotation of the wheel stopped. The specimen was carefully removed from the holder and reweighed.

The abrasion test results were reported as volume loss in cubic millimeters in accordance with the specified procedure used in the test. The mass loss was converted to volume loss using the formula shown below and density of ASTM A532 Class III Type A, (**7.6g**/cm^3). The surface morphologies of the worn surface of the composites were studied in a scanning electron microscope.

Volume loss (mm^3) = (Mass Loss (g)/Density (g/cm^3)) x 1000……….Equation 3.1

Since the mass for all specimens before testing was not exactly the same it was decided that the results be presented as percentage mass loss in order to make comparisons (*Mass Loss = ((Original Mass - Final Mass)/Original Mass)) x 100.*

3.9.3. Ball mill testing

High chromium white cast and carbidic austempered nodular iron grinding balls subjected to different heat treatments, hence with different amounts of retained austenite, were tested in a ball mill to study their behaviour when subjected to a combined impact and abrasive wear. Prior to ball milling tests each ball was marked for identification purposes. A spark eroder (electro discharge machining, EDM) was used to mark each set of the balls. The identification marks were about 10mm deep and were similar in size.

This technique [92] is commonly used to mark grinding balls because it does not transform the microstructure, and also does not induce significant stress compared with mechanical drilling. A small-scale ball mill shown in Figures 3.15 and 3.16, with a diameter of 600 mm and barrel length of 600 mm was used for the test. The material charged into the mill consisted of grinding balls and UG2 ore (-6mm size fraction) for these 70mm diameter balls [92]. For this project UG2 ore was used because the high chromium white cast iron balls are commonly used in the platinum mining industry. During the tests ore was charged through the hopper at a feed rate of about 300g per minute using a vibrating feed mechanism. The water feed was regulated by a flow meter to achieve a pulp density of about 75%. The mill speed was monitored and kept at 46 rpm (i.e. ~82% of the critical speed).

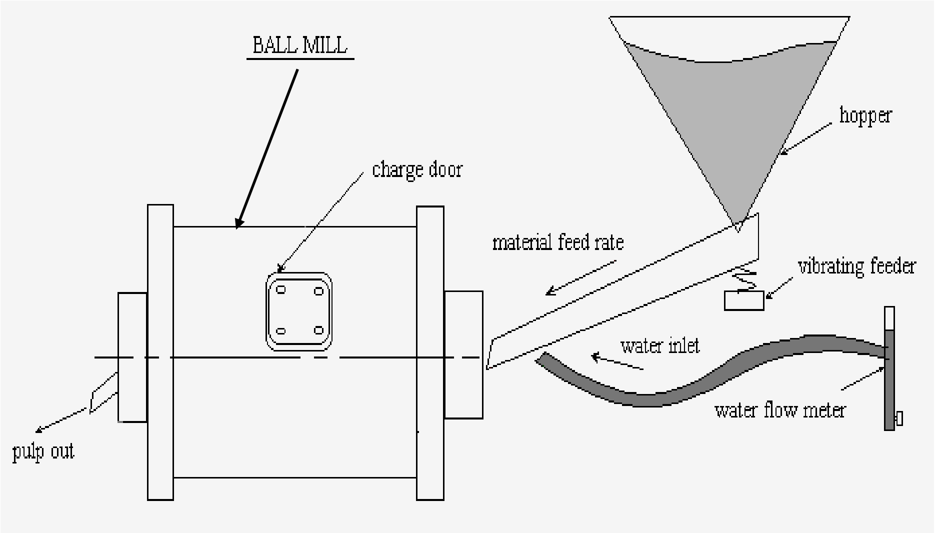

Figure 3.15. The experimental ball mill – schematic.

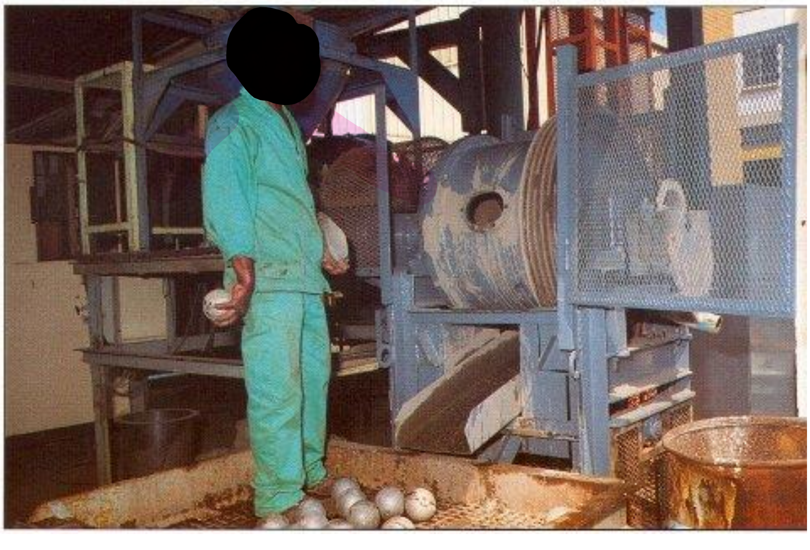

Figure 3.16. The 0.6m x 0.6m experimental ball mill in operation.

Prior to recording the weight losses of the balls as a function of the mill running time, a conditioning run of 20 hours was first performed to remove any adhering scale and surface decarburised layer from the balls. The balls were then tested for five separate 20 hour runs (i.e. for a total of 100 hours, excluding the conditioning). The masses of the balls (ten balls from each set) were measured after each run and the wear rate determined. The wear rates obtained in this type of experimental ball mill cannot be directly converted to predict the wear rates in a full-size mill, however, but are suitable to rank different types of balls. This ranking for abrasion, however, is expected to be the same in an industrial mill [93].

3.10. General Metallurgical Characterisation

3.10.1. Optical metallography

One as-cast and heat treated grinding ball was selected from each set of alloys (i.e. high chrome white cast and carbidic austempered nodular iron) and visually examined for surface and internal defects on the sectioned surfaces. The other half of each of the balls was prepared for metallography. This involved grinding, polishing and etching to study the microstructures, by swabbing the surface, in order to reveal the general microstructure. The etchant does not attack any carbides (white), enabling good contrast between the carbides (primary and secondary carbides) and the remainder of the microstructure. Microstructural investigation was performed on representative samples to study the carbide's morphology and matrix.

The carbide content of the high chromium white cast iron balls was obtained using the empirical relationship according to Maratray [94] for determining the eutectic carbide volume (CV) based on the bulk carbon and chromium composition as shown in Equation 3.2. The lower than eutectic C and Cr levels suggest lower carbide content than predicted for a eutectic composition [94].

$$(\%CV = 12.33(\%C) + 0.55(\%Cr) - 15.2) \text{……………..Equation 3.2}$$

Laird [95] recommends caution in using this empirical relationship according to Maratray [94] because of its limited accuracy while Dupin et al. [96] found variations in the carbide volume between surface and core regions of white iron castings and believed to be due to cooling rate variations [96]. The latter suggests that the prediction of carbide volume is based solely on the bulk chemical composition. The volume fraction is, of course, also governed by the %C and the other carbide forming elements (such as molybdenum (Mo), vanadium (V), boron (B) and others) exceeding their solubility limits.

The Le-Pera tint etchant that combines sodium metabisulfite ($Na_2S_2O_5$) and picric acid was also used. The samples were also etched with Groesbeck a selective carbide etchant in order to identify the carbide type, or any variation in the carbide type which might have been present. These different etching techniques applied in order to characterize the microstructure of the cast iron by light microscopy, are summarized in Table 3.7. To enhance the contrast between the phases, different etchants were used consecutively and different etching methods were combined [97].

Table 3.7. Selective carbide etchant composition and procedure applied [97].

Etchant	Composition	Etching principle
Nital	100 ml ethanol 99%, 3 ml nitric acid 65%	Grain boundary etching
Le-Pera	50 ml $Na_2S_2O_5$ 1% in aqueous dilution, 50 ml picric acid 4% in ethanol	Anodic surface layer etching
Groesbeck	40g/l NaOH, 40g/l $KMnO_4$	Immersion at 20 °C, ~3 min

3.10.2. Scanning Electron Microscopy

To analyse the type of carbides the specimens were examined using a scanning electron microscope (SEM) equipped with an energy dispersive X-ray spectroscopy (EDS) capability. The EDS was used to determine the compositional variations within the microstructure. EDS is not that accurate therefore, electron microprobe analysis (EMPA) was conducted to determine the carbon content in the matrix and in the carbides. The samples were mounted in the Cameca SX 50 Electron Microprobe for analysis of the C, Cr, Mn and Fe content of phases in the samples. Randomly selected points of the phases observed in each sample were analysed. An accelerating voltage of 20 kV and a beam current of 30 nA were used. The system was calibrated using pure reference standards and checked against a reference standard (Cr-16).

Some selected specimens were metallographically prepared for electron backscattered diffraction (EBSD) examination with a final polishing step of 0.5 mm, using an oxide polishing solution (OPS) suspension [98]. The last specimen-preparation step was electrolytic polishing with an electrolyte consisting of 78 ml perchloric acid, 90 ml distilled water.

4. CHAPTER 4: RESULTS

4.1. Effect of Austenitising Treatment

Sections 4.1.1 and 4.1.2 show the results of the retained austenite contents obtained during the heat treatment of the experimental high chromium white cast iron and carbidic austempered nodular iron studied in this project. Various temperatures were selected and used so that they could produce different amounts of retained austenite (γ_{res}) content. The chemical compositions of all the produced grinding balls were within the targeted chemical composition range and are summarized in Table 4.1. The chemical compositions of the commercial alloys that were used as reference were also within the chemical composition range given in Table 4.2.

Table 4.1. Chemical composition for the produced HCWCI grinding balls.

Alloy Tested	**Elements wt%**							
	C	**Si**	**Mn**	**Cr**	**Cu**	**Mo**	**Ni**	**V**
HCWCI *(Experimental)*	2.55	0.91	0.55	12.4	0.12	0.05	0.14	0.07

Table 4.2. Chemical composition for the produced CANI grinding balls.

Alloy Tested	**Elements wt%**								
	C	**Si**	**Mn**	**Cr**	**Cu**	**Mo**	**Ni**	**Mg**	**V**
CANI	3.08	2.24	0.96	0.89	0.78	0.36	0.11	0.043	0.02

The property diagrams of the two alloys studied in this work i.e. HCWCI and CANI, were calculated using the Thermo-Calc^{TM} computer software, see Figures 4.1 and 4.2 respectively. As expected, a higher volume fraction of graphite was predicted in CANI due to the higher Si content and the converse was true for the HCWCI, i.e. higher volume fraction of M_7C_3 and M_3C were predicted at higher and lower temperatures respectively. These Thermo-Calc phase transformation predictions agreed with the observations that were made. It can be seen that as the temperature increased, more carbides dissolved and upon quenching, more carbon was trapped in solid solution. This resulted in more retained austenite after quenching from the austenitisation temperature. After solution treatment and quenching, the carbon re-precipitated during tempering, hence, the decreased and less variation of the carbon content in the matrix.

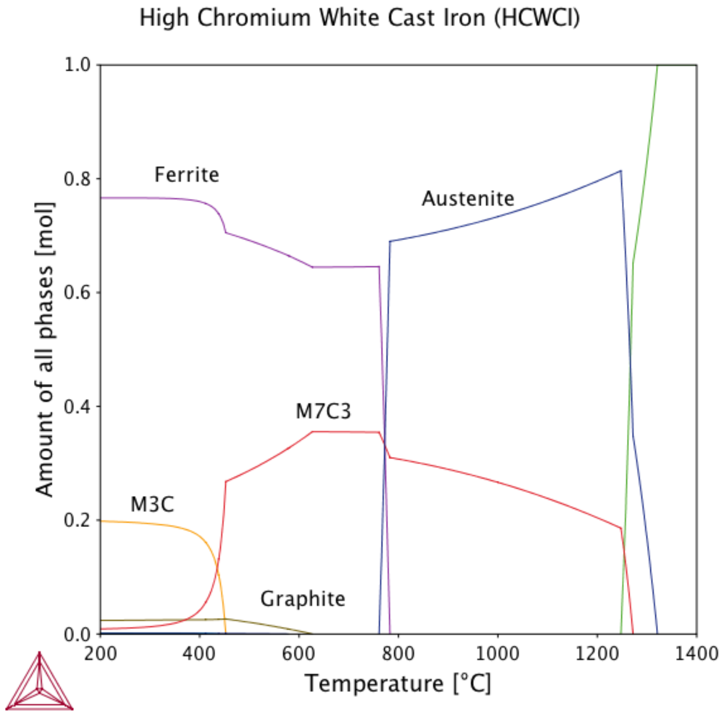

Figure 4.1. Property diagram for the produced 12 %Cr white cast iron showing amounts of phases present at range of temperature, note the decrease in amounts of carbide phases as the temperature increases to dissolution temperature.

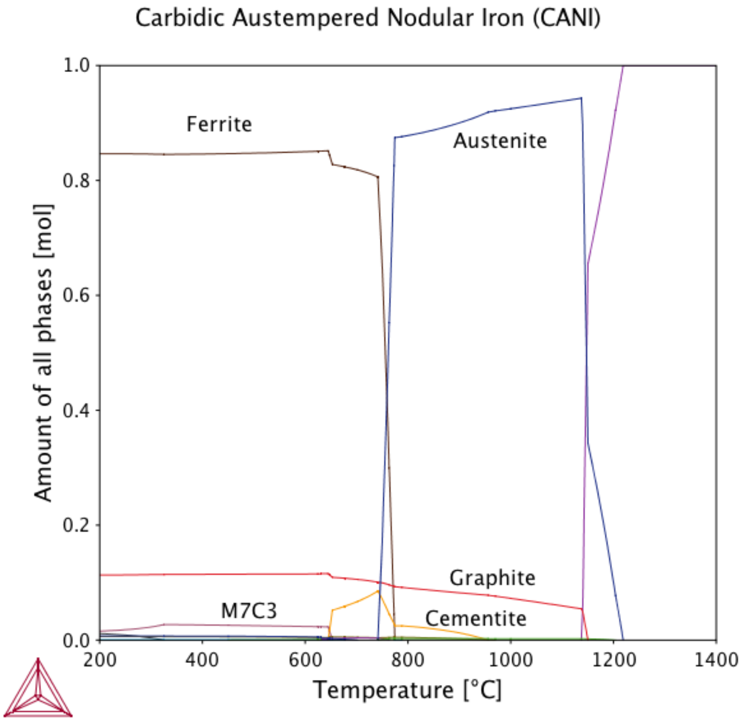

Figure 4.2. Property diagram for the produced CANI with the composition showing phases present at range of temperatures.

4.1.1. XRD Analysis of high chrome white cast iron

X-ray diffraction analyses were performed on the samples removed near the surface of the 70 mm diameter grinding balls to determine the volume percentage of retained austenite. The XRD analysis identified five phases within the as-quenched, first temper and final temper samples, which included ferrite, austenite, M_3C, M_7C_3 and Mo_2C carbides. The amount of retained austenite produced through various heat treatments is summarized in Table 4.3.

Table 4.3. The percentage of retained austenite of HCWCI grinding balls.

Austenitising Temperature °C	**% Retained austenite content**		
	Forced air quenched	**Tempering at 350 °C**	**Tempering at 450 °C**
875	10.6	8.9	6.4
925	9.2	10.6	2.9
1000	32.0	33.2	11.5
1050	40.5	32.2	22.6
1100	57.3	54.9	50.8

The relationship between retained austenite and temperature is also graphically presented in Figure 4.3. It is clear that the percentage of retained austenite increased with an increase in austenitising temperature. A significant increase in the percentage of retained austenite was observed when the specimen was destabilised at higher temperatures such as 1000 °C to 1100 °C.

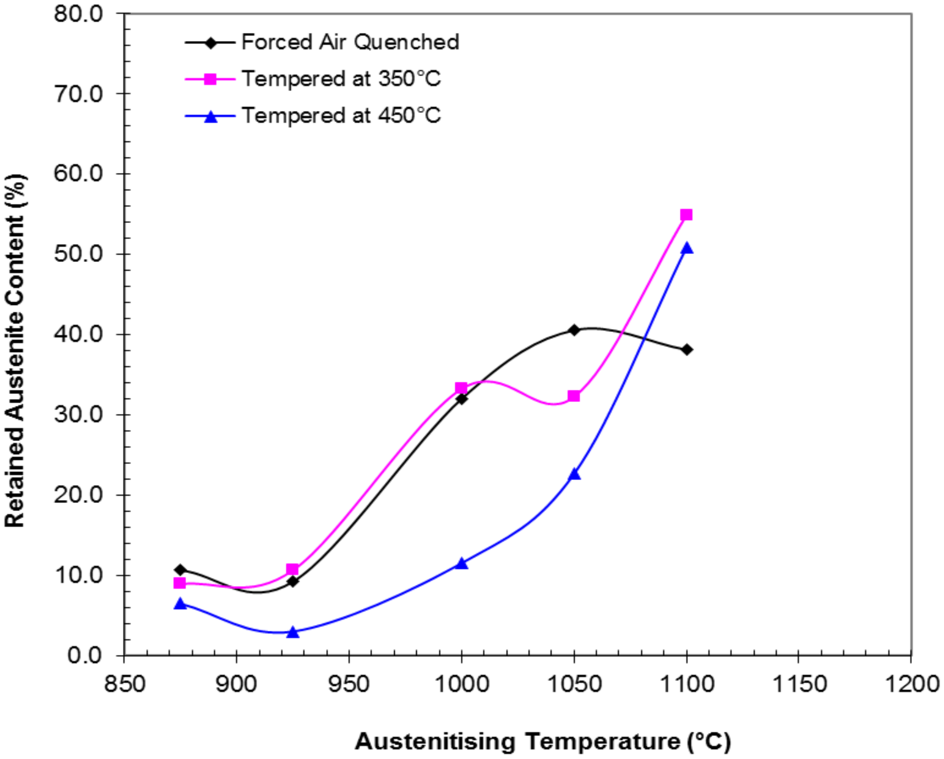

Figure 4.3. The influence of destabilisation and tempering temperature on the retained austenite of HCWCI.

4.1.2. *Carbidic Austempered Nodular Iron (CANI)*

The CANI alloy was austempered at various temperatures to vary the retained austenite content. The XRD analyses identified phases within the as-cast and austempered samples, which included ferrite, austenite, M_3C carbides. The effect of austempering temperature on the amount of retained austenite for the CANI is shown in Table 4.4. The relationship between retained austenite and austempering temperature is also graphically presented in Figure 4.4. As the austempering temperature was raised from 275 °C to 400 °C the amount of retained austenite was found to increase in the matrix from 17% to a maximum of 26% at 350 °C then decreased at higher temperatures, i.e. above 375 °C. In other words, 350 °C was found to be the optimal partitioning temperature where the volume fraction of retained austenite was found to be maximum in this alloy. At low austempering temperatures, an acicular (needle-like) ferritic phase was formed with only a small amount of retained austenite with high hardness. With increased austempering temperatures, the ferrite became coarser with increased amounts of retained austenite; with a typical "ausferrite" structure. This resulted in a substantial reduction in strength and hardness.

Table 4.4. The amounts of % retained austenite of CANI alloy.

Alloy Identity	**Austenitising temperature °C**	**Austempering temperature °C**	**%RA**
CNI_275°C	900	275	17.0
CNI_300°C	900	300	21.8
CNI_350°C	900	350	26.1
CNI_375°C	900	375	16.4
CNI_400°C	900	400	16.6

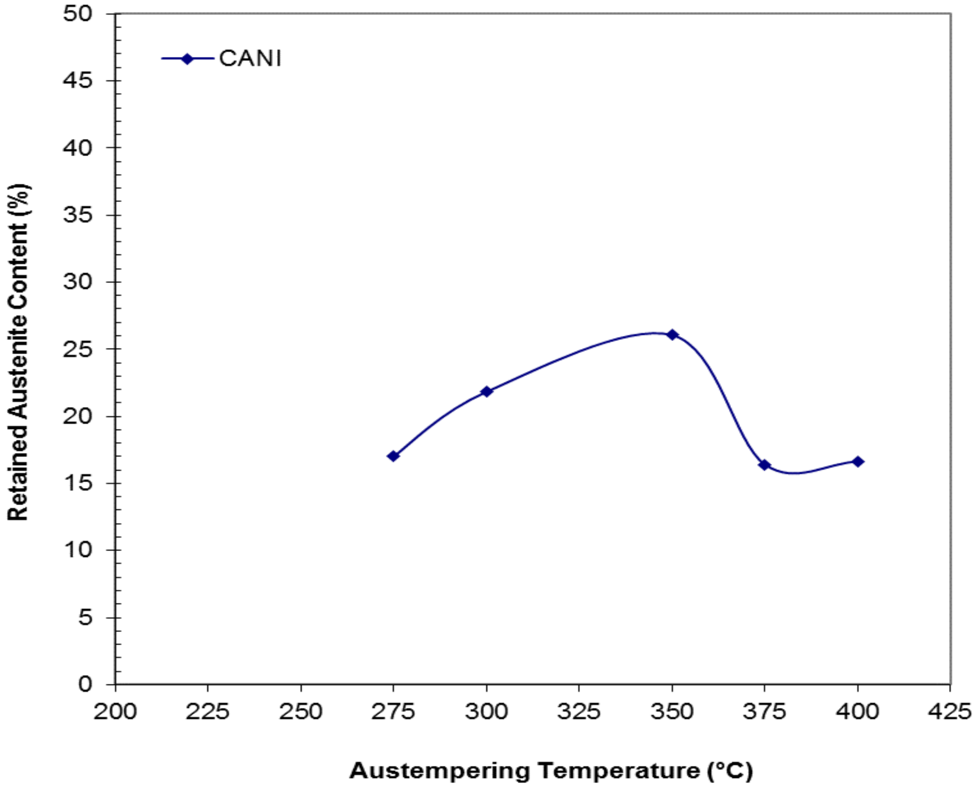

Figure 4.4. The effect of austempering temperature on the % retained austenite in the structure of CANI.

4.2. Effect of destabilisation temperature on the microstructures of HCWCI and CANI alloys

The effect of destabilisation temperature on the microstructures of HCWCI and CANI alloys are presented in Sections 4.2.1 and 4.2.2 respectively.

4.2.1. Microstructures of high chrome white cast iron (HCWCI) after various heat treatments

Figures 4.5 and 4.6 show the microstructures observed in the as-cast balls, forced air quenched from 875 °C, and subsequently tempered at 350 °C and 450 °C. It can be seen that the as-cast microstructures comprised eutectic carbides in a pearlitic matrix.

The as-cast microstructure of the hypoeutectic white cast iron consisted of a primary phase pearlite (i.e. austenite which decomposed) with eutectic phases (austenite and M_7C_3 carbides). Figure 4.6 shows eutectic carbides in an un-tempered martensitic matrix after forced air quenching from 875 °C and eutectic carbides in a tempered martensitic matrix after tempering at 350 °C and 450 °C for 4 hours respectively. The hypoeutectic primary austenite dendrites were surrounded by eutectic M_7C_3 and austenite.

Figures 4.7 to 4.10 show the resultant microstructures of the high chromium balls that were destabilised at 925 °C, 1000 °C, 1050 °C and 1100 °C for 3 hours and forced air quenched. These were then subsequently tempered at 350 °C and 450 °C. When the balls were heated to the high temperatures of 1050 °C to 1100 °C and forced air quenched, the resultant microstructures consisted of eutectic carbides in a matrix of martensite and a significant amount of retained austenite, see Figures 4.9 and 4.10. On tempering at 350 °C and 450 °C, the retained austenite transformed to martensite, see Figures 4.9 and 4.10. The analysis of X-ray diffraction indicates that the microstructure consisted of retained austenite, martensite and eutectic carbides. The retained austenite contents of samples destabilised at temperatures above 1000 °C were high.

The microstructures are changed as the soaking temperature increased, see Figures 4.6 to 4.10. There was less eutectic carbide as the temperature increased due to dissolution and there were an increased in secondary carbides (amounts of white phase within the matrix). The precipitation of secondary M_7C_3 carbides at elevated temperatures reduces the carbon and chromium content in the matrix.

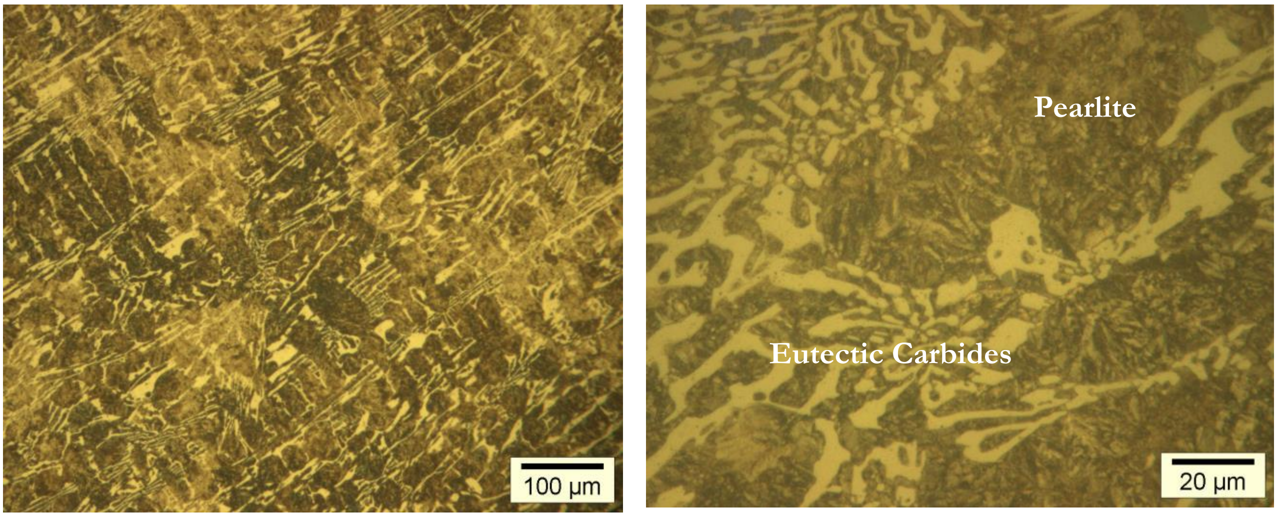

Figure 4.5. Optical micrographs showing microstructure of the as-cast high chromium white iron at low and high magnification showing the eutectic carbide's morphology (white phase) in a pearlitic matrix (etched with 3% Nital).

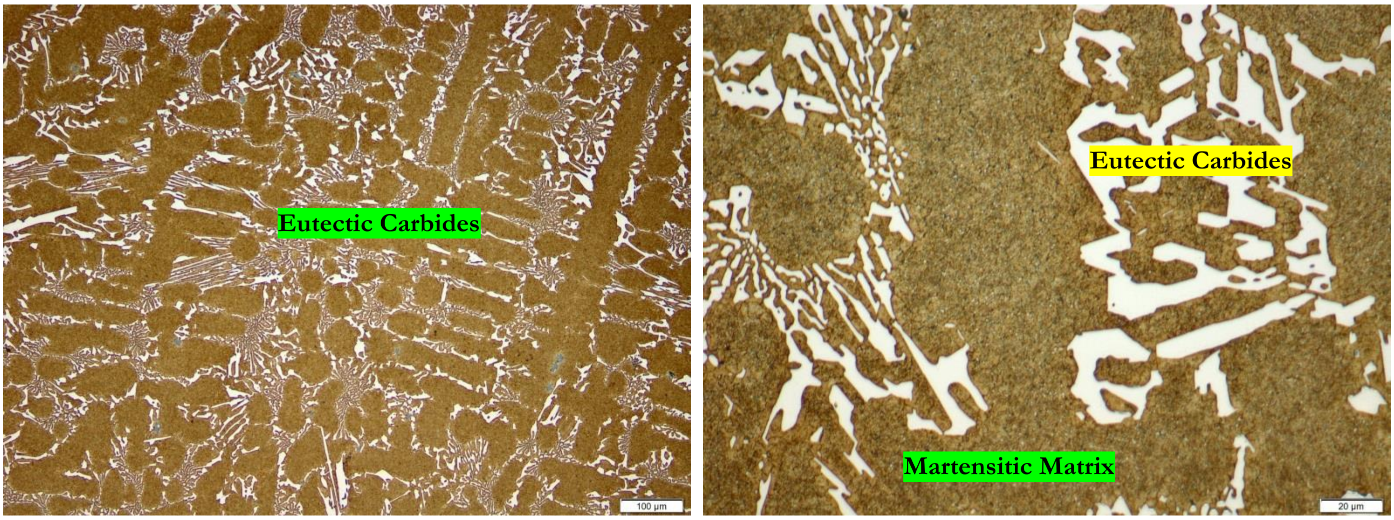

875 °C +FAQ (etched with Le Pera) 10.6 %RA

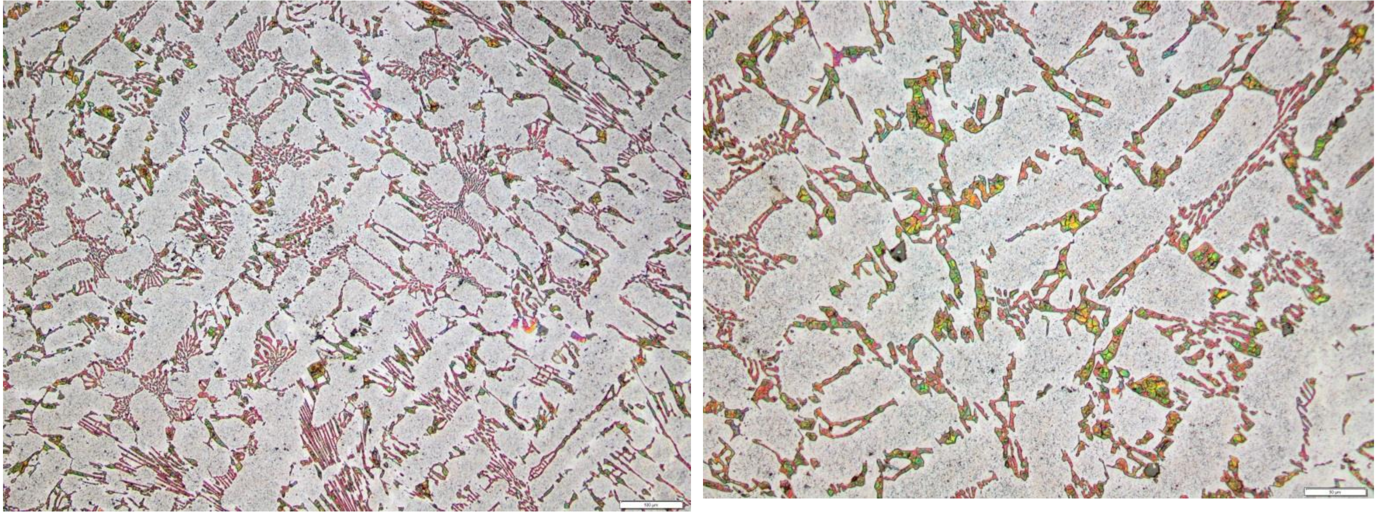

875 °C +FAQ + 350 °C T (etched with Groesbeck) 8.9 %RA

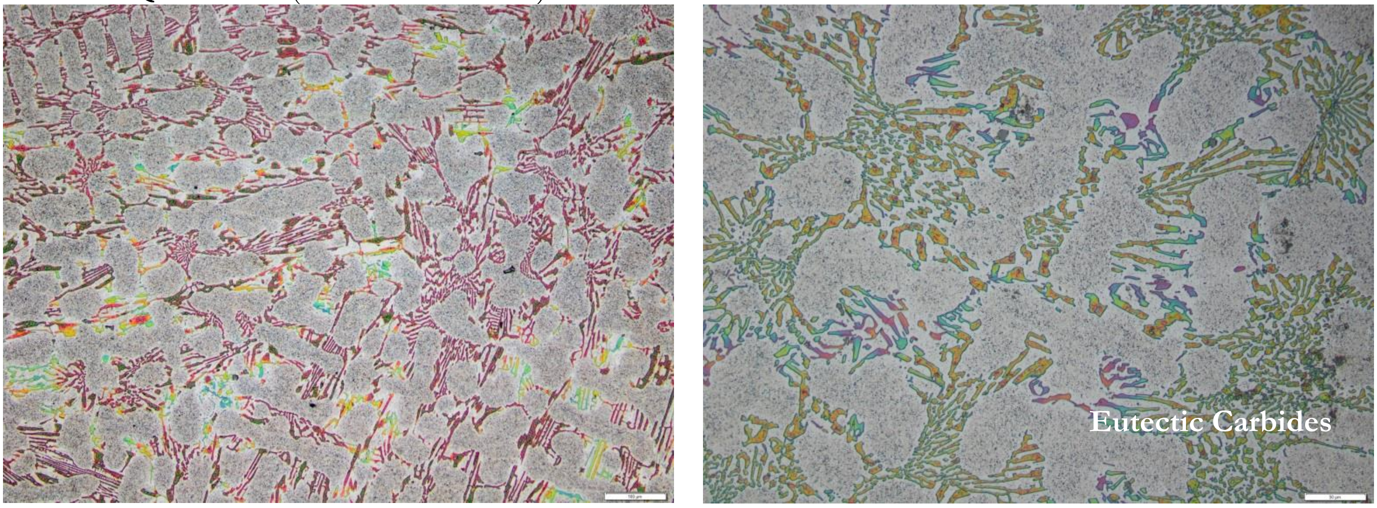

875 °C +FAQ + 450 °C T (etched with Groesbeck) 6.5 %RA

Figure 4.6. Optical micrographs showing microstructure of high chromium white iron showing eutectic carbides in an un-tempered martensitic matrix after forced air quenching from 875 °C and eutectic carbides in a tempered martensitic matrix after tempering at 350 °C and 450 °C for 4 hours, left at low and right at high magnification, (etched with Le-Pera and Groesbeck).

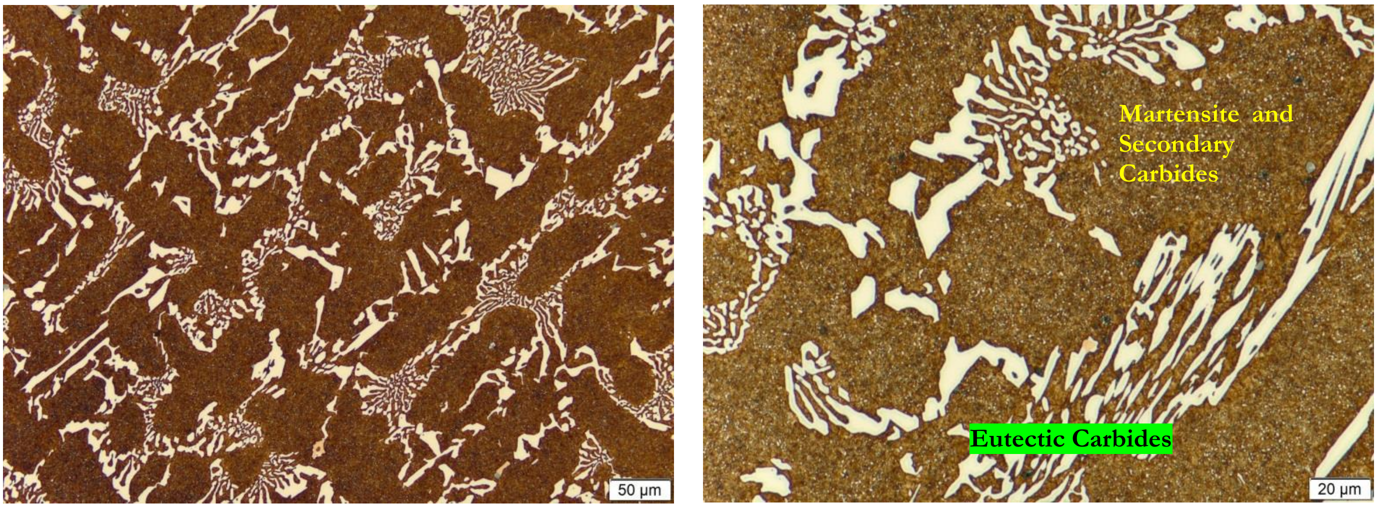

925 °C +FAQ (etched with Le Pera)

9.2 %RA

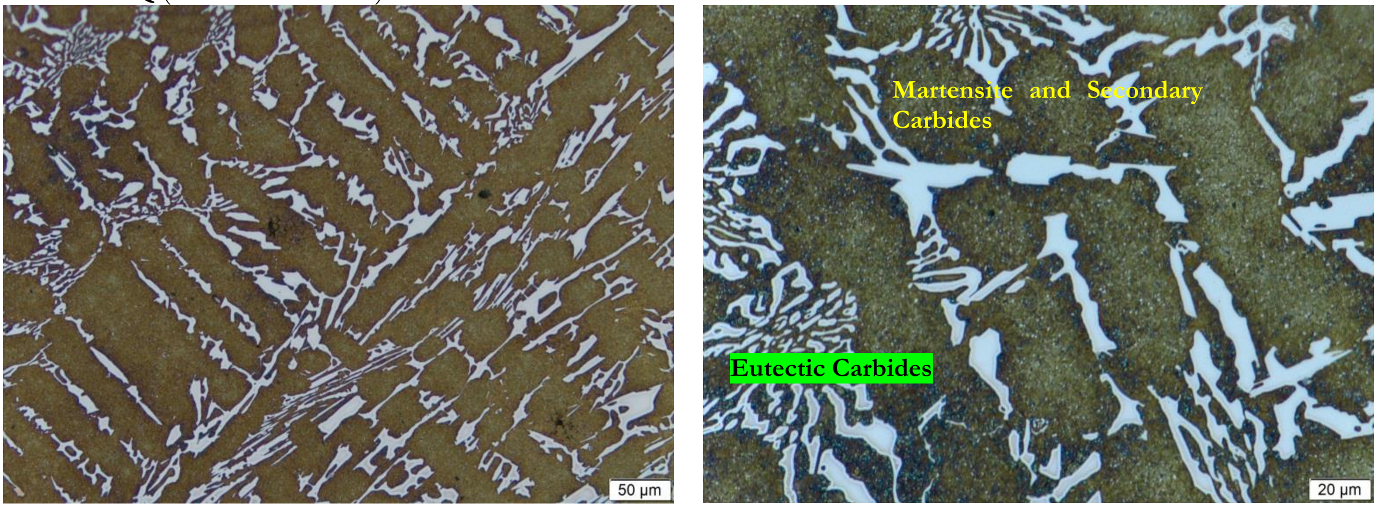

925 °C +FAQ + 350 °C T (etched with Le Pera)

10.6 %RA

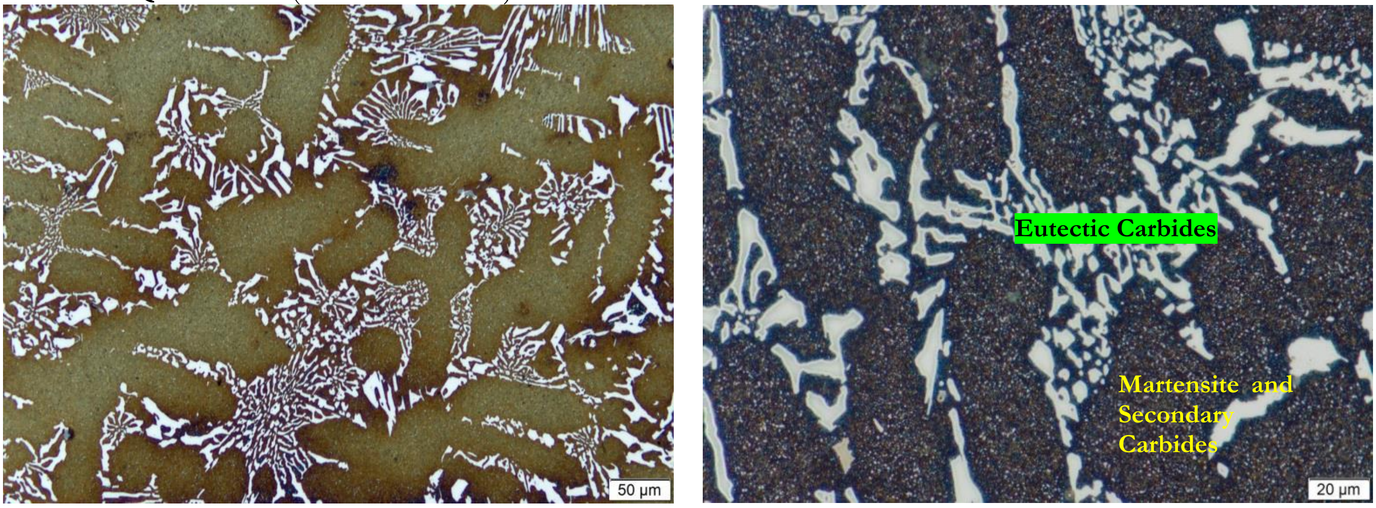

925 °C +FAQ + 450 °C T (etched with Le Pera)

3.0 %RA

Figure 4.7. Optical micrographs showing microstructure of high chromium white iron showing eutectic and secondary carbides (white phases) and retained austenite in an un-tempered martensitic matrix (after forced air quenching at 925 °C). Also eutectic carbides in a tempered martensite matrix, possibly with some residual retained austenite after tempering at 350 °C and 450 °C respectively for 4 hours, left at low and right at high magnification, (etched with Le Pera).

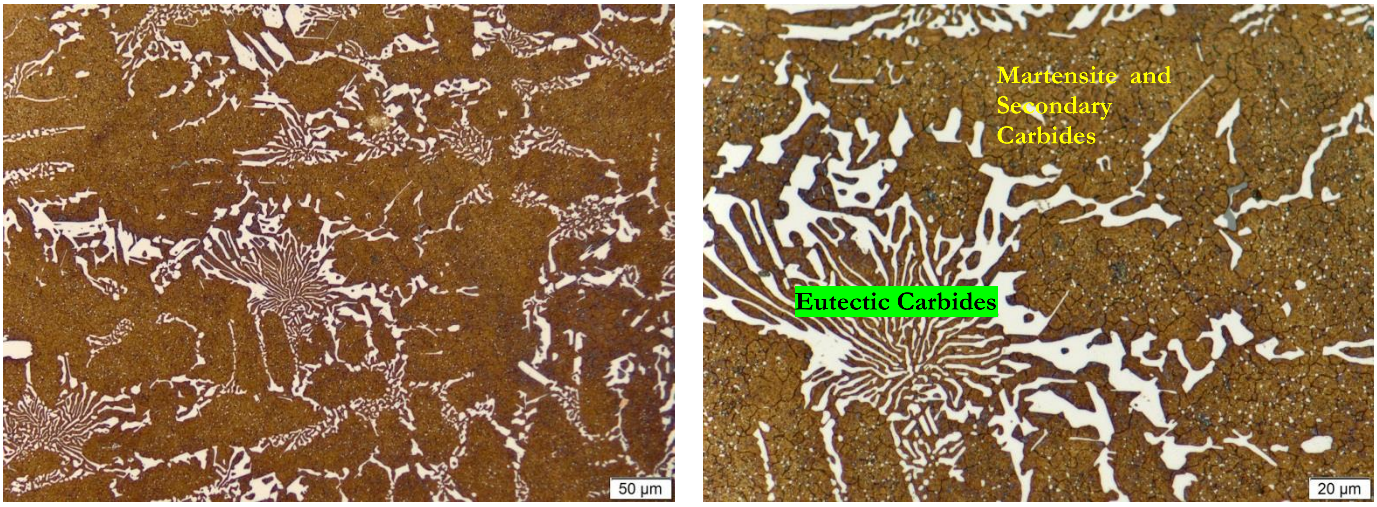

1000°C +FAQ (etched with Le Pera)

32.0 %RA

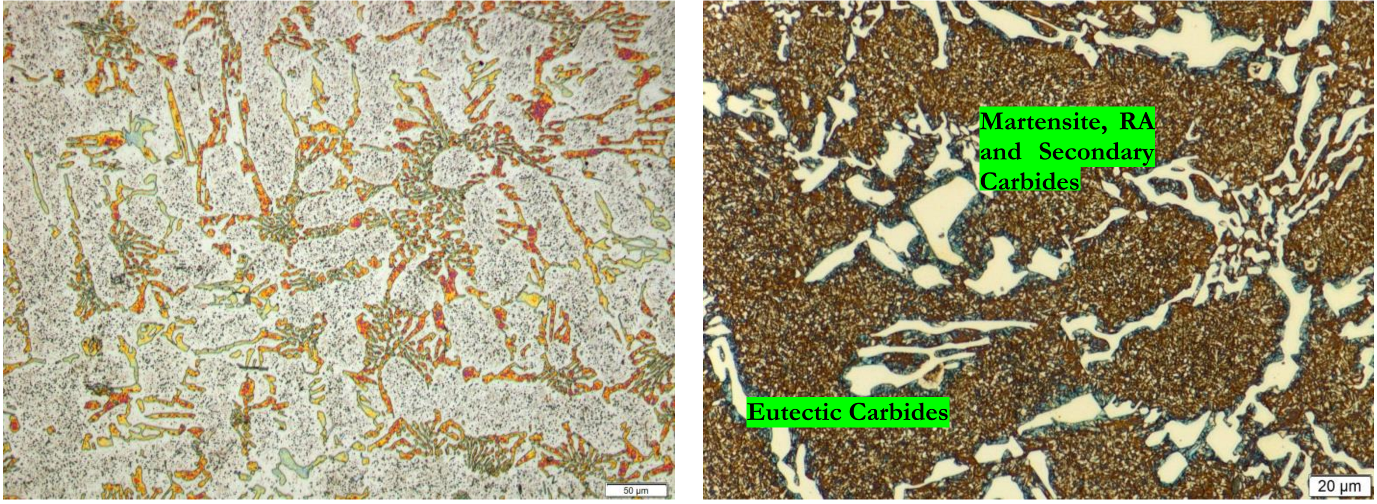

1000°C +FAQ + 350°C T (etched with Le Pera)

33.2 %RA

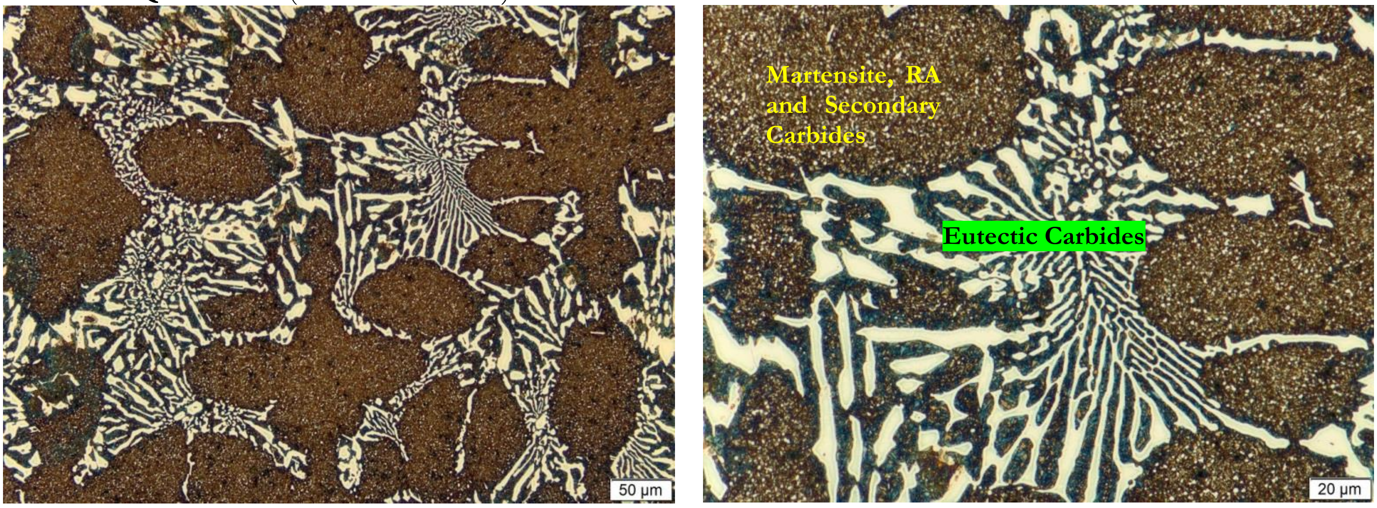

1000 °C +FAQ + 450 °C T (etched with Le Pera)

11.5 %RA

Figure 4.8. Optical micrographs showing microstructure showing eutectic carbides and retained austenite in a matrix of martensite after forced air quenching from 1000 °C. It also shows eutectic and secondary carbides and retained austenite in a tempered martensite after tempering at 350 °C and 450 °C respectively for 4 hours, left at low and right at high magnification, (etched with Le Pera).

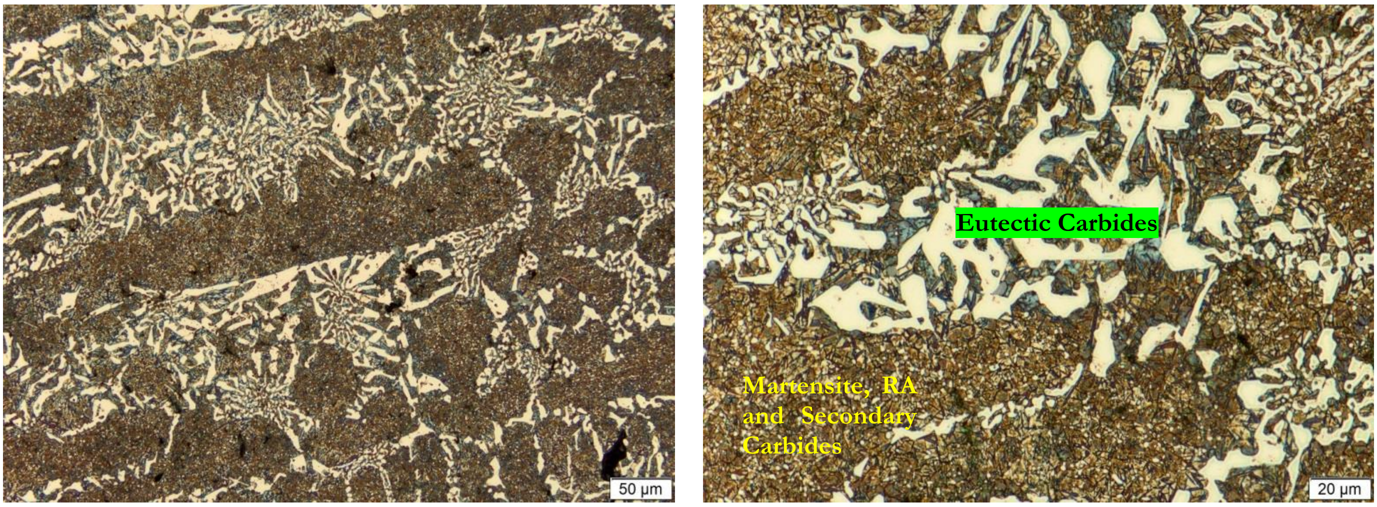

1050 °C +FAQ (etched with Le Pera)

40.5 %RA

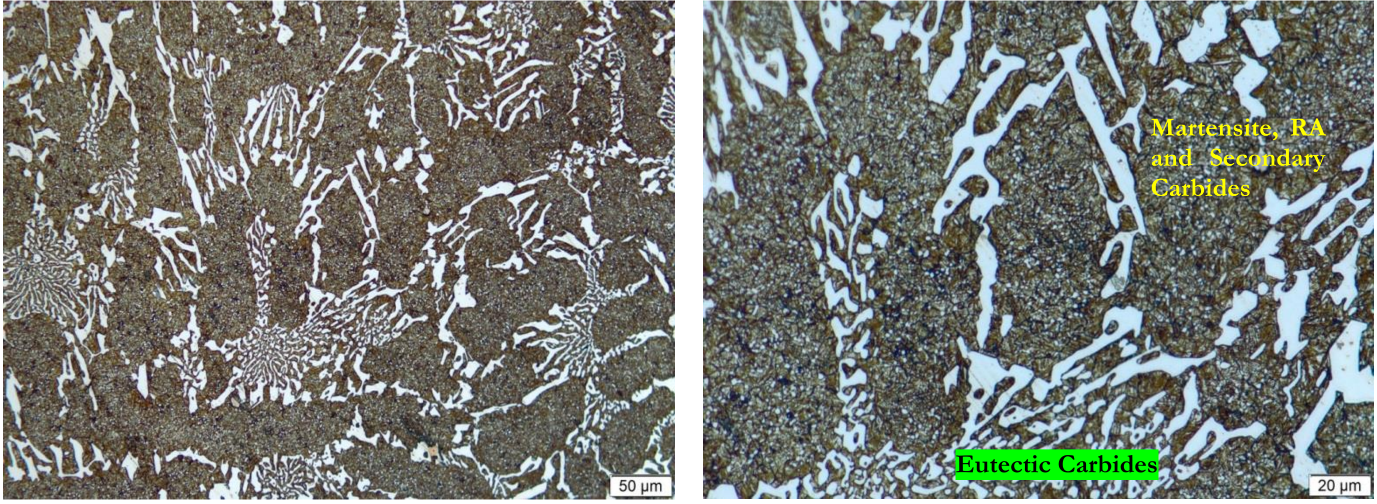

1050 °C +FAQ + 350 °C T (etched with Le Pera)

32.3 %RA

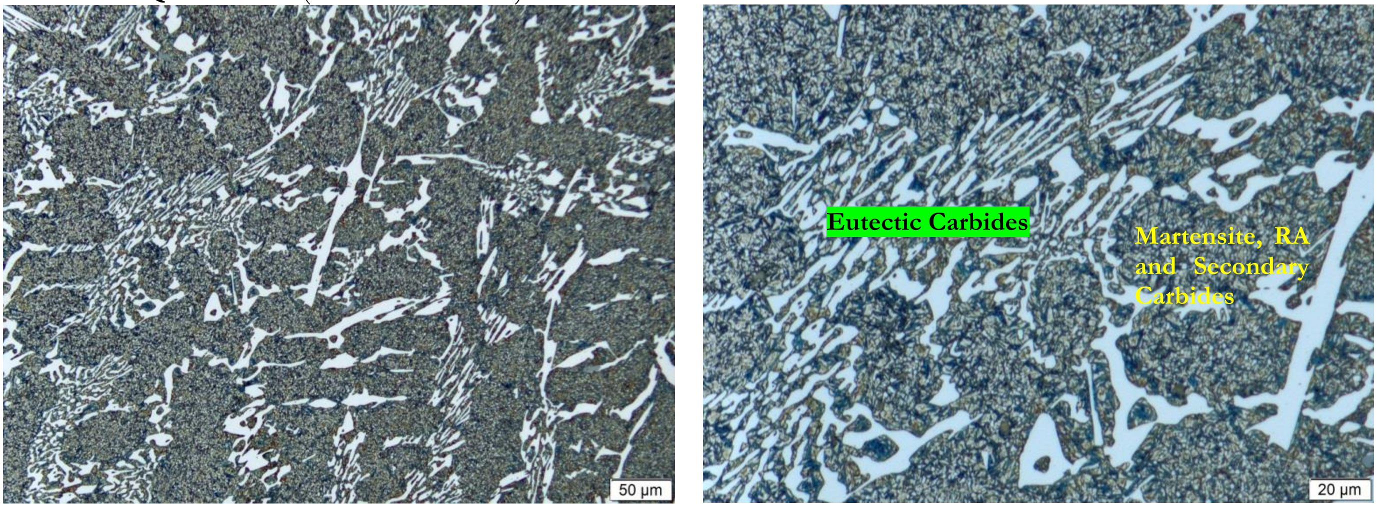

1050 °C +FAQ + 450 °C T (etched with Le Pera)

22.7 %RA

Figure 4.9. Optical micrographs showing microstructure showing eutectic carbides and retained austenite in a martensitic matrix after forced air quenching from 1050 °C. It also shows eutectic and secondary carbides and retained austenite in a tempered martensite matrix after tempering at 350 °C and 450 °C respectively for 4 hours, left at low and right at high magnification, (etched with Le Pera).

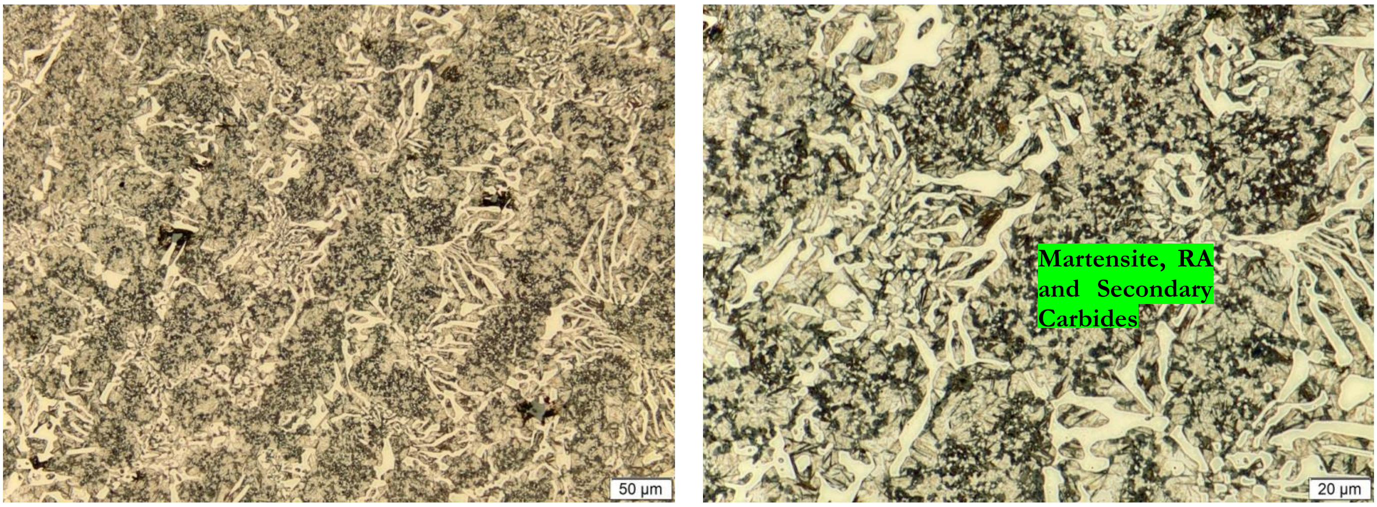

1100 °C +FAQ (etched with Le Pera) 57.3 %RA

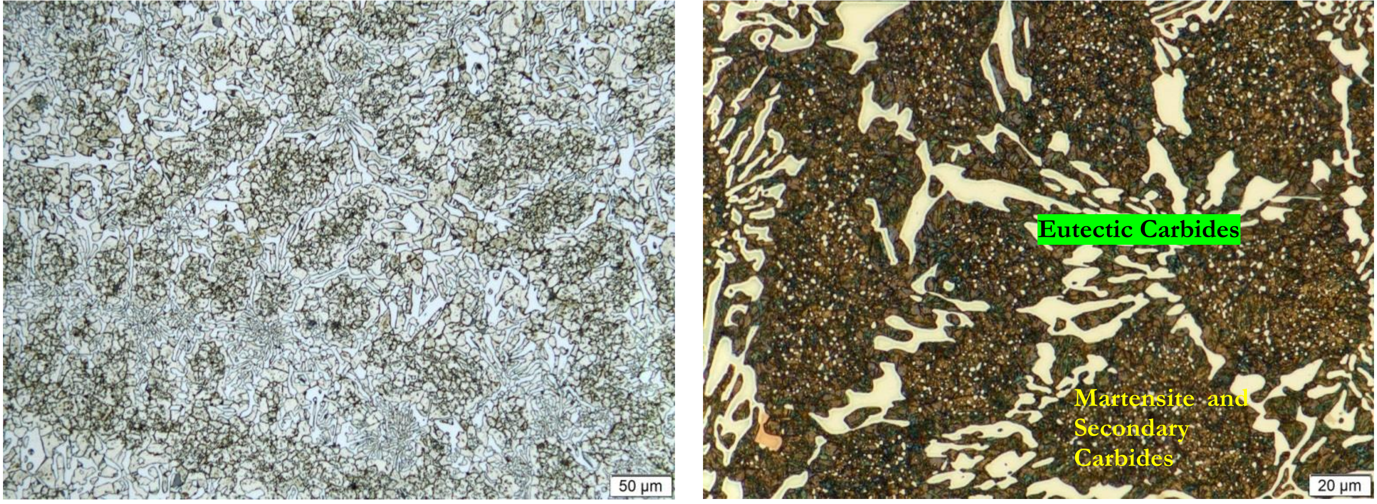

1100 °C +FAQ + 350 °C T (etched with Le Pera) 54.9 %RA

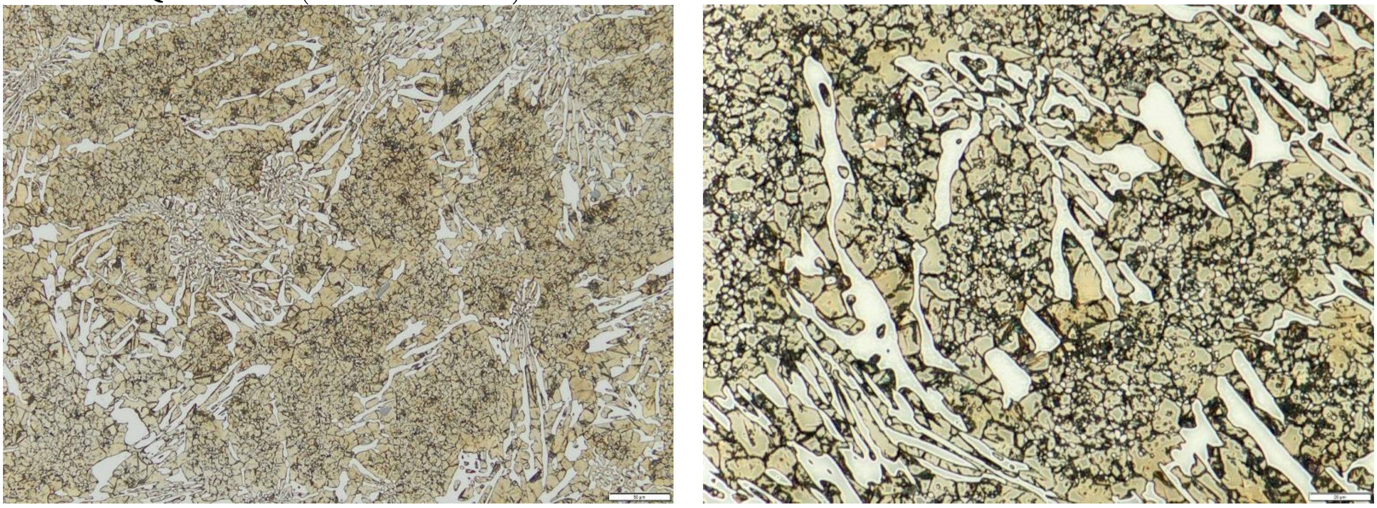

1100 °C +FAQ + 450 °C T (etched with Le Pera) 50.87%RA

Figure 4.10. The microstructure showing eutectic and secondary carbides in an austenitic matrix, after forced air quenching from 1100 °C. It also shows eutectic and secondary carbides in a tempered martensitic-austenite matrix, with residual retained austenite after tempering at 350 °C and 450 °C respectively for 4 hours, left at low and right at high magnification, (etched with Le Pera).

4.2.2. Carbidic Austempered Nodular Iron

Figure 4.11 shows the microstructures of a conventional ductile iron compared to Figures 4.12 and 4.13 with the microstructures of carbidic nodular iron set aside for austempering to yield carbidic austempered nodular iron (CANI). The as-cast ductile iron exhibited a microstructure of pearlite and ferrite around the graphite nodules; often referred to as the "bull's eye" microstructure. The carbidic ductile iron, which was alloyed with both molybdenum (Mo) and chromium (Cr), had a microstructure of pearlite and iron carbides, while some graphite nodules were also evident. The carbides were of the type M_3C, with chromium partially substituting iron.

Figure 4.12 and 4.13 shows the microstructures of the alloyed carbidic ductile iron cooled in a sand mould after casting, fettled then austenitised at 900 °C and austempered (i.e. directly quenched in molten salt) at various temperatures to produce carbidic austempered nodular iron (CANI) with different amounts of retained austenite. Figures 4.12 and 4.13 show the microstructures of carbidic nodular iron austempered as follows:

(**a**) 275 °C showing nodules, carbides, a fine ausferrite matrix and retained austenite,
(b) 350 °C showing graphite nodules, retained austenite, carbides and acicular ferrite,
(c) 375 °C showing graphite nodules, retained austenite and feathery ferrite,
(d) 400 °C showing coarse ausferrite (austenite + ferrite) and carbides.

It must be noted that as the austempering temperature increased from 275 °C to 375 °C, the ferrite became more feathery. The size of the ferrite needles in the ausferrite matrix increased as the austempering temperature increased. The carbides formed during solidification did not dissolved during the austempering process.

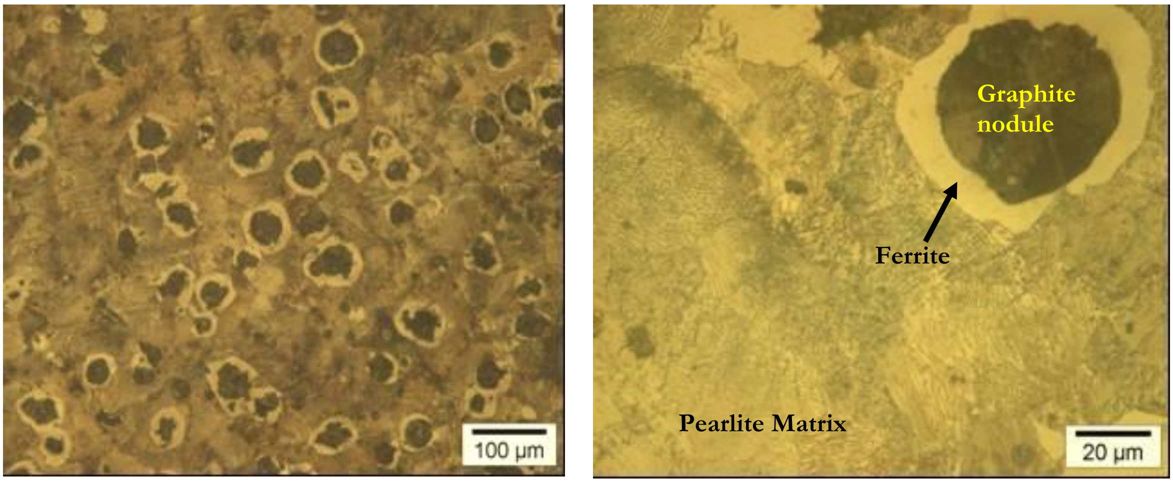

Figure 4.11. Optical micrographs showing microstructure of as-cast ductile iron showing graphite nodules surrounded by ferrite in a pearlitic matrix (etched with 3% Nital).

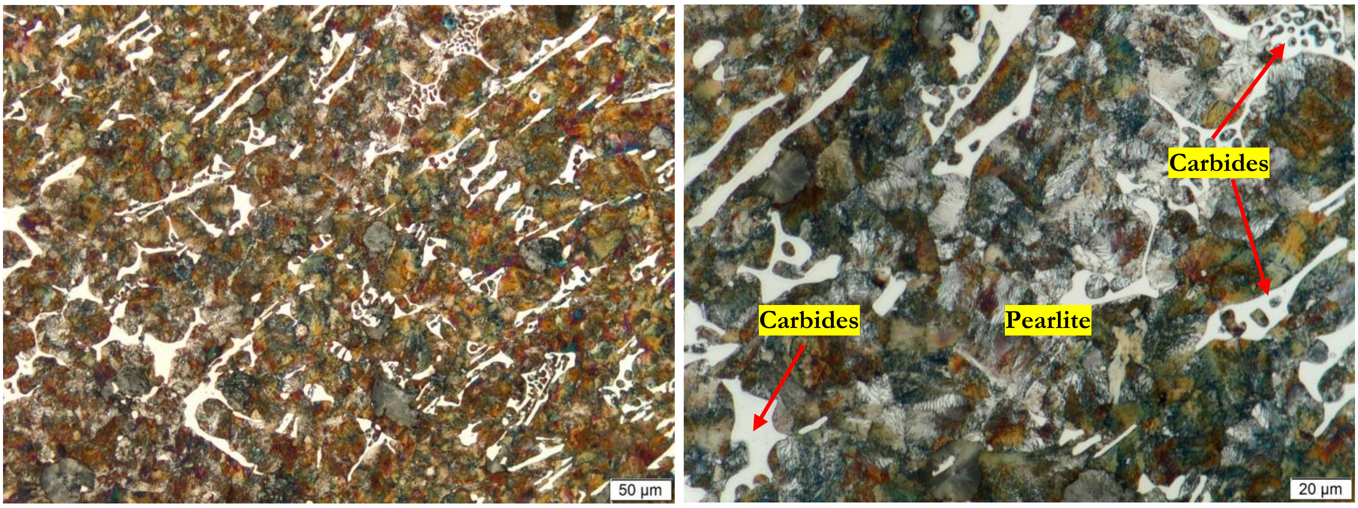

(a) As-cast carbidic nodular Iron, **Showing cementite carbides in pearlite matrix**

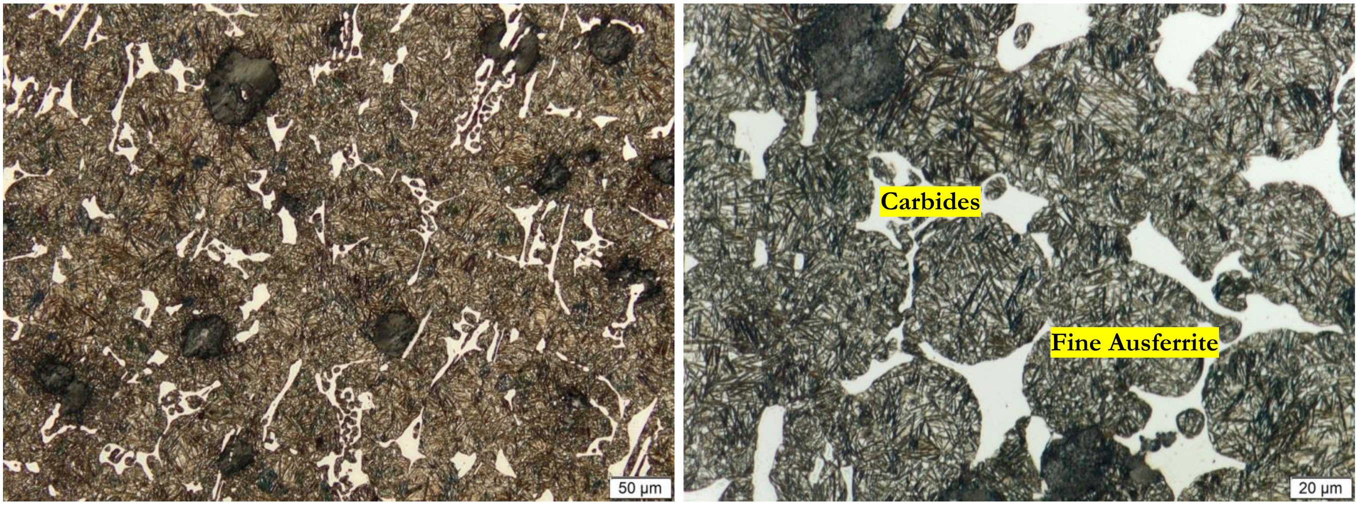

(b) 900°C + 275 °C Austempered 26.0 %RA

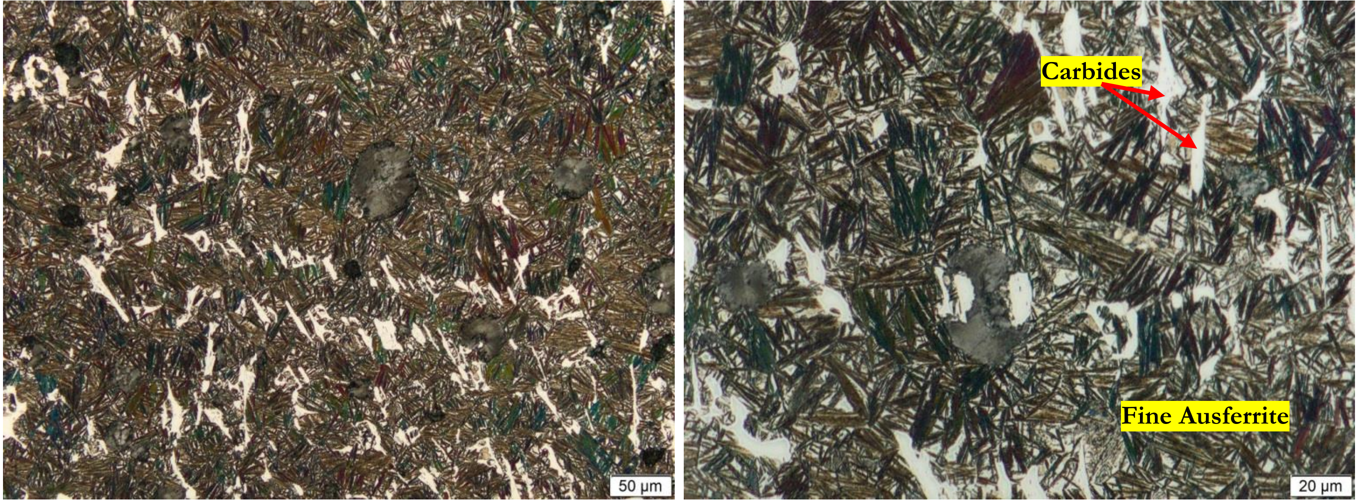

(c) 900°C + 350 °C Austempered 26.1 %RA (showing ausferrite, carbide and nodular graphite)

Figure 4.12. Optical micrographs showing microstructure of the as-cast carbidic nodular iron showing graphite nodules and carbides in a matrix of pearlite. Also shown is the carbidic nodular iron austempered respectively at 275 °C showing acicular ferrite and retained austenite, and after austempering at 350 °C showing graphite nodules, retained austenite, cementite carbides and ausferrite (etched with 3% Nital).

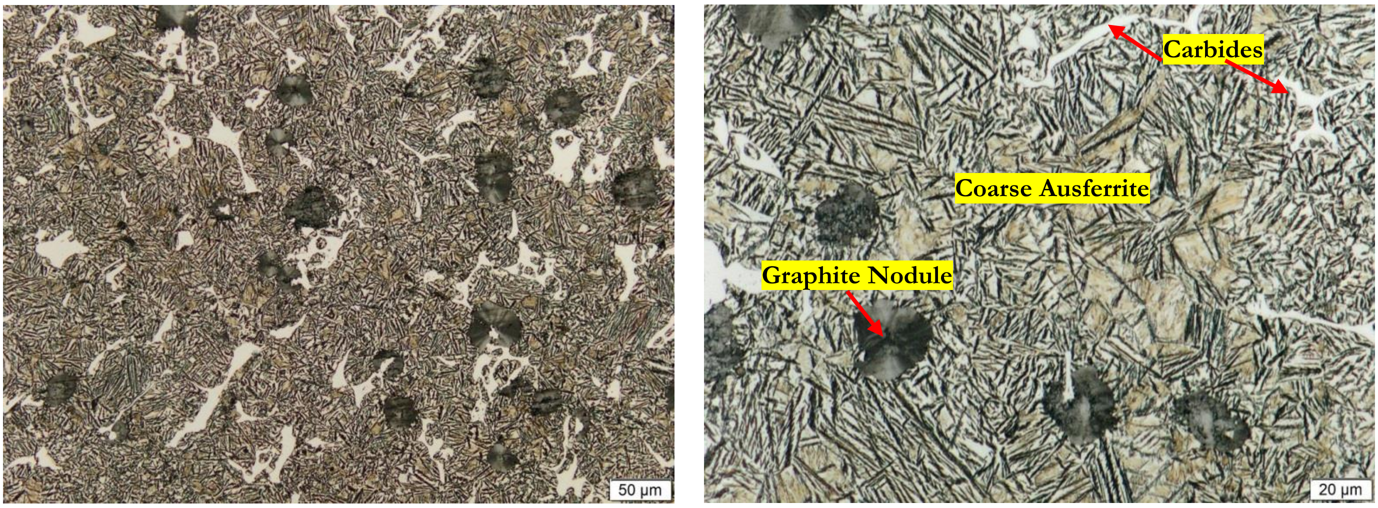

(d) 900°C + 375°C Austempered 16.41 %RA

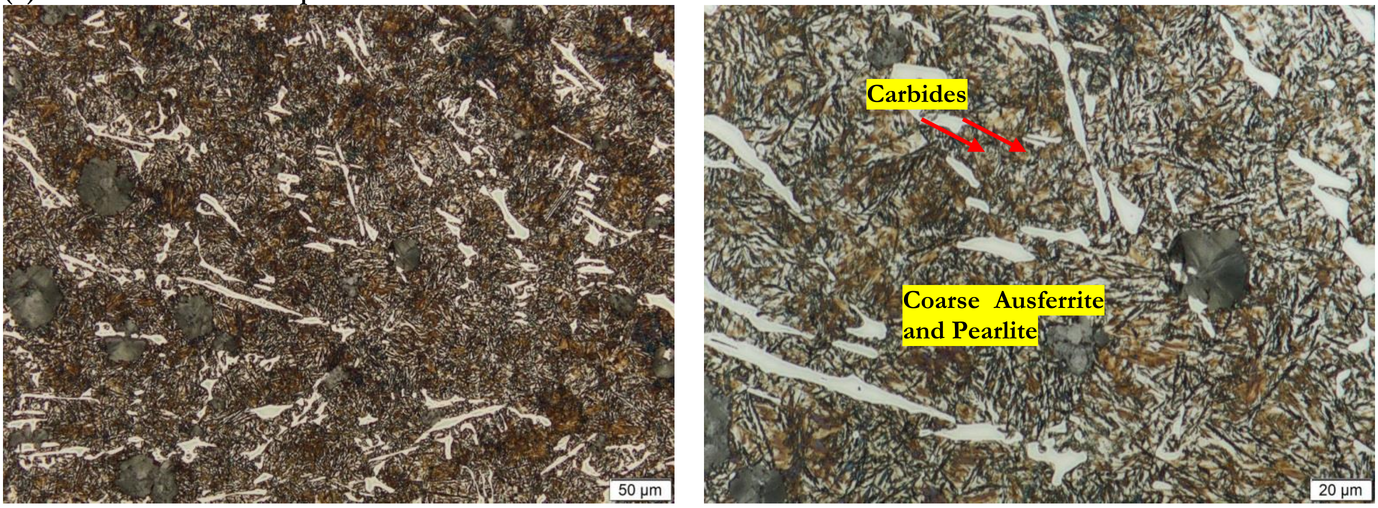

(e) 900°C + 400°C Austempered 16.6 %RA

Figure 4.13. Optical micrographs showing microstructure of the carbidic nodular iron respectively austempered at 375 °C showing graphite nodules, retained austenite and feathery ferrite, and after austempering at 400 °C showing a predominantly pearlitic microstructure with islands of ausferrite (austenite + ferrite) and carbides (etched with 3% Nital).

4.3. Electron probe micro-analyses (EPMA)

The microstructures of CANI alloys revealed graphite nodules (dark phase) with good nodularity and a carbide (white phase), in an ausferrite matrix. The chemical composition of the carbides, see Table 4.5 and that of the matrix, are summarised in Tables A and B in the Appendix. The type of carbides for both HCWCI and CANI were found to be M_7C_3 and M_3C respectively. EDX analysis of these carbides confirmed the stoichiometries as the M_7C_3 and M_3C type carbides.

Table 4.5. Electron probe micro-analyses (EPMA) results of HCWCI and CANI alloy.

Alloy	**Elemental (wt%)**					**Phase**
	C	**Si**	**Cr**	**Mn**	**Fe**	
HCWCI	8.45	0.03	40.40	0.77	50.80	Carbide
CANI	5.77	0.28	2.60	1.87	91.80	Carbide

The matrix carbon content determined by the EMPA method was also used as input data to calculate the carbon concentration $\boldsymbol{x_\gamma}$ of the austenite. Unfortunately, the results from the EPMA technique showed that the amount of carbon in the matrix increased with an increase in destabilisation temperature. This was due to the fact that the EMPA carbon content measurement included the secondary carbides whose volume fraction increased with an increase in temperature. Hence, the results could not be relied upon.

According to the results from the Thermo-Calc^{TM} prediction, it can be seen that as the temperature increases more carbides dissolve and upon quenching, more carbon is trapped in solid solution, Figures 4.2 and 4.3. During tempering obviously the carbon re-precipitated, hence, the decrease in the carbon content of the matrix.

4.4. Effect of Retained Austenite on Hardness

Sections 4.3.1 and 4.3.2 show the hardness test results obtained after the different heat treatments of the two HCWCI and CANI alloys. Selected temperatures were used so that a different amounts of retained austenite content were achieved in order to study their effect on hardness.

4.4.1. Effect of retained austenite on hardness of HCWCI and CANI alloys

The hardness traverse values for all the 70 mm diameter grinding balls that had been heat treated and tempered at various temperatures, are shown in the Appendix. The surface hardness values are also graphically presented in Figure 4.14. The hardness of the forced quenched (FAQ) grinding balls was higher if compared to that of the tempered ones.

As may be seen from Table C in the Appendix, there is a significant variation in hardness of the grinding balls from the surface to the centre of all the heat treated HCWCI grinding balls and this may be ascribed to the variations in cooling rate. As expected, the surface hardness decreased as the destabilisation temperature and amount of retained austenite increased.

Figure 4.15 shows the influence of destabilisation temperature on the hardness and the retained austenite content. The carbon content of the austenite just before quenching determines the hardness of the martensite and the amounts of retained austenite after quenching. The retained austenite is only free if all γ_{ret} transforms to martensite.

As may seen, the hardness did not drop significantly up to 1050 °C and this was probably, be due to the presence of fine secondary carbides.

The bulk hardness values of the specimens subjected to different austenitising treatments were higher than those for the as-cast conditions (525 to 550 BH) due to the secondary carbide precipitation. The maximum bulk hardness was obtained in the specimen austenitised at 875 °C and 925 °C and air quenched. A decrease in the hardness values was observed with increasing austenitising treatment temperatures due to the increasing contents of retained austenite and coarsening of secondary carbides.

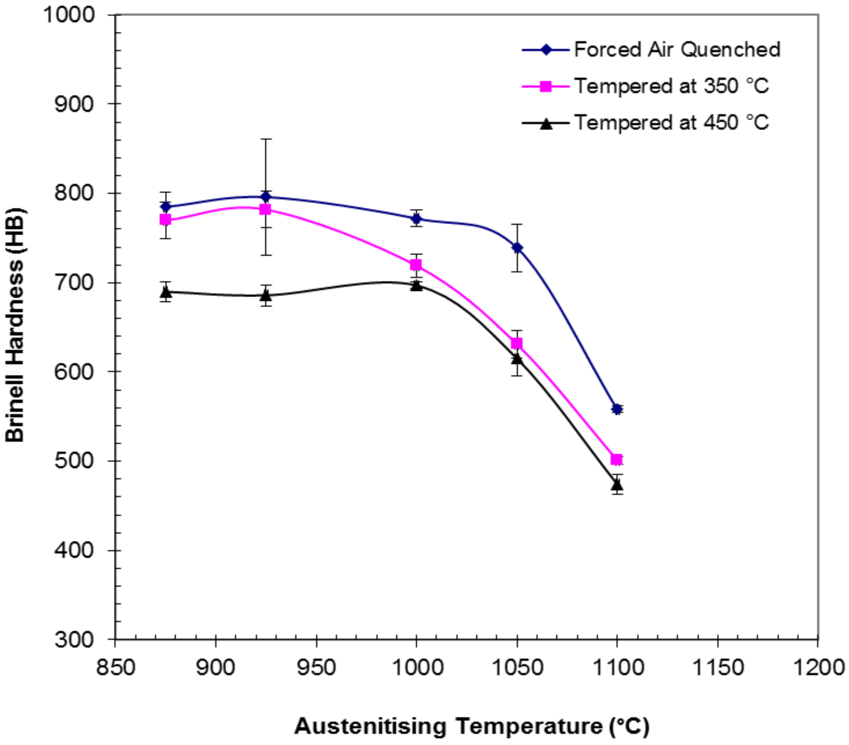

Figure 4.14. The influence of destabilisation and tempering temperature on the hardness of the high chromium white cast iron.

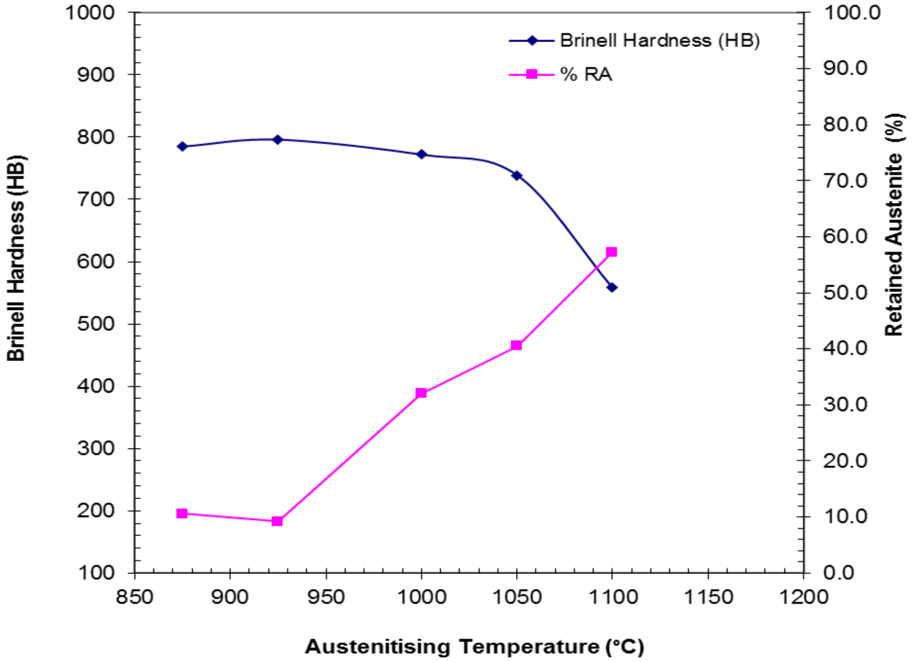

Figure 4.15. The influence of destabilisation temperature on the hardness and retained austenite content for the high chromium white cast iron.

4.4.2. Hardness traverse values across the diameter of the grinding balls

The hardness traverse values for all the 70 mm diameter carbidic nodular iron grinding balls austempered at various temperatures, are shown in Table D in the Appendix. As may be seen, there was a significant variation in hardness of the grinding balls from the surface to the centre in their austempered condition. The surface hardness values of the balls are graphically presented in Figure 4.16. It is clear that the surface hardness decreased as the austempering temperature and the amount of retained austenite increased.

Figure 4.16 also shows the influence of austempering temperature on the surface hardness and the retained austenite amount. The hardness trend matched the volume fraction of the retained austenite.

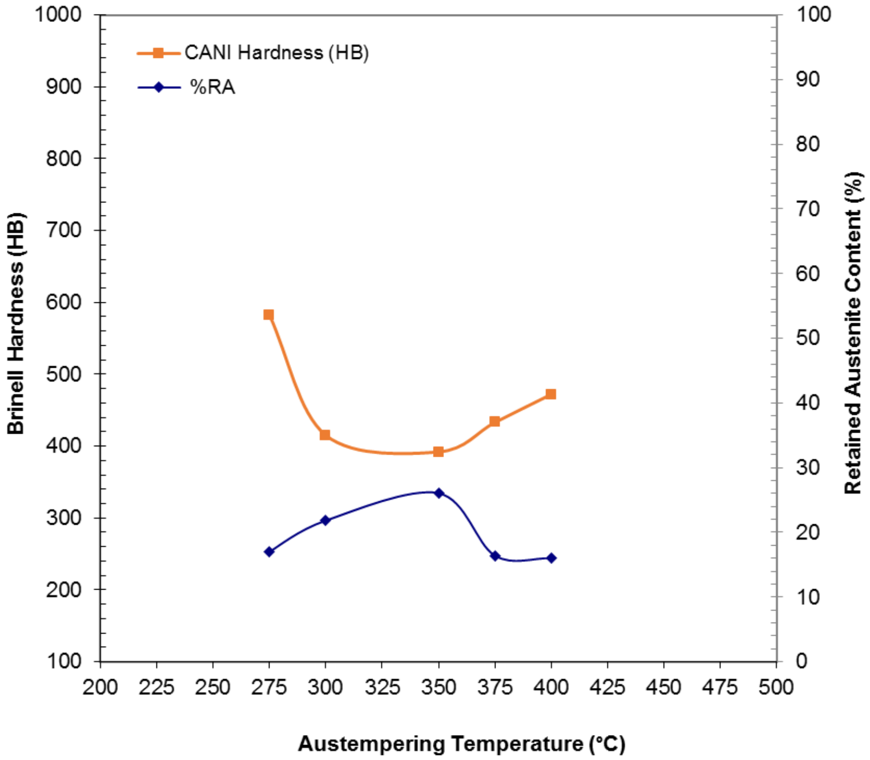

Figure 4.16. The influence of austempering temperature on the hardness and retained austenite for the carbidic austempered nodular iron.

4.5. Effect of Retained Austenite on High Stress Abrasion Wear (POB)

Sections 4.4.1 to 4.4.3 cover the influence of retained austenite on high stress, low stress and ball mill wear tests of the HCWCI and CANI alloys respectively.

4.5.1. Pin-on-belt (POB) high stress abrasion test of HCWCI

The surface retained austenite amounts before and after the pin-on-belt abrasion test were measured and are summarised in Tables E and F in the Appendix. The influence of austenitising temperature on the retained austenite before and after high stress abrasive wear (POB), is graphically presented in Figure 4.17. It can be seen that the retained austenite amount of the alloy before the abrasion wear test was significantly higher if compared to after testing. The decrease in retained austenite is an indication that transformation from retained austenite to martensite (α') occurred during high stress abrasion wear test. The effect of tempering temperature on retained austenite amount after high stress abrasive wear (POB) is evident.

As may also be seen from Figure 4.17, the amount of retained austenite before the test significantly decreased as the tempering temperature increased from 350 °C to 450 °C as a result of lower stability of austenite.

The percentage mass loss and retained austenite results obtained after the pin-on-belt abrasion wear tests are also graphically presented in Figure 4.18**.** Generally, it can be seen that the trend in the percentage mass loss decreased as the destabilisation temperature increased, within the experimental scatter. This is most likely attributed to possibly an increase of strain induced martensite (SIM).

The tempering temperature has an opposite effect if compared to the austenitising temperature. As the tempering temperature increased the percentage mass loss to a limited extend decreased, i.e. after tempering at 350 °C and 450 °C. The effect of retained austenite on high stress abrasion is also illustrated in Figure 4.18. As the retained austenite increased the percentage mass loss decreased very slightly. The retained austenite transformed to the harder martensite phase during high stress abrasion wear and this led to reduced wear. Taking into account the scatter, one could enclose these graphs in a band showing improvement in wear with increased in retained austenite and austenitizing temperature up to 1100 °C.

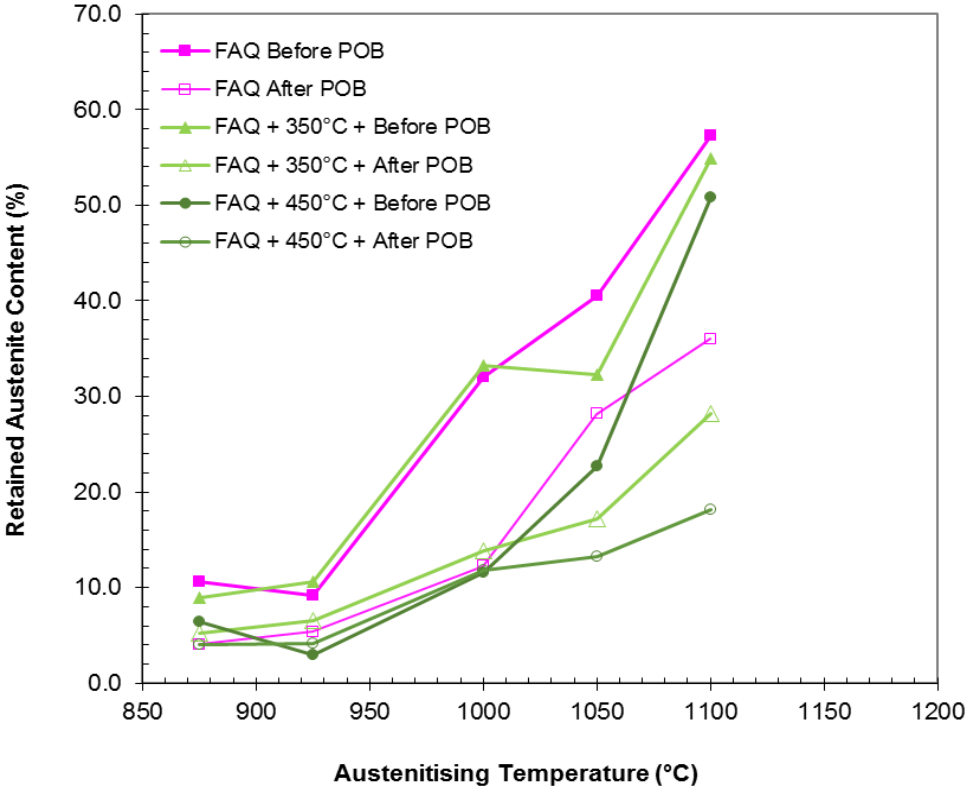

Figure 4.17. The influence of austenitising and tempering temperature on the retained austenite before and after high stress abrasive wear (POB) of HCWCI.

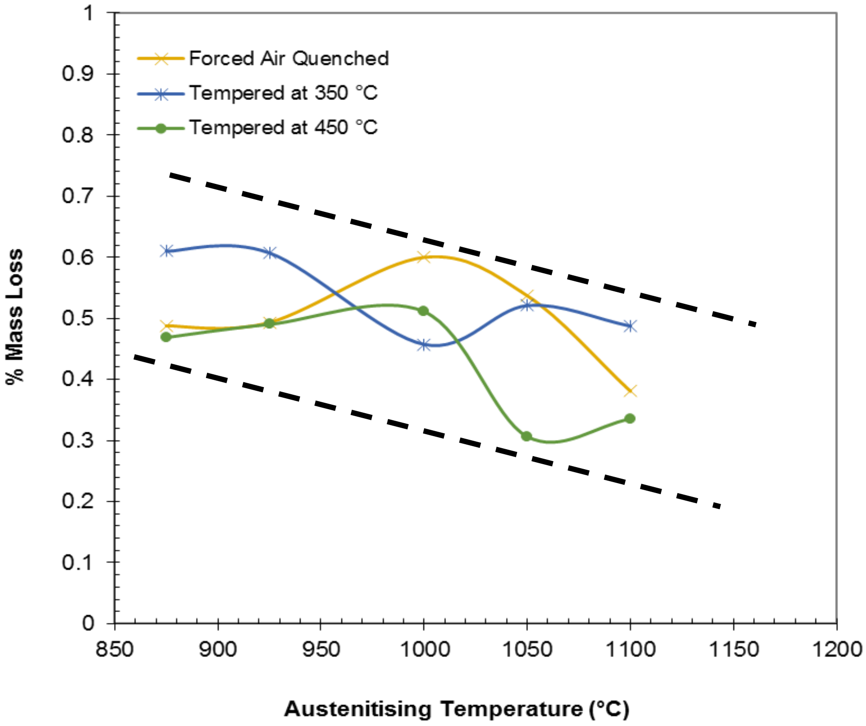

Figure 4.18. The effect of austenitising and tempering temperature on the high stress abrasive wear (POB) of high chromium white cast iron.

4.5.2. Pin on belt (POB) high stress abrasion test of CANI

The retained austenite amounts of the carbidic austempered nodular iron before and after the pin-on-belt abrasion test were measured and is summarised in Table E in the Appendix. The retained austenite on as-cast carbidic ductile iron was not measured since the matrix was purely pearlitic. The influence of austempering temperature on the retained austenite before and after high stress abrasive wear (POB), is graphically presented in Figure 4.19. It can be seen that the retained austenite amount of the alloy before the high stress wear test, was significantly higher if compared to after testing. The decrease in retained austenite is an indication that transformation to SIM occurred during high stress abrasion wear test.

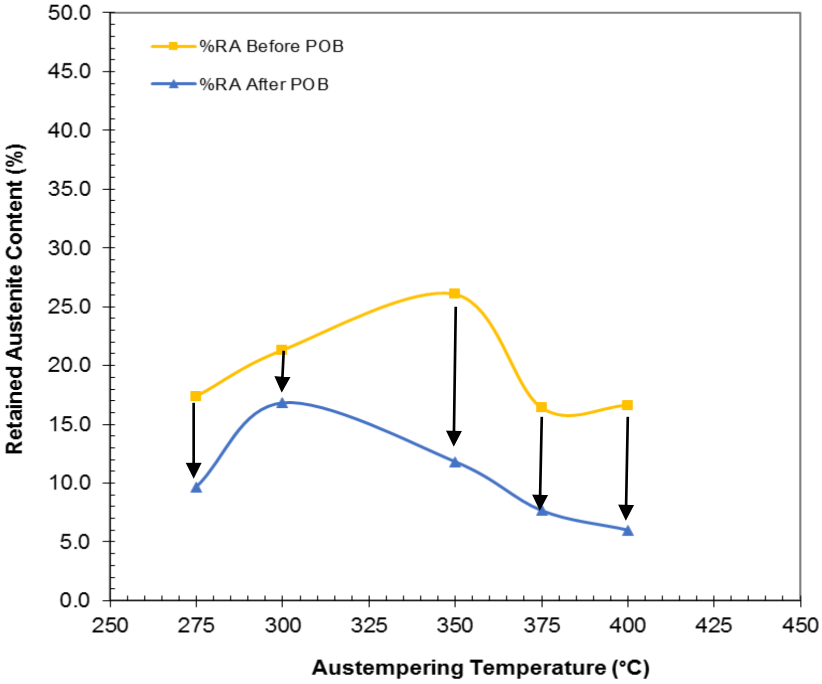

Figure 4.19. The influence of austempering temperature on the retained austenite before and after high stress abrasive wear (POB) of CANI.

The weight loss of CANI pin samples after the high stress abrasion wear test is graphically presented in Figure 4.20. It is evident that the retained austenite initially increased rapidly until 350 °C, and then decreased with a further increment in austempering temperature. As expected, at high austempering temperatures (375 °C and 400 °C), the specimens exhibited a high percentage mass loss during POB testing. On the other hand, at lower austempering temperatures, the percentage mass loss was relatively lower. The reasons for this type of behaviour are discussed in Sections 2.9 (theory) and 5.1.

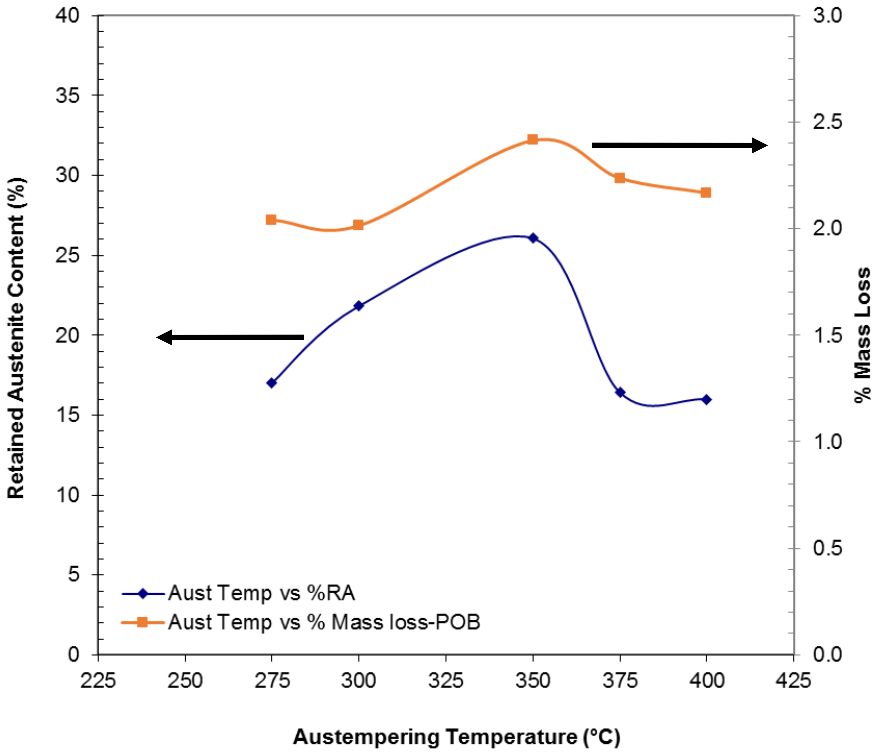

Figure 4.20. The influence of austempering temperature on the amount of retained austenite and percentage mass loss after high stress abrasion wear (POB) on CANI.

The possibility of retained austenite transforming to martensite under high stress sliding conditions for both HCWCI and CANI was also investigated by X-ray diffraction analysis. Here, retained austenite was measured on the specimen before and after the pin on belt abrasive wear test. This was necessary to ascertain if there was actually a transformation of retained austenite to martensite during abrasion. A test sample of 10x10x15mm which was sampled from near the surface of a 70 mm diameter grinding ball was prepared for this test.

Computer software, which utilised the integrated areas of both the austenite (220) and (311) and ferrite (200) and (211) peaks, was used in the determination of the volume fractions of retained austenite and ferrite before and after abrasion. The results revealed that there was a decrease in retained austenite after the pin on belt wear test. This was a result of the transformation of retained austentite to martensite; i.e. for the HCWCI alloy, see the XRD results in Figures 4.21 to 4.25.

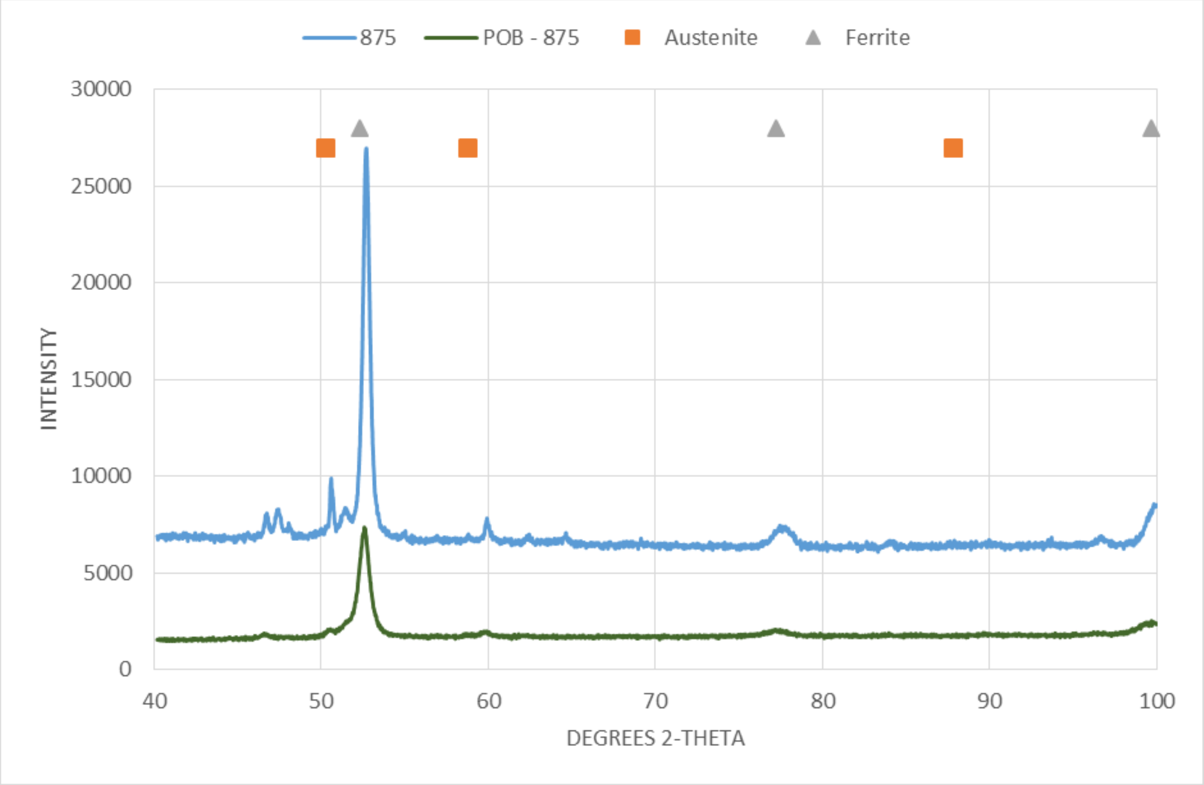

Figure 4.21. The X-ray diffraction diagram showing no deformation induced martensite transformation in HCWCI sample heat treated at 875°C and after a fast air quenched (FAQ). The diagram shows the austenite and ferrite peaks before and after high stress abrasion (POB).

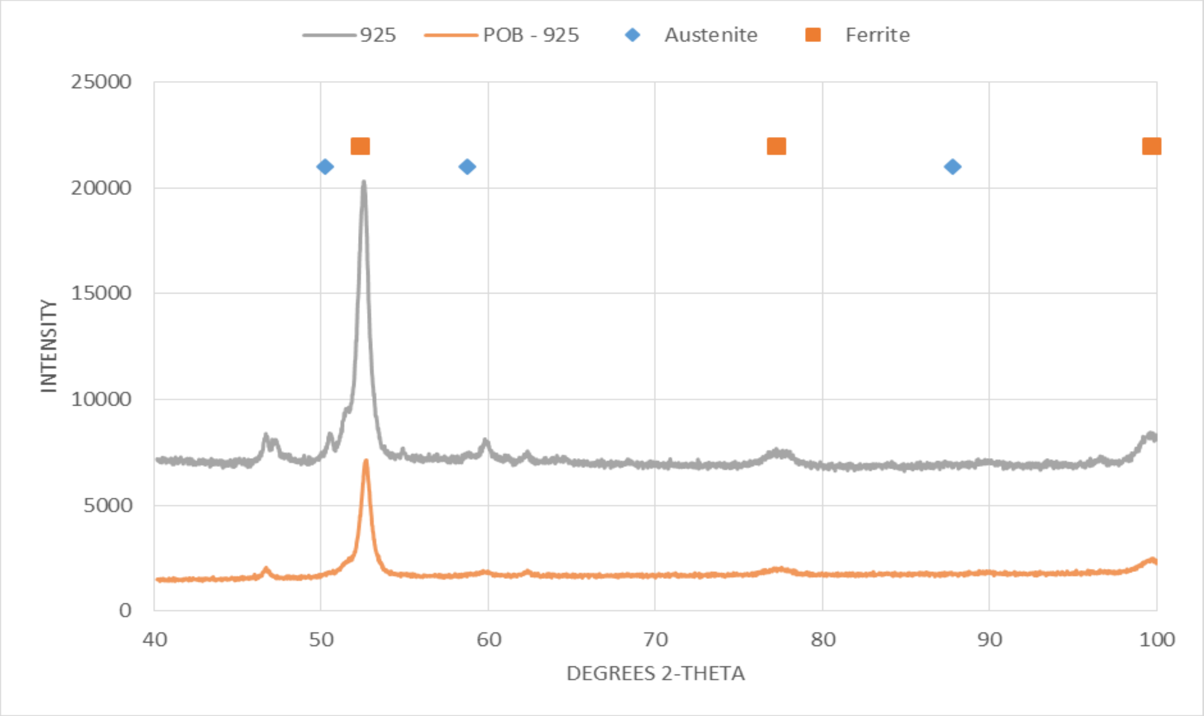

Figure 4.22. The X-ray diffraction diagram showing deformation induced martensite transformation in a HCWCI sample heat treated at 925°C and after a FAQ. The diagram shows the austenite and ferrite peaks before and after high stress abrasion (POB).

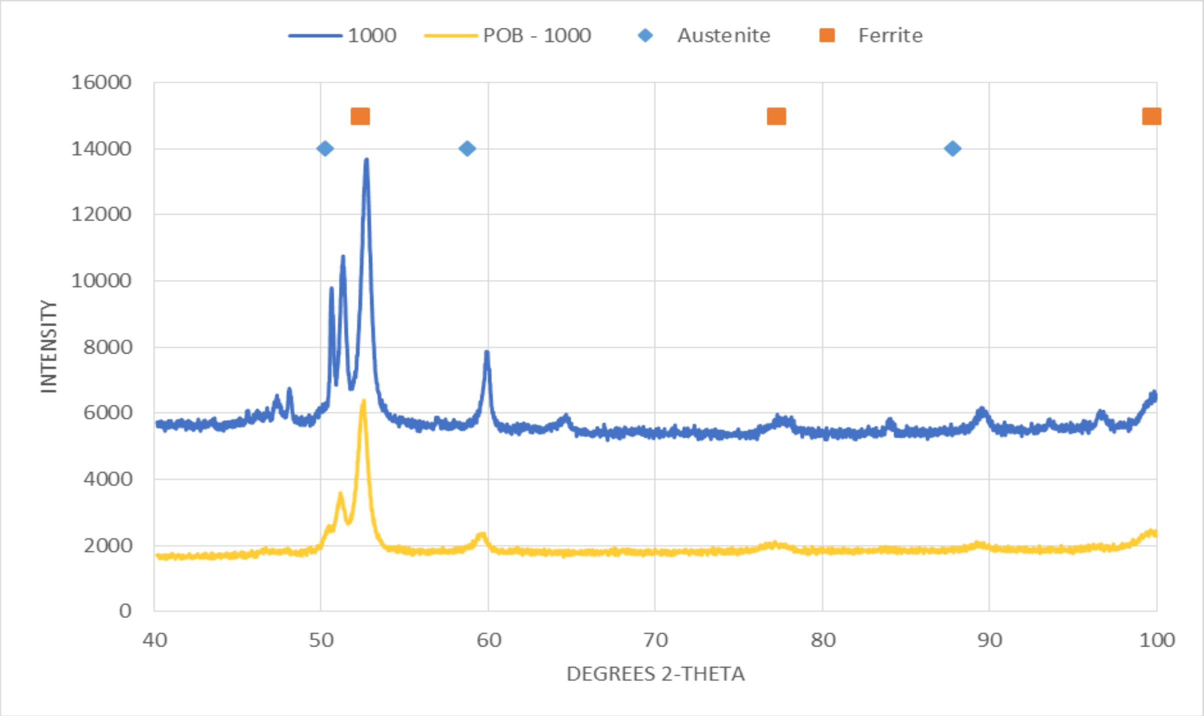

Figure 4.23. The X-ray diffraction diagram showing some deformation induced martensite transformation in a HCWCI sample heat treated at 1000°C and after a FAQ. The diagram shows the austenite and ferrite peaks before and after high stress abrasion (POB).

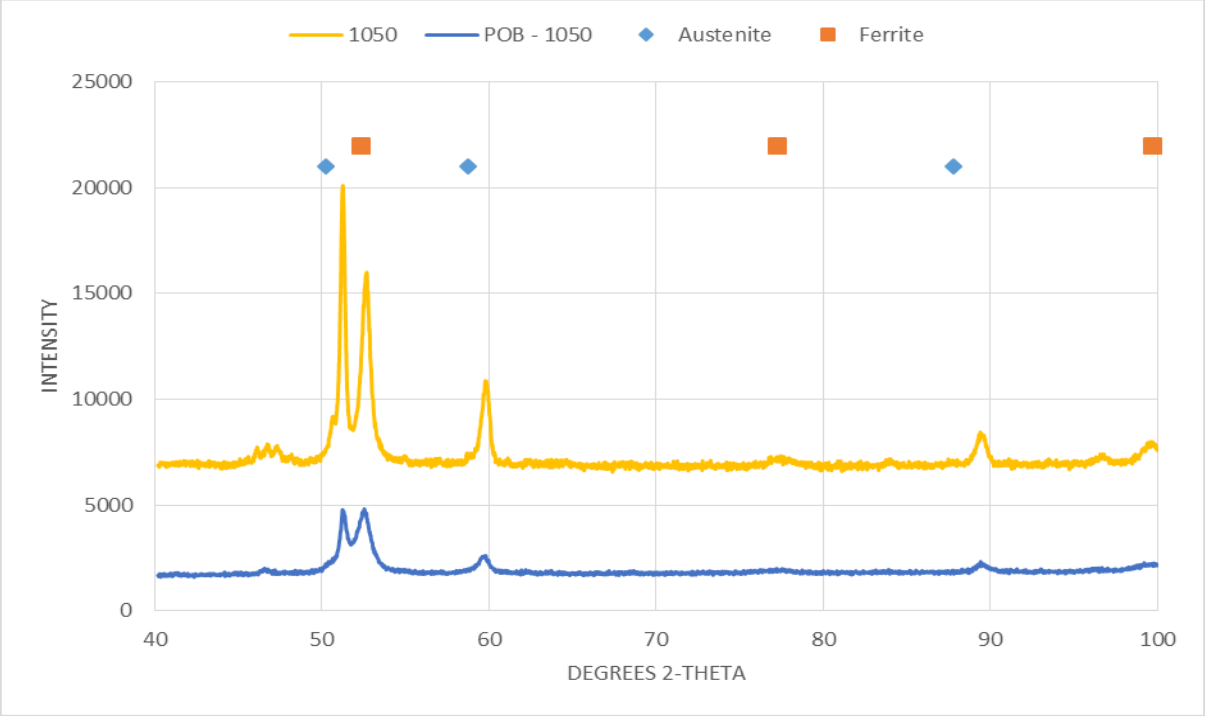

Figure 4.24. The X-ray diffraction diagram showing some deformation induced martensite transformation in a HCWCI sample heat treated at 1050°C and after FAQ. The diagram shows the austenite and ferrite peaks before and after high stress abrasion (POB).

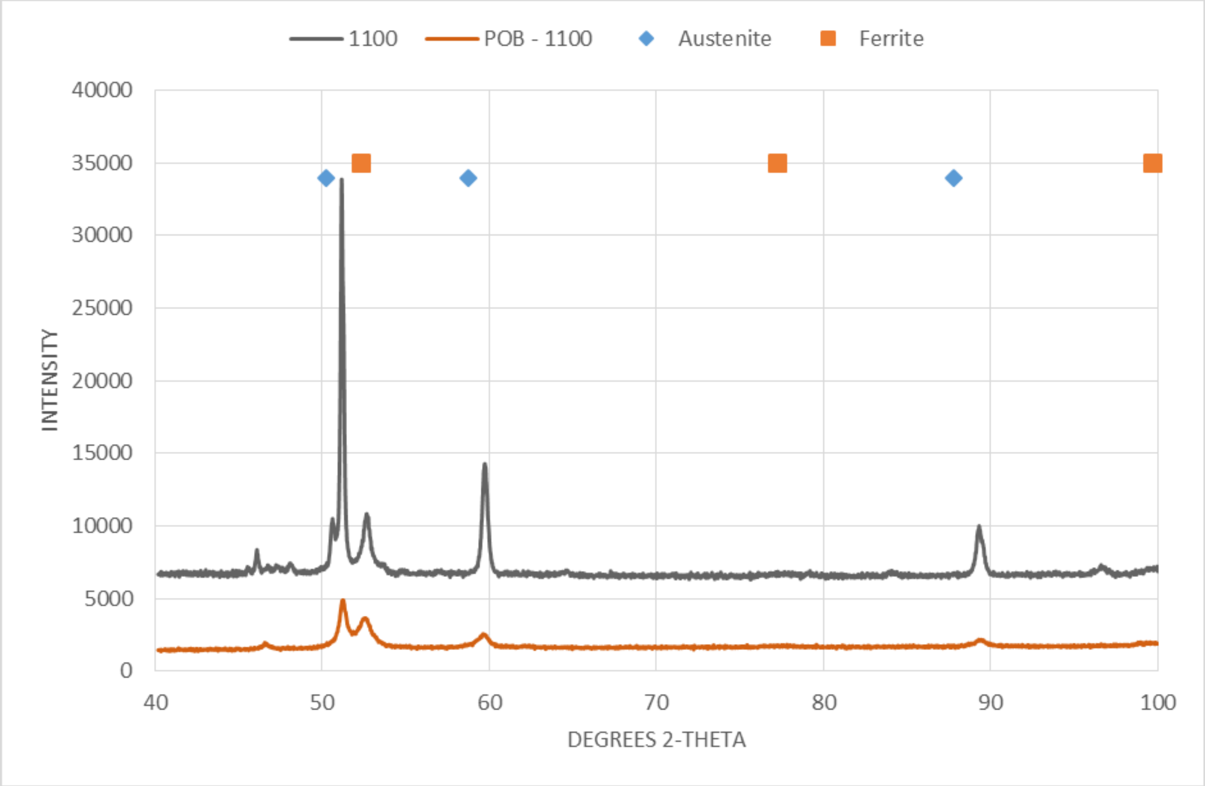

Figure 4.25. The X-ray diffraction diagram showing some deformation induced martensite transformation in a HCWCI sample heat treated at 1100°C and after a FAQ. The diagram shows the austenite and ferrite peaks before and after high stress abrasion (POB).

Figures 4.26 to 4.29 show the austenite and ferrite peaks before and after abrasion for CANI specimen's austempered at 275°C to 400°C, respectively. After the abrasive wear tests the prominent austenite peaks were reduced to nearly background noise levels. This reduction in the size of the austenite peaks coupled with some broadening of the ferrite/martensite peaks in Figures 4.26 to 4.29 after abrasion testing, suggests that deformation induced transformation of the retained austenite had occurred. The broadening of peaks is there because there is a difference between **c** and **a** parameters in martensite, whereas ferrite is cubic, so has no difference.

It must be noted that the grinding ball samples being maintained at the selected intercritical temperature, were subjected to an <u>austempering stage</u>, rather than to <u>water quenching</u>. This led to the austenite to ausferrite transformation rather than from austenite to martensite. This was confirmed by the microstructures of the austempered samples in Figures 4.12 and 4.13.

The X-ray diffraction peaks before and after the wear test for the specimens that were austempered at 400 °C do not seem to vary significantly. This is in agreement with the coarse ausferrite microstructure that was observed in Figure 4.13.

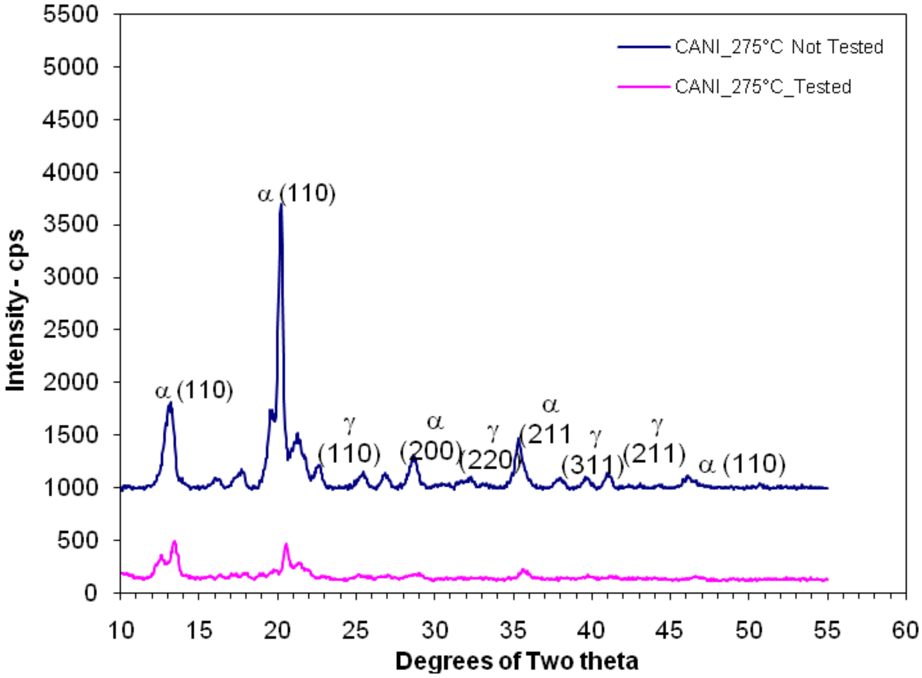

Figure 4.26. The X-ray diffraction diagram showing some deformation induced austenite to martensite transformation in a CANI sample austempered at 275°C. The diagram shows the austenite peaks, labelled (110), (220), (311) and (211) before and after high stress abrasion test (POB).

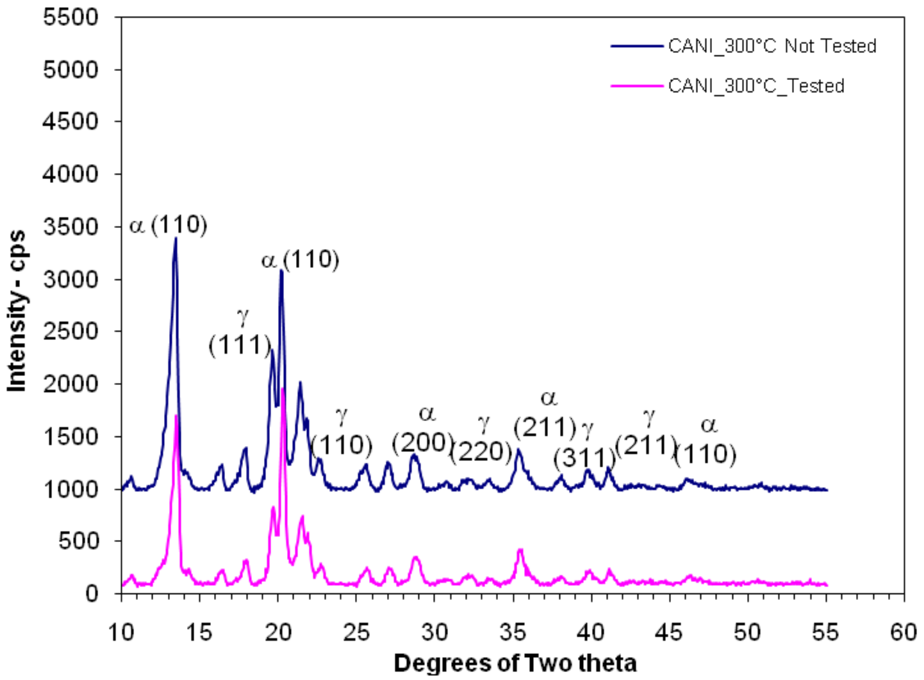

Figure 4.27. The X-ray diffraction diagram showing some deformation induced austenite to martensite transformation in a CANI sample austempered at 300°C. The diagram shows the austenite peaks, labelled (110), (220), (311) and (211) before and after high stress abrasion test (POB).

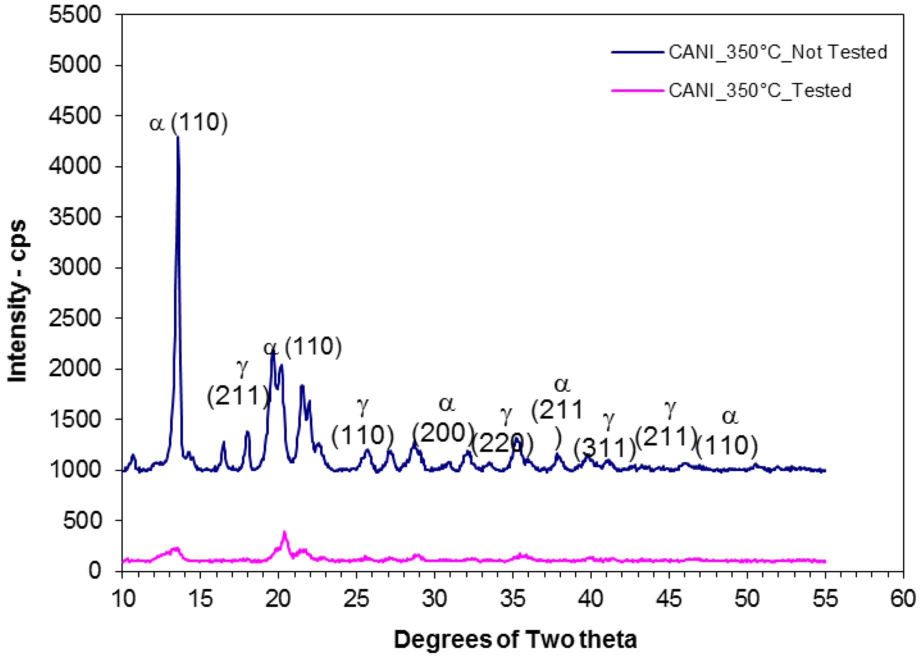

Figure 4.28. The X-ray diffraction diagram showing some deformation induced austenite to martensite transformation in a CANI sample austempered at 350°C. The diagram shows the austenite peaks, labelled (110), (220), (311) and (211) before and after high stress abrasion test (POB).

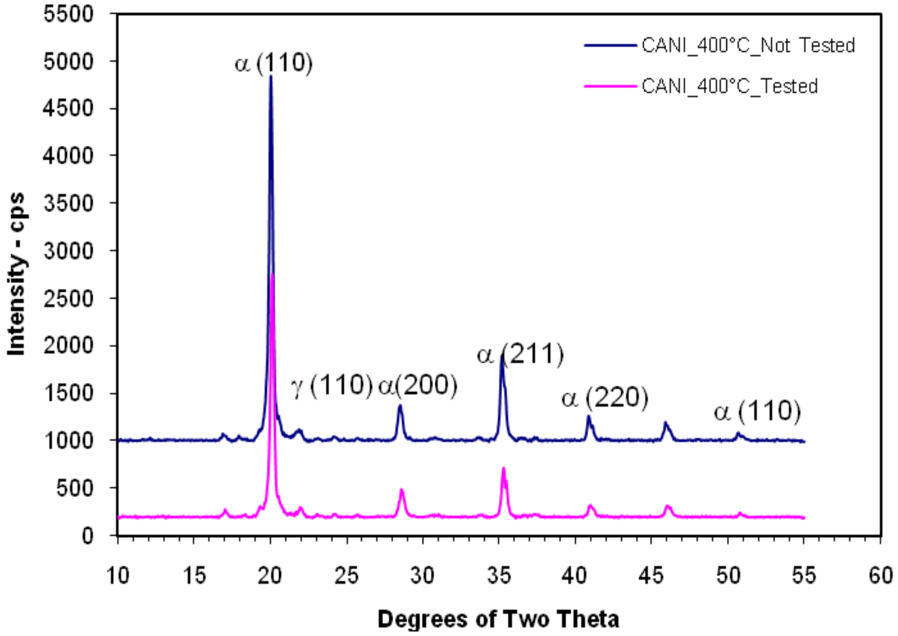

Figure 4.29. The X-ray diffraction diagram showing no deformation induced austenite to martensite transformation in a CANI sample austempered at 400°C. The diagram shows the ferrite peaks, labelled (200), (211), (110) and (110) before and after high stress abrasion test (POB).

4.5.3. Scanning electron microscopy (SEM) studies of worn surfaces of HCWCI and CANI

In order to study the wear mechanisms that occurred during the SiC induced high stress abrasion wear test, worn surfaces of HCWCI and CANI samples were examined using a scanning SEM. Figure 4.30 shows a SEM micrograph of the 120grit SiC particles on the belt that was used as abrasive material. Figures 4.31 to 4.32 show the representative appearances of worn surfaces in the POB abrasion test of HCWCI. The long scars show that cutting and grooving by the abrasive particles occurred on the specimen surface. The worn surface of the as-cast alloy appeared heavily deformed and smeared. These deformed grooves within the channels compare fairly well to the shape of the SiC particles. Comparing the hardness of the SiC (2500 – 2600HV) with that of chromium carbides, M_7C_3 (1200 – 1800HV), the abrasive particles (SiC) can abrade the specimen effectively. Figure 4.31(a) shows a ploughing mode of abrasion where a groove is formed which has ridges on both sides and wear debris is formed. Fewer micro-cracks were seen in the martensitic structures, see Figures 4.31b and 4.32a. It appeared that the abrasive particles could cut through the matrix and fractured the carbides very easily.

The surface topography of CANI consisted typically of shallow wear scars and grooves with small pits. Figures 4.34 to 4.36 show the wear scar mechanism that occurred in the CANI alloy under high stress abrasion. It can be seen that the as-cast samples showed deformed or ploughed grooves as a sign of the soft matrix. As the austempering temperature increased, samples were less resistant to high stress wear showing a ploughing mode of abrasion whereby grooves were formed which has ridges on both sides.

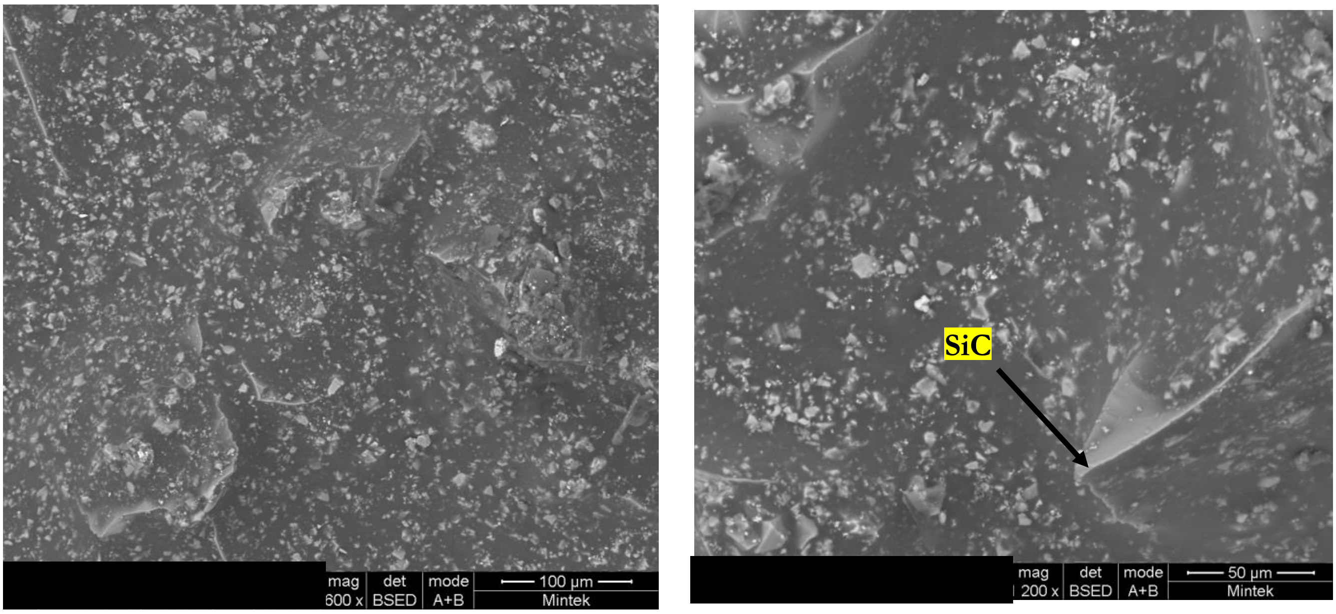

Figure 4.30. SEM-backscatter electron mode picture of the 120grit SiC abrasive paper on belt that was used as abrasive material showing silicon carbide particles.

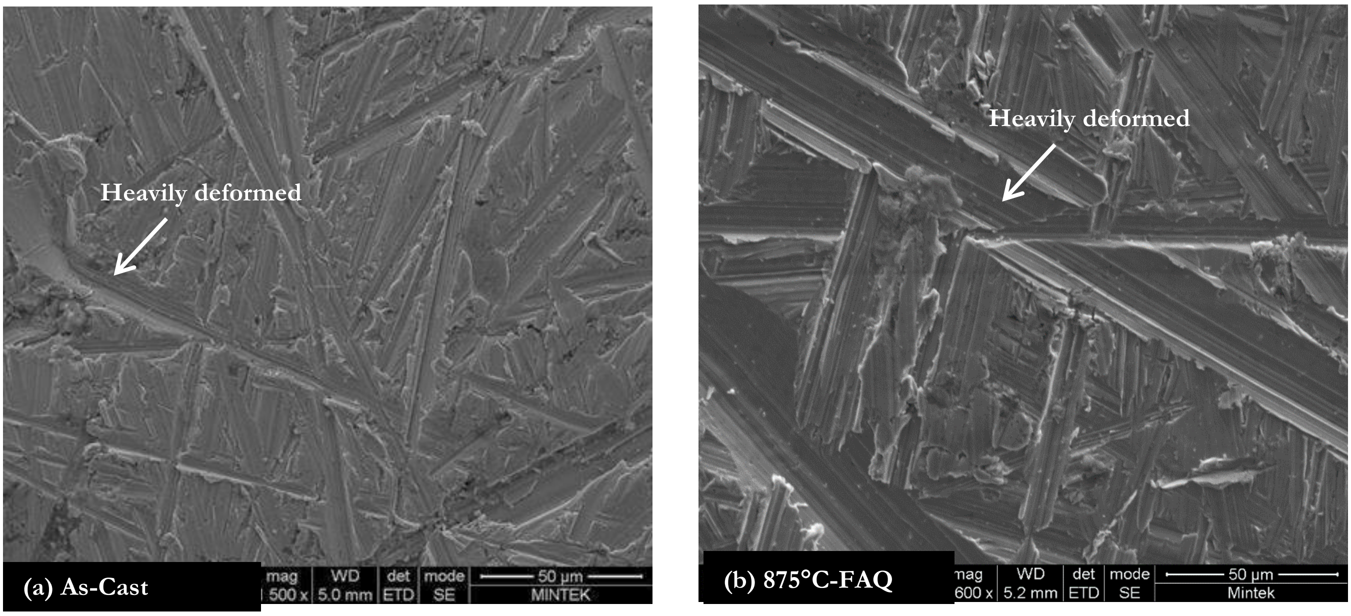

*Figure 4.31. SEM-secondary electron mode micrograph of the worn surface obtained after the high stress abrasion test (**a**) showing deformed rims of the wear grooves indicating a fair degree of ductility, (**b**) showing wear scars that are terminated abruptly due to carbide fracture.*

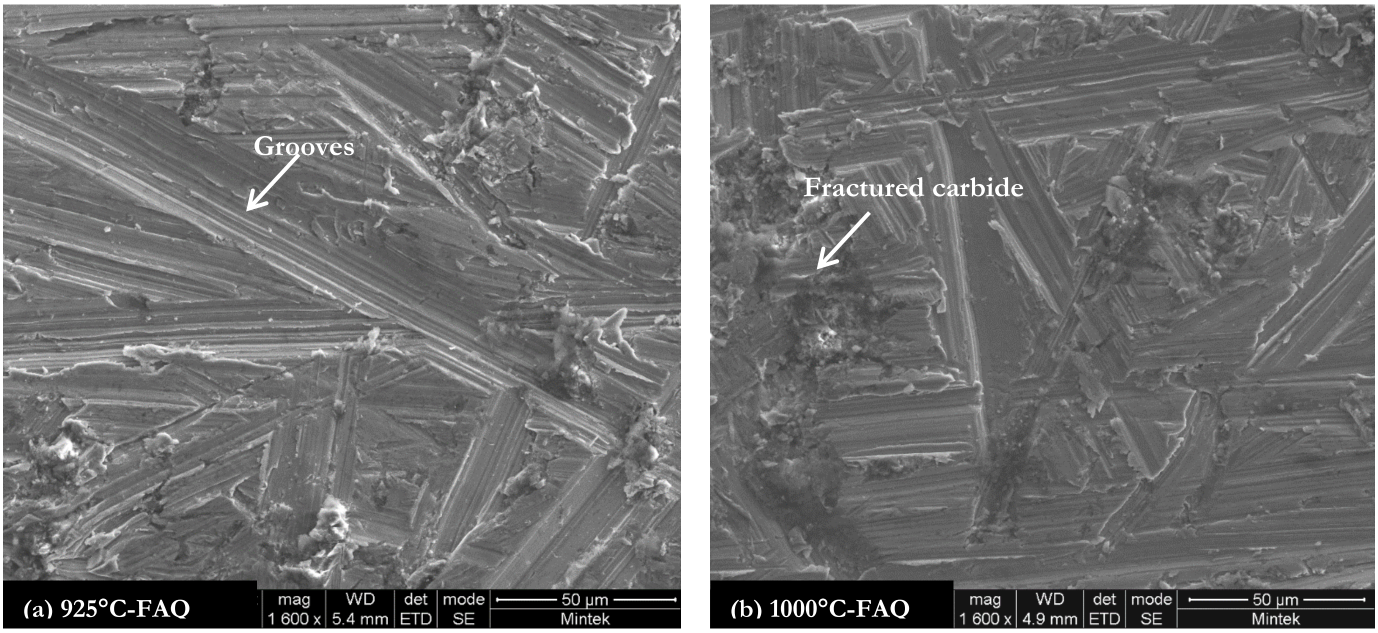

*Figure 4.32. SEM-secondary electron mode micrographs of the worn surface obtained after the high stress abrasion test (**a**) showing deformed rims of the SiC induced wear grooves (**b**) showing a wear track terminated probably due to fracturing of the abrasive particle – fractured carbide.*

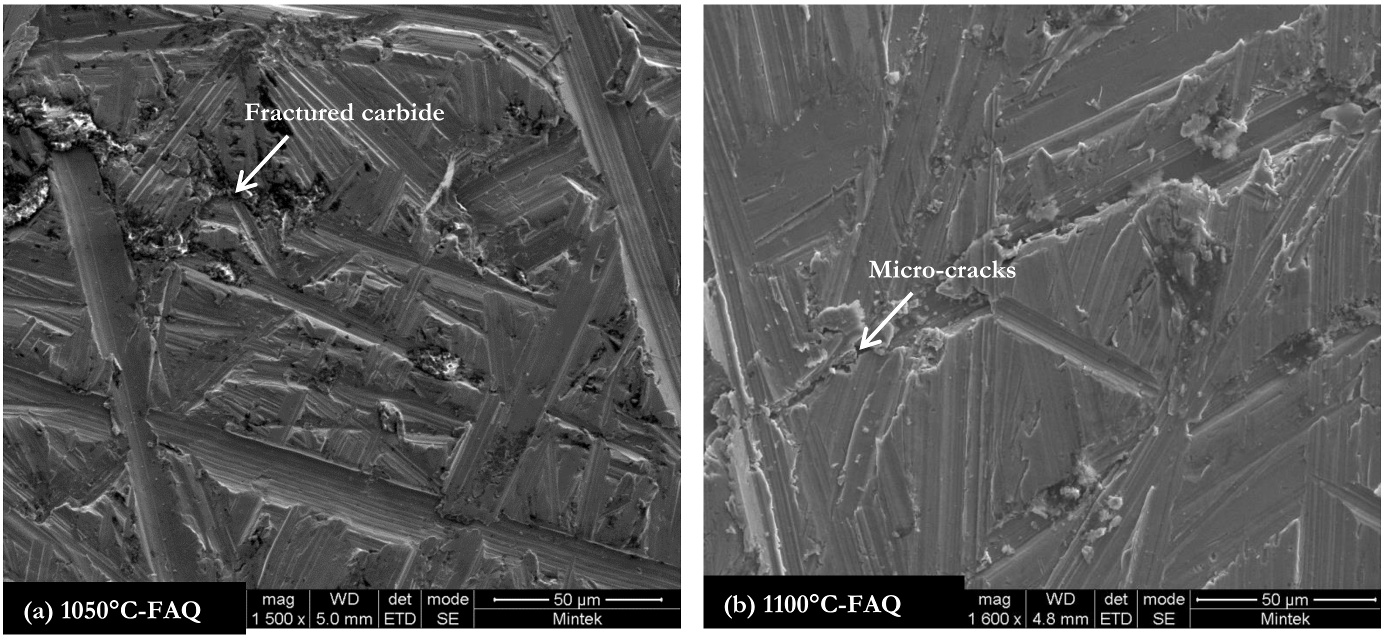

Figure 4.33. SEM-secondary electron mode micrographs of the worn surface obtained after the high stress abrasion test, (a) showing the wear track interrupted by a SiC carbide particle resisting the cutting action of the abrasive, (b) micro-cracks and wear grooves indicating fair a degree of ductility.

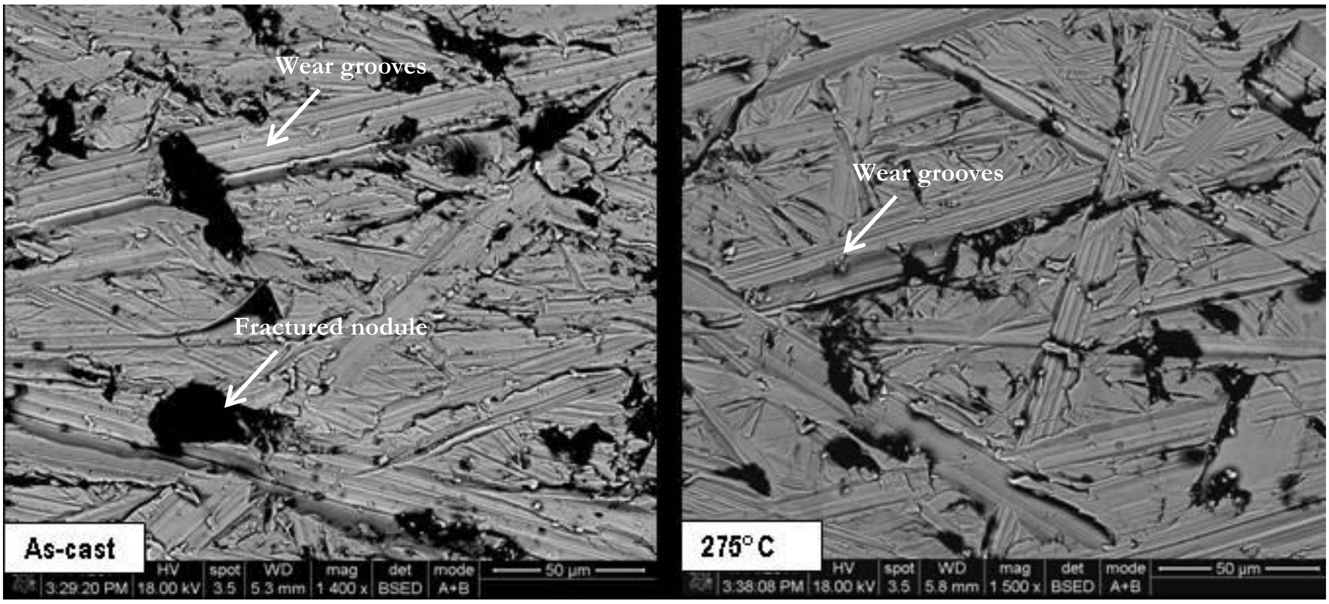

Figure 4.34. SEM-backscattered electron mode micrographs of the worn surfaces of the CANI, as cast and austempered at 275 °C.

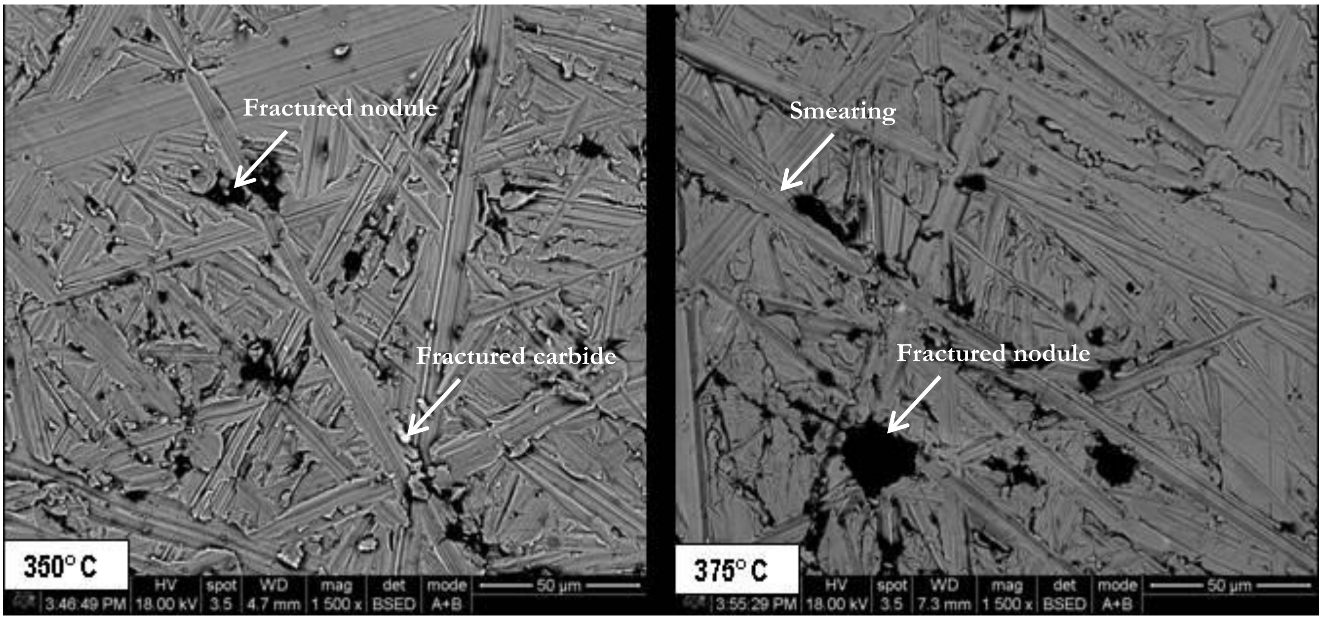

Figure 4.35. SEM-backscattered electron mode micrographs of the worn surfaces of the CANI, austempered at 350°C and 375 °C.

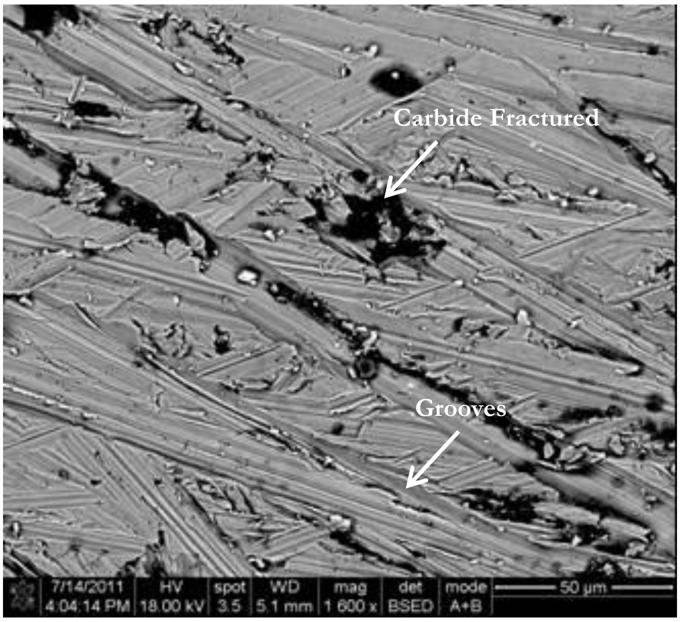

Figure 4.36. SEM-backscattered electron mode micrographs of the worn surfaces of the CANI austempered at 400 °C.

4.6. Effect of Retained Austenite on the Abrasion Wear (DRWAT)

4.6.1. Dry rubber wheel abrasion test (low stress) of HCWCI and CANI

The results of the dry rubber wheel abrasion tests carried out on HCWCI and CANI are summarised in the Appendix and graphically presented in Figures 4.37 and 4.38. The low stress three-body abrasive dry rubber wheel abrasion test (DRWAT) was carried out on as-cast samples that were air quenched at 875 °C plus tempered at 350 °C and 450°C.

As seen from Figure 4.37, the wear resistance of HCWCI samples which were quenched from 875 °C was the highest and only deteriorated after tempering heat treatment. The percentage volume loss of the HCWCI samples which were quenched from 875 °C appears to remain relatively constant after 600 s, i.e. remain at about 16 mm^3. However, the rest of the heat treatment led to a steady increase in mass loss with time.

It is apparent from Figure 4.38 that the wear of the CANI alloy was related to the austempering temperature. As the austempering temperature was increased from 275 °C to 400 °C the volume loss increased. The wear resistance was highest after austempering at 275 °C and this is probably due to the higher hardness and lower volume fraction of the retained austenite.

It is, therefore, noticeable that there was a running-in period prior to the wear rate becoming linear with time. This behaviour is illustrated more clearly in Figure 4.38 which shows the volume loss of the CANI as a function of time. Both Figures 4.37 and 4.38 show that there was an optimum amount of retained austenite and volume fraction of carbides for both HCWCI and CANI alloys, i.e. the HCWCI alloy which was quenched from 875 °C and the CANI alloy which was austempered at 275 °C exhibited the best performance. Clearly hardness and matrix structure largely determine the abrasion resistance of the alloys.

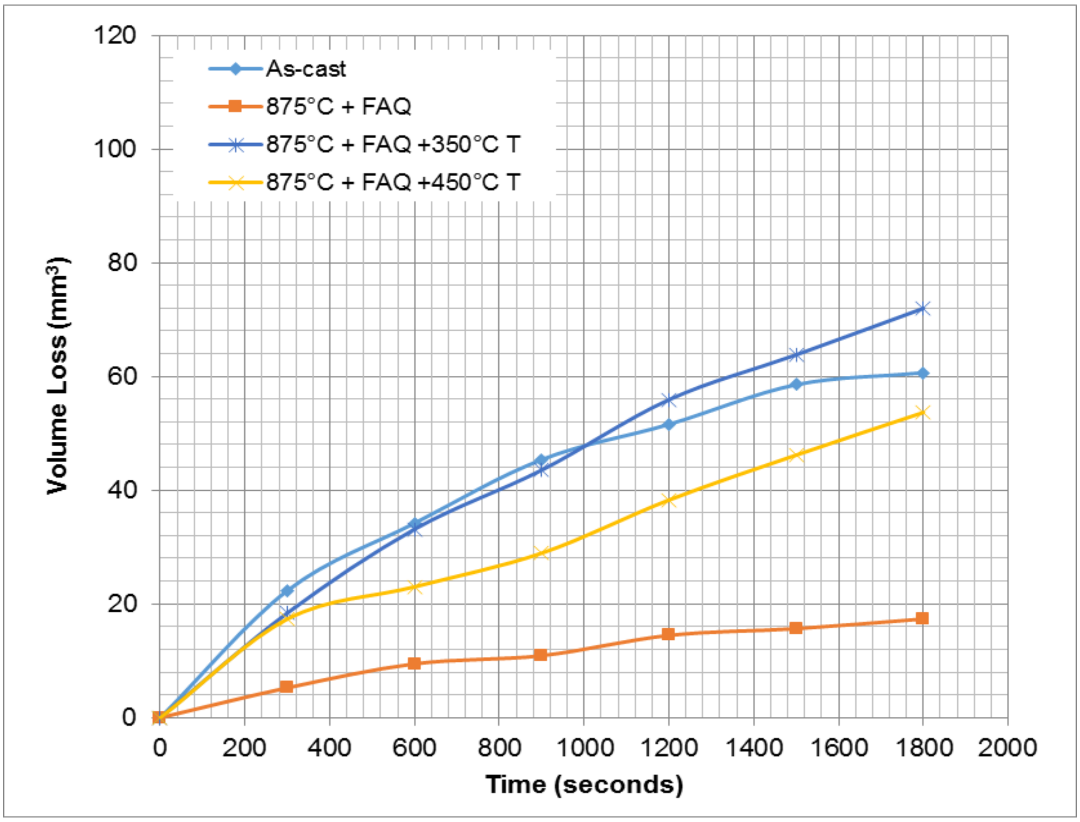

Figure 4.37. The volume loss versus time for the HCWCI after low stress abrasion testing (DRWAT).

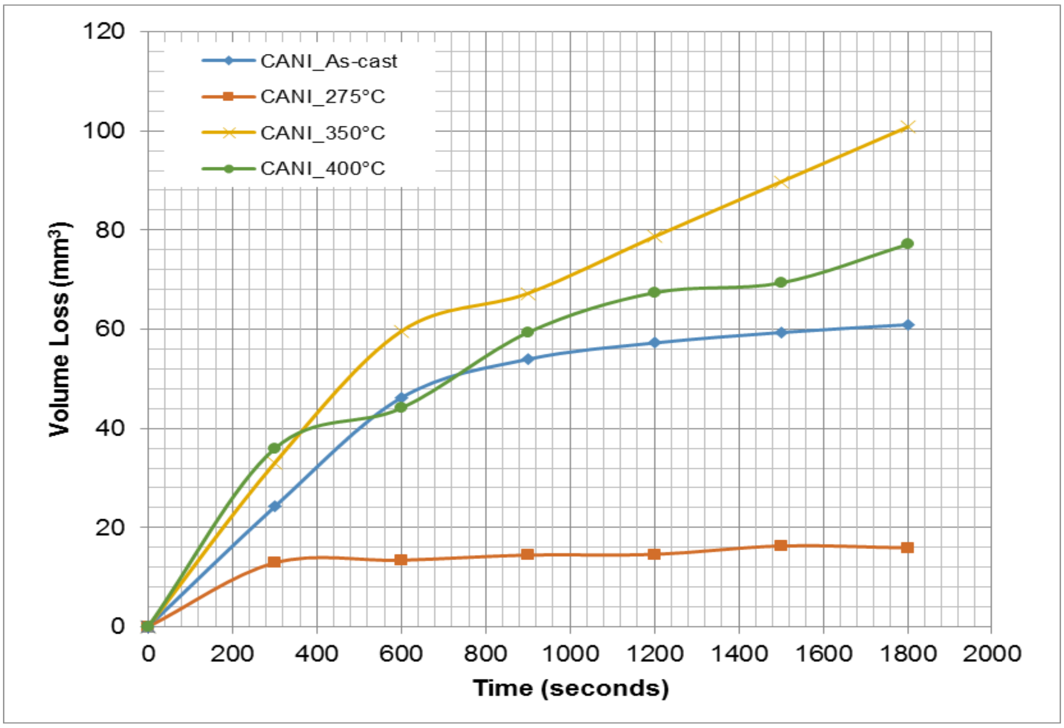

Figure 4.38. The volume loss versus time for the CANI after low stress abrasion testing (DRWAT).

4.7. Effect of Retained Austenite on Abrasion Wear (Ball Mill simulation)

4.7.1. Abrasive wear test (Ball Mill simulation) of HCWCI and CANI

A conditioning run of 20 hours was first performed to remove any adhering scale and surface decarburised layers, which was not representative of the 70 mm diameter grinding media. The balls were then tested for five separate 20 hours runs (runs 1 to 5) to give a total of 100 hours, excluding the 20 hour conditioning run. The masses of the grinding balls were measured after each 20 hour cycle. One ball from the 875°C batch broke during the test probably due to casting defects and the results are based on a total of four balls. The masses of the CANI balls which were austempered at 350 °C were also measured after each 20 hour cycle. Four of these balls broke during the test and results are based on a total of only 3 grinding balls.

The total mass loss per 20 hour cycle of all the balls over the test period and the cumulative and average weight loss values after 100 hours of both HCWCI and CANI are detailed in the Appendix. The results are graphically presented in Figures 4.39 and 4.40. The HCWCI grinding balls which were heat treated at 1000 °C and forced quenched and tempered at 350 and 450 °C, showed the best results with the lower percentage mass loss of **1.6** as compared to the other temperatures.

Similarly, CANI grinding balls austempered at 275 °C showed the best abrasion wear results with a lower percentage mass loss of **1.5**. Therefore, it shows that the tempering temperature does play a significant role on abrasive ball mill wear of grinding balls. In other words, within the assumed experimental scatter, the performance of CANI-900 °C-275 °C was the same as HCWCI-1000 °C - 350 and 450 °C.

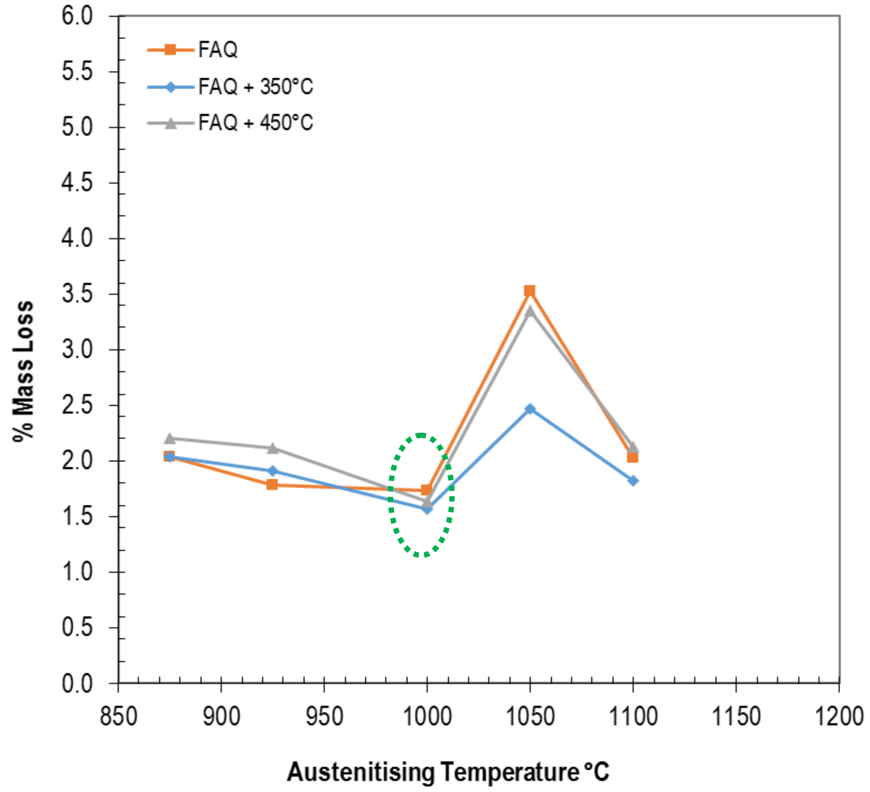

Figure 4.39. Influence of retained austenite on ball mill wear values of the HCWCI grinding balls.

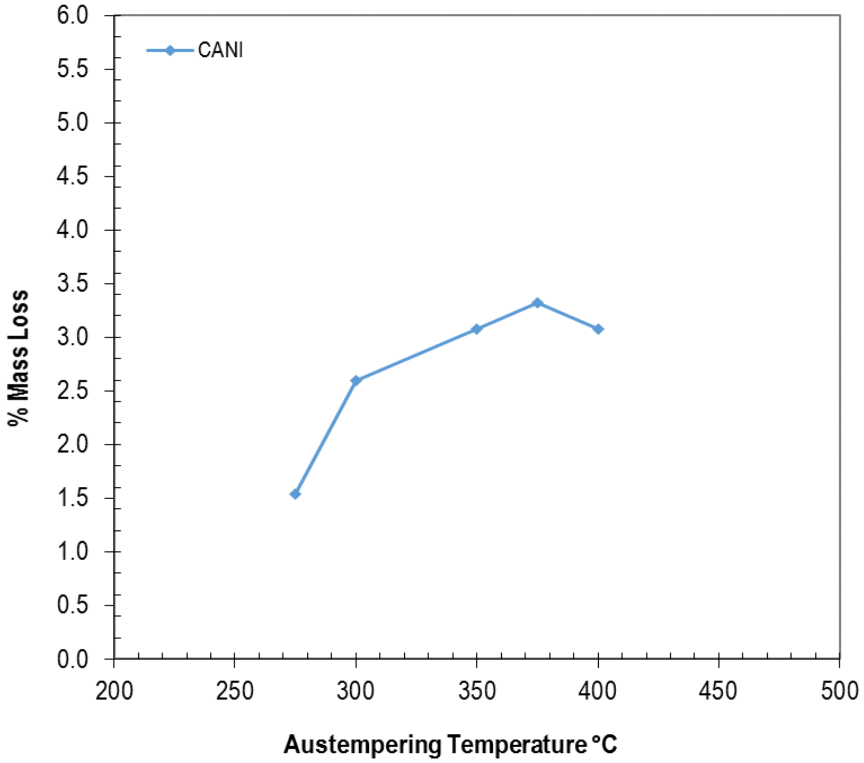

Figure 4.40. Influence of austempering temperature on ball mill wear of the CANI grinding balls.

5. CHAPTER 5: DISCUSSION

A detailed comparative study of the performance of CANI milling balls versus HCWCI as a benchmark in various environments was performed. Therefore, this chapter discusses the results of the retained austenite amounts obtained during the heat treatment of the experimental high chromium white cast iron and carbidic austempered nodular iron studied in this project. It discusses in depth the metallurgical phenomena (such as carbon partitioning) that occurred by the changes in austenitising, tempering and austempering temperatures and how these are expected to affect the amount of retained austenite (RA) through changes in the deformation induced martensite transformation temperature, M_d. This chapter addresses the question of "**why**" the abrasion wear (i.e. high stress, low stress and ball mill) of the two alloys (CANI and HCWCI) were different since up to Chapter 4 the question "**what**" was extensively addressed.

In order to investigate the "**what"** and the "**why"**, the resulting microstructures and subsequent mechanical properties of the specimens which were subjected to twenty various heat treatments, i.e. as-cast, forced quenched (FAQ), FAQ+350T (tempered at 350 °C), FAQ+450T (tempered at 450 °C), and austempered between 275 and 400 °C were evaluated under:

- high stress abrasive wear (POB)
- low stress abrasive wear (DRWAT)
- abrasive and impact wear (wet ball mill simulation).

Various temperatures were selected and used so that they could produce different amounts of retained austenite. The results of the retained austenite amounts obtained during the various heat treatments are summarised and compared in Table 5.1. The effect of retained austenite is correlated to either purely abrasive wear (i.e. high and low stress), combination of abrasive and impact wear (i.e. wet ball mill simulation), or with hardness.

The influence of retained austenite on hardness and abrasive wear behaviour of both HCWCI and CANI specimens was determined, and their comparison is also shown in Table 5.1.

Table 5.1. General comparison of mechanical and metallurgical results between HCWCI and CANI alloys.

Alloy Identity	**% RA**	**% Mass Loss - POB**	**Volume Loss - DRWAT**	**% Mass Loss – Ball Mill**	**Microstructures**	**Surface Hardness (HB)**
875°C + FAQ	10.6	0.49	12.2	2.04	M+EC+RA	785
925°C + FAQ	9.2	0.49	-	1.78	M+EC+RA	796
1000°C + FAQ	32.0	0.60	-	1.74	M+EC+RA	772
1050°C + FAQ	40.5	0.54	-	3.53	M+EC+RA	739
1100°C + FAQ	57.3	0.38	-	2.03	M+EC+RA	558
875°C + FAQ +350°C T	8.9	0.61	47.8	2.04	M+EC+SC+RA	770
925°C + FAQ +350°C T	10.6	0.61	-	1.91	M+EC+SC+RA	782
1000°C + FAQ +350°C T	33.2	0.46	-	1.57	M+EC+SC+RA	719
1050°C + FAQ +350°C T	32.3	0.52	-	2.47	M+EC+SC+RA	631
1100°C + FAQ +350°C T	54.9	0.49	-	1.83	M+EC+SC+RA	501
875°C + FAQ +450°C T	6.5	0.47	34.6	2.20	M+EC+SC+RA	690
925°C + FAQ +450°C T	3.0	0.49	-	2.11	M+EC+SC+RA	686
1000°C + FAQ +450°C T	11.5	0.51	-	1.64	M+EC+SC+RA	697
1050°C + FAQ +450°C T	22.6	0.31	-	3.35	M+EC+SC+RA	615
1100°C + FAQ +450°C T	32.7	0.34	-	2.13	M+EC+SC+RA	474
CANI_275°C	17.4	2.04	14.6	1.54	AF+C	582
CANI_300°C	21.8	2.01	-	2.59	AF+C	415
CANI_350°C	26.1	2.41	71.5	3.07	AF+C	392
CANI_375°C	16.4	2.24	-	3.32	AF+C	433
CANI_400°C	16.6	2.17	58.9	3.08	AF+C	472

M = martensite, EC = eutectic carbides, SC = secondary carbides, RA = retained austenite, AF = ausferrite and C = carbides

The main objective of this study was to determine the optimal heat treatment process for the 12%Cr HCWCI and 0.5%Cr CANI balls that will give the best abrasive wear performance. The results emanated from different heat treatment processes were individually compared and the optimal thermal process from each of the alloys was then taken forward.

The best heat treatment process in terms of performance under high stress, low stress and ball mill abrasion wear conditions from each alloy are compared as summarised in Table 5.1. The ball mill is one of the critical steps in the comminution of minerals in the mining industry . Therefore, the comparison of the results from ball mill abrasion wear simulation is of paramount importance. In the next sections, the retained austenite results from tempered HCWCI and austempered CANI alloys are correlated to all properties and wear behaviour.

5.1. Effect of retained austenite on high stress abrasion wear – POB

The wear resistance of both HCWCI and CANI pin samples before and after the high stress abrasion wear test (POB) is graphically presented in Figures 4.17 to 4.20. There is no clear correlation between the amount of retained austenite and high stress abrasion wear for CANI as compared to the HCWCI. As may be seen from Figure 4.18 for HCWCI, as the retained austenite increases the high stress abrasion wear resistance increases too. Some of the retained austenite of the HCWCI transformed to martensite during high stress abrasion wear due to strain induced martensite (SIM) mechanism. As the austempering temperature was raised from 275 °C to 400 °C the amount of retained austenite was found to increase in the matrix from 17% to a maximum of 26% at an optimal austempering temperature of 350 °C but then decreased at higher temperatures.

As shown in Figures 4.18 and 4.20, the HCWCI alloys showed a significant low percentage mass loss of between 0.3 and 0.6% as compared to the CANI that was greater than 2%. For both alloys, the amount of retained austenite that underwent the deformation induced martensite transformation was between 10 and 15%. Therefore, the better performance of HCWCI can only be attributed to its higher volume fraction of the hard eutectic and secondary carbides, especially M_7C_3 that formed in the matrix. On the contrary, the CANI's matrix structure was predominantly ausferrite with a low volume fraction of M_3C carbides. According to literature [99], the hardness of a grinding ball is governed by mainly the hardness and volume fraction of the primary carbides, which are mostly of the Cr-rich type M_7C_3 in most Cr-containing HCWCI irons with a Knoop hardness of about 1600 KHN. The only other harder carbides would be the type MC, i.e. typically VC and NbC as shown in Figure 5.1 below, with a hardness exceeding 2200 KHN. The preferred primary carbide is the Cr-rich M_7C_3 type (and not M_6C or M_3C).

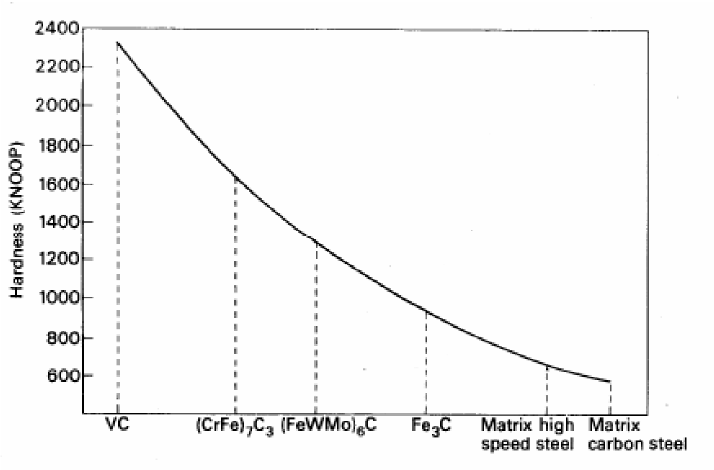

Figure 5.1. Figure on Vickers/Knoop hardness's of carbides [99].

As may be seen from Figure 4.17 and Table 5.1, the amount of retained austenite after tempering was found to be insensitive to the latter up to 350 °C and only began to decline beyond this temperature. This observation is in agreement with what Zhang et al. [100] found where the tempering of HCWCI below 400 ºC did not affect the amount of retained austenite and its mechanical properties. The amount of retained austenite drastically reduced when tempering was carried out above 400 ºC, i.e. the retained austenite became unstable.

Overall, the best high stress abrasion (POB) resistance was obtained on HCWCI specimens that were austenitised at 1050 °C and 1100 °C and then tempered at 450 °C as compared to CANI. The percentage mass loss values of these specimens after high stress abrasion wear are 0.31 and 0.34 respectively. It is known that the excellent wear resistance of HCWCI is largely due to the *in situ* hard carbides, especially M_7C_3 that formed in the microstructure [101].

The presence of retained austenite in the martensitic matrix also provides strain hardening capability that is needed to delay the material displacement, ploughing and cutting that is produced by the abrasive particles striking on the surface during wear [102].

The interaction between carbide precipitation and martensitic transformation during the heat treatment process (i.e. at 1050 °C and 1100 °C, then tempered at 450 °C) led to considerable fine secondary carbides and stable carbon-enriched retained austenite, see Figures 4.9 and 4.10. Unfortunately, the hardness values of these samples were below 615HB which is not ideal for other environments. This was probably due to competition between the processes of carbon partitioning from the martensite into the residual austenite, and the precipitation of excess carbon in the martensite.

By comparing the amount of deformation induced martensite of the two casts which were austenitised at 900 °C (CANI) and 920 °C (HCWCI), see Tables E and F in the Appendix, the values for CANI were found to be higher than those of the HCWCI. However, the CANI's performance was found to be poor under high stress abrasion wear (POB) as compared to the HCWCI alloy. This suggests that the better performance of the HCWCI alloy was due to the higher volume fraction of the M_7C_3 carbides and not necessarily to the deformation induced martensite.

However, within the CANI, the best high stress abrasion (POB) resistance was obtained after austempering at 275 °C. This is attributed to the higher hardness and finer microstructures. During the austempering heat treatment process of as-cast carbidic ductile iron the ausferrite preferentially forms instead of pearlite matrix. This ausferrite has very good abrasive wear properties because of its tendency to "strain transform" i.e. transforms to martensite which has higher hardness on the abraded surface [103]. The austempering temperature range between 350 and 400 °C led to lower strength, hardness and wear resistance as a result of a coarse ausferrite matrix, while below 350 °C, the converse was true, see Figure 4.20. From this work, it has been found that the austempering temperature of 275 °C was the threshold temperature for optimum mechanical properties of CANI for POB tests.

As shown in Figures 4.31 to 4.36, the worn surface of all specimens showed ploughing grooves and micro-cutting. These results showed that both the micro-ploughing and micro-cutting took place simultaneously. The micro-ploughing, however, was found to be the dominant mechanism during all the tests.

A strain induced martensite (SIM) transformation phenomenon occurs only if appropriate conditions are fulfilled [103], namely: presence of metastable, low carbon-enriched, retained austenite; and local pressure on the metal matrix is sufficient. This SIM was therefore prevalent in a high stress abrasive environment.

5.2. Effect of retained austenite on low stress abrasion wear – DRWAT

As shown in Figures 4.37 and 4.38, the best low stress abrasive wear resistance was achieved from the CANI samples austempered at 275 °C and this was due to the combination of high hardness due to finer microstructures. Unfortunately, samples from only one destabilisation temperature were used for this low stress abrasion test.

Both Figures 4.37 and 4.38 show that there was an optimum amount of retained austenite for HCWCI and CANI. As may be seen, a higher hardness as a result of higher volume fraction of carbides and lower amount of retained austenite largely contributed to better abrasion resistance of the alloys.

By comparing the mass loss against testing time for the two casts austenitised at 900 °C (CANI) and 875 °C (HCWCI), the loss in mass values of CANI were found to be significantly lower than those of the HCWCI. The CANI samples from all austempering temperatures performed better under low stress abrasion wear (DRWAT) than the HCWCI.

In other words, the volume fraction of carbides did not play a significant role on low stress abrasion tests. The improvement in the wear resistance of the austempered specimens may be attributed to the lubricity inherent in the graphite nodules [104].

Overall, the best low stress abrasion (DRWAT) resistance was obtained by the samples that were austempered at 275 °C and this was due to the finer microstructures and high hardness. The ausferrite matrix had very good abrasive wear properties because of its tendency to "strain transform" on the abraded surface [103]. With respect to the matrix, it is generally accepted that a higher hardness promotes higher abrasion resistance.

In this work, the influence of the matrix microstructure and its corresponding hardness given in Table 5.1, where the highest wear resistance (under the present experimental conditions) corresponds to the matrix with the highest hardness and the lowest wear resistance, corresponds to that of the matrix with the lowest hardness.

5.3. Effect of retained austenite on abrasion and impact wear – Ball Mill simulation

As may be seen from Figures 4.39 and 4.40, the better abrasive wear resistance for the ball mill simulation was achieved from the CANI samples austempered at 275 °C with 17% retained austenite and percentage mass loss of 1.54%. This performance was comparable to HCWCI after austenitising at 1000 °C and tempering at 350 °C whereby the percentage mass loss was found to be 1.57%. CANI consists of carbides, graphite nodules embedded in an ausferrite matrix. Graphite lubricates the working interfaces and improves the wear resistance [104].

It was also observed in Figure 4.40 that as the hardness decreased with an increase in austempering temperature, the abrasion wear resistance decreased and the converse was true. At a lower austempering temperature of 275 °C, finer ferrite and a lower volume fractions of high carbon austenite are present which in turn raises the hardness of the alloy, i.e. yielding higher hardness values up to ~580 HB. With an increase in austempering temperature (≥350 °C), the acicular/fine ferrite became thicker and bigger and the hardness decreased. As the austempering temperature was raised from 275 °C to 400 °C, there was a marginal decrease in the hardness at 350 °C which was the maximum stabilisation temperature for the CANI, see Figure 4.16.

The second best performance from abrasive ball mill tests was exhibited by the HCWCI specimen that was austenitised at 1000 °C, FAQ and tempered at 450 °C as shown in Figure 4.40. The percentage mass loss after abrasion wear was found to be 1.64%. The set of HCWCI grinding balls that showed best abrasive ball mill wear resistance of 1.57% and 1.64%, had the retained austenite content of 33% and 11% respectively. The wear properties of high-chromium white cast iron depends on the optimal combination of matrix hardness and toughness, i.e. coarsening of carbides and increasing content of retained austenite which inhibits crack formation [105].

6. CHAPTER 6: CONCLUSIONS

The influence of retained austenite on hardness and abrasive wear behaviour of both HCWCI and CANI alloys in various test environments including simulating ball mill conditions, was determined, and the following conclusions were made:

- The HCWCI performed best in the high stress abrasion tests and this was due to the type and relatively high volume fraction of carbides present in addition to the mixture of retained austenite and martensite in the matrix as compared to CANI which had less carbides.

- The best low stress abrasion (DRWAT) resistance was exhibited by the CANI samples that were austenitized at 900 °C and austempered at 275 °C. This was due to the finer microstructure and high hardness. The ausferrite matrix exhibited good abrasive wear properties because of its tendency to "strain transform" on the abraded surface.

- The better abrasive wear resistance for ball mill simulation was achieved from the CANI samples austempered at 275 °C with a percentage mass loss of 1.54%. This performance was comparable to HCWCI after austenitising at 1000 °C and tempering at 350 °C whereby the percentage mass loss was found to be 1.57%. This is attributed to the graphite nodules embedded in the ausferrite matrix that lubricates the working interfaces and the optimal combination of matrix hardness and toughness, i.e. coarsening of carbides and increasing content of retained austenite.
- The optimum amount of retained austenite was not conclusive to good wear resistance since the role of carbides and matrix microstructural variations could not be isolated to see the effects of retained austenite acting alone. Therefore, a significant amount of controversy still exists on the levels and extent to which it is beneficial.

7. CHAPTER 7: FUTURE WORK

As part of future work, the following investigations could be considered:

- Dilatometry tests to help in interpreting phase transformation that occurred on the two cast materials.
- Neutron diffraction using HRPD to confirm the amount of retained austenite measured by XRD on samples austenitised, tempered and austempered at various temperatures
- High definition field ion microscopy atom probe tests to study the partitioning of carbon from martensite to retained austenite during heat treatment during austempering process and the type of martensite/ausferrite present. Also to study the formation, shape, size, morphology, and distribution of secondary carbides using scanning electron microscopy (SEM) and transmission electron microscopy (TEM).
- The dry rubber wheel abrasion test (DRWAT) was carried out only on HCWCI samples austenitised at 875°C and air quenched and, therefore, other quenching temperatures should be studied in order to determine the effects of the austenitising temperature on DRWAT.
- The behaviour of retained austenite under conditions of impact for both the HCWCI and CANI was not studied in this work and it is proposed that this be conducted in future. This is required to further develop the understanding of the influence of retained austenite on impact wear.

8. CHAPTER 8: REFERENCES

1. R. Fuoco, Wear Resistant Cast Materials for the Mining Industry, 2nd BRICS Foundry Forum, China, May 2012
2. Mining Review Africa 2003, *The milling process in mineral processing,* Issue 4, 2003, www.miningreview.com, accessed in 2007
3. DRA News Bulletin, *New mining process plant design and project management*, www.drasa.co.za/news, accessed in 2007
4. http://practicalaction.org/practicalanswers, Practical Action, *Mineral Processing Milling - Mining and minerals* , accessed in 2007
5. S.L. Gay, *A liberation model for comminution based on probability theory,* Minerals Engineering 17 (2004) pp. 525–534
6. J. Kruttschnitt Mineral Research Centre (JKMRC), Lecture 1, *Comminution and Classification Equipment*, 2006
7. U. Cloos., (Doering GmbH, West Germany). Cylpebs: An alternative to balls as Grinding media. *World Mining,* **36**, (10) 59. 1989
8. E.T. Stamboliadis, *The energy distribution theory of comminution specific surface energy, mill efficiency and distribution mode*, Minerals Engineering 20 (2007) pp140–145
9. B. Clermont, *Optimize mill performances by using on-line ball and pulp Measurements*, The 6th International Comminution Symposium (Comminution 08) June 17-20, 2008
10. P. Radziszewski, Rena Varadi, Tapiwa Chenje, Lena Santella, AnthonySciannamblo, Tumbling mill steel media abrasion wear test development, Minerals Engineering 18 (2005) 333–341
11. W. K. Tolley. I. Nichols. and J. Huiatt, Corrosion Rates of Grinding Media in Mill Water, Bureau of Mines Report of Investigations 8882, 1984
12. L.A. Vermeulen and D.D. Howat, “Quantitative Assessments of Abrasive and Impactive Wear from Ball-Size Distributions in Rotary Mills”, Mintek Report No. M201, 6 May 1985
13. http://www.themininggrindingoffice.com/ accessed in 2013
14. B. Pålsson, B Jarousseau, and S Persson, *Influence of oxygen content in grinding mills*, The 6th International Comminution Symposium (Comminution 08) June 17-20, 2008
15. B.A. Wills., 1992. Mineral Processing Technology. Pergamon Press, Oxford, England.
16. Magotteaux Fond, Patent specification number GB1315203 – Balls and Lining plates for crushing and grinding mills and or other castings intended to withstand abrasion and repeated impact shock loads and the steels for their manufacture, 1973, Belgium
17. D.D. Howat, Spotlight on wear and abrasion in industry Journal of the South African Institute of Mining and Metallurgy, June 1981
18. M. Van Eck, A.N. Mainza, and M.S. Powell, Investigating the Products from Different Modes of Particle Breakage Testing, MSc. Thesis submitted to the University of Cape Town, October 2007
19. R.T. Jones, Platinum Smelting in South Africa, Platinum is produced in South Africa by Amplats, Impala Platinum, Lonrho Platinum, 2001

20. L.A. Cramer, The Extractive Metallurgy of South Africa's Platinum Ores, JOM, October 2001
21. L.A. Cramer, J. Basson and L.R. Nelson, The Impact Of Platinum Production From Ug2 Ore On Ferrochrome Production In South Africa, Proceedings: Tenth International Ferroalloys Congress INFACON X: 'Transformation through Technology; February 2004'
22. Platinum Group Metals in SA, Impala Platinum Holdings Limited Annual Report 2003
23. J. Nell, Melting of platinum group metal concentrates in South Africa, The Journal of The South African Institute of Mining and Metallurgy, volume 104, number 07, p423, August 2004
24. http://wwwu.edu.uni-klu.ac.at/mmessner/sites/rsa/wits/wits.htm, accessed 2013
25. http://nevada-outback-gems.com/prospect/gold_specimen, Natural Gold Ores and Minerals, accessed 2009
26. D.D. Howat, An Assessment of the merits of various types of ball in the milling of ores, Mintek Private Communication Report No. M117, November 1993
27. E. Albertin, A. Sinatora, Effect of carbide fraction and matrix microstructure on the wear of cast iron balls tested in a laboratory ball mill, Wear 250 (2001) 492–501
28. https://www.google.co.za/SAG mills, accessed 2013
29. R.T Warren and B. Chicco, "The Iron Rich Corner of the Metastable C-Cr-Fe Liquidus Surface", *Met. Trans.,* 16A, (9) pp.1541-1549 (1985)
30. J.R. Davis, Ed., Cast Irons, ASM Specialty Handbook, ASM International, 1996
31. S. Kuyucak and R. Llewellyn, High-Chrome White Irons Incorporating Ultra-Hard Carbide-Forming Elements for Improved Wear-Resistance, Paper 06-097(05), AFS Transactions 2006 © American Foundry Society, Schaumburg, IL USA
32. J.R. Brown, FOSECO Foundryman's Handbook. London: Butterworth Heinemann, 1994.
33. T. Noguchi, K. Shimizu, N. Takahashi, T. Nakamura, Strength evaluation of cast iron grinding balls by repeated drop tests, Wear 231, 301–309, 1999
34. J.S. Moema, Wear test and characterisation of grinding balls, Mintek Private Communication, 2005
35. http://pauloabbe.com/productLines/millingEquipments/images, Principles of grinding, accessed in 2007
36. http://www.steelballs.cc/grinding-steel-balls, China Shandong Huamin Casting and Forging Joint-Stock Co.,Ltd. Design:Luck-Star, , accessed in 2008
37. X. Fan, H.E. Lin and Z. Qingdel, A structural study of high Cr cast iron as a grinding ball material, China Journal Metallurgical Scientific Technology., Vol 5, 1989
38. V.L.L.J. Joiret, United States Patent 4043842 (US4043842), Grinding Members or Magotteaux Patent Number GB1315203, July 1977
39. J.R. Keough, Ductile Iron Data for Design Engineers, *Austempered Ductile Iron*, Ductile Iron Society, Strongsville, Ohio, USA, August 1998
40. J.R. Keough and K.L. Hayrynen, Carbidic Austempered Ductile iron (CADI), Presented at DIS Meeting on November 14, 2000

41. K. Hayrynen, Carbidic Austempered Ductile Iron (CADI) – The New Wear Material, Transactions of the American Foundry Society Vol. 111, Paper No 03-088 P 845-850, 2003).(SIMBA International, www.simba.co.uk)
42. K.L. Hayrynen and K.R. Brandenberg, Carbidic Austempered Ductile Iron (CADI) – The New Wear Material, Transactions of the American Foundry Society V 111 Paper No 03-088 P 845-850, 2003
43. S. Laino, J.A. Sikora, R.C. Dommarco, Development of wear resistant carbidic austempered ductile iron (CADI), Wear 265 (2008) 1–7
44. A. Nofal, *Advances in the Metallurgy and Applications of ADI*, Journal of Metallurgical Engineering (ME), Volume 2, Issue 1, January 2013, www.me -journal.org
45. C.P. Tabrett and I.R. Sare, Effect of heat treatment on the abrasion resistance of alloy white irons, Wear, 203-204(1997), p.206 - 219
46. http://www.stle.org/resources/lubelearn/wear/, accessed in 2013
47. B Bhushan, *Types of Wear Mechanism*, Principles and Applications of Tribology, ISBN 0471 59407-5, p479-583, March 1999
48. K. Hokkirigawa., and K. Kato, An experimental and theoretical investigation of ploughing, cutting and wedge formation during abrasive wear, *Tribology Int.,* 21, 1, 51-57, 1988
49. K. Kato. K, Hokkirigawa, The effect of hardness on the transition of the abrasive wear mechanism of steels, Wear 123, (1988) p241-251
50. ASTM G132-96, Standard Test Method for Pin Abrasion Testing, West Conshohocken, PA 19428-2959, United States.
51. R. Blickensderfer, J. H. Tylczak, and B. W. Madsen, Laboratory Wear Testing Capabilities of the Bureau of Mines, Bureau of Mines Information Circular, 1985
52. R. Blickensderfer, J.H. Tylczak and G.Laird, Spalling of High-Chromium White Cast Iron Balls Subjected to Repetitive Impact, 'Wear of Materials 1989', Denver, CO, April 1989, Vol. 1, 175-182, 1989, ASME
53. M. Izcilera, H. Celik, *Two- and three-body abrasive wear behaviour of different heat-treated boron alloyed high chromium cast iron grinding balls*, Journal of Materials Processing Technology 105 (2000) 237-245
54. T.E. Norman., Climax Finds New Austenitic Alloy Ideal for Ultra-Abrasive Mine •Mill Applications. Eng. and Min. J., v. 166, No.4, 1965, pp. 86-90.
55. ASTM G65-04, Standard Test Method for Measuring Abrasion using the Dry Sand/Rubber Wheel Abrasion Tests, ASTM International, West Consholocken, PA, USA, 2004
56. G Agarwal, A Patnaik, R Kumar Sharma, *Parametric Optimization and Three-Body Abrasive Wear Behaviour of Sic Filled Chopped Glass Fibre Reinforced Epoxy Composites*, International Journal of Composite Materials 2013, 3(2): p32-38
57. M. Izcilera, *The effects of chromium content and heat treatments on abrasive wear behaviour of cast irons under different temperature sliding conditions*, Ph.D. Thesis, Firat University, 1997
58. ASTM G105, Standard Practice for Conducting Wet Sand/Rubber Wheel Abrasion Tests, ASTM G105, Wear and Erosion: Metal Corrosion, Vol. 03.02, ASTM
59. M. Fiset, G. Huard, M. Grenier, C. Jacob, G. Comeau, Three-body impact-abrasion laboratory testing for grinding ball materials, Wear 217 (1998) 271-275

60. R.D Morrison, Shi, F. and Whyte, R. (2007). Modelling of incremental rock breakage by impact – For use in DEM models. Minerals Engineering. 20, 303-309.
61. R. Blickensderfer and J.H. Tylczar. A large scale Impact spalling Test. Wear, Vol. 84, No. 3, 1983, pp. 361 -373.
62. L.I. Wei, Effect of Microstructure on Impact Fatigue Resistance and Impact Wear Resistance of Medium Cr-Si Cast Iron, Journal of Iron and Steel Research, International. 2007, 14(3): 47-50.
63. T. Noguchi, Kazumichi Shimizu, Norio Takahashi and Takashi Nakamura, Strength evaluation of cast iron grinding balls by repeated drop tests, Wear 231 (1999), 301–309
64. T. Hayashi, Y. Tanaka, Shogeki Kogaku, Impact Engineering, Nikkan Kogyo Shinbun, 1988, 145.
65. L.A. Vermeulen, D.D. Howat, and C.L.M. Gought, Theories of ball wear and the results of a Marked-ball test in ball milling, Journal of the South African Institute of Mining and Metallurgy, Vol. 083, No. 08, August 1983 pp189-197.
66. M Legros and Johan Dahner, Milling circuit optimization Methodology and objectives, Innovation and Optimization in Difficult Times MMMA Seminar – 08 May 2009.
67. M.S. Powell and R.D. Morrison, International Journal of Mineral Processing, Vol. 84, Issues 1-4, 19 October 2007, pp 228-239.
68. M.J. Meulendyke and J.D. Purdue, Wear of grinding media in the mineral processing industry: Overview, Minerals and Metallurgical Processing, Nov 1989, p. 167-172.
69. J.G. Speer, D.V. Edmonds, F.C. Rizzo F.C. and D.K. Matlock: Curr. Opin. Solid State Mater. Sci., 2004, 8, 219-237.
70. J. Speer, D.K. Matlock, B.C. De Cooman, and J.G. Schroth, Acta Material., 2003, vol. 51, pp. 2611–22.
71. X. Jia, X. Zuo, Y. Liu, N. Chen, and Y. Rong, High Wear Resistance of White Cast Iron Treated by Novel Process: Principle and Mechanism, Metallurgical and Materials Transactions A, 5514, Vol. 46A, December 2015.
72. S.W. Ooi, Y. R. Cho, J. K. Oh and H. K. D. H. Bhadeshia, Carbon enrichment in residual Austenite during martensitic transformation, The Minerals, Metals & Materials Society (TMS), pp179 – 185, ICOMAT 08, 2009.
73. Y. Toji, G. Miyamoto and D. Raabe, Carbon partitioning during quenching and partitioning heat treatment accompanied by carbide precipitation, Acta Materialia 86 (2015) 137–147
74. A.J.S.T. da Silva, M.F. de Campos, A.S. Nishikawa, W.L. Guesser and H. Goldenstein, Quenching and Partitioning process in Ductile Cast Irons, 10th International Symposium on the Science and Processing of Cast Iron – SPCI10.
75. D.J. Dyson and B. Holmes: Design of novel high-strength bainitic steels, Journal of the Iron and Steel Institute, 1970, Vol. 208, pp469-470.
76. N. Bhople, S. Patil, M. Harne, S. Dhande, Austempering Parameters and Machinability of Austempered Ductile Iron: A Comprehensive Review on Effective Parameters, International Journal of Innovative Research in Science, Engineering and Technology, Vol. 5, Issue 2, February 2016, pp1197 - 1211

77. T. Thein, L. Kay, “Optimizing the microstructure and mechanical properties of ADI for automobile differential gear”. Journal of Metals, Materials and Minerals, Vol.18 No.2 pp.199-205, 2009.
78. Z. Mohammad, A.P. Hamid, A.P Hamed, (2013). Wear characteristics of ADIs; A comprehensive review on mechanisms and effective parameters. Journal of Basic Applied Science Research. 3(2)646-656, ISSN 2090-4304, text road publication, 2013.
79. T Zhang, Effect of Chromium on Microstructure and Mechanical Properties of Carbidic Austempered Ductile Iron, Thesis on Materials Processing Engineering, 2010-02-24
80. J. Liu, G. Li, X. Zhao, X. Hao, and J. Zhang, Effect of Austempering Temperature on Microstructure and Properties of Carbidic Austempered Ductile Iron, Materials and Design 10.4028/www.scientific.net/AMR.284-286
81. K.S. Swain, K.R. Panda, J.P. Dhal, S.C. Mishra, and S. Sen, “Phase Investigation of Austempered Ductile Iron”. Orissa Journal of Physics, Vol. 19, No.1, ISSN 0974-8202, pp. 73-80, 2012.
82. K. Aslantas, I. Ucun, K. Gok, “Evaluation of the performance of CBN tools when turning austempered ductile iron material”. Journal of Manufacturing Science and Engineering, October 2008, Vol. 130 / 054503-1, 2008.
83. Z. Ławrynowicz and S. Dymski, Carbon Concentration of Austenite in Austempered Ductile Iron (ADI), Archives of Foundry Engineering, ISSN (1897-3310) Volume 7 Issue 3/2007
84. ASM Special Handbook, Cast Iron, Metallurgy and Properties of High Alloy White Iron, ASM International, 1996
85. W.P. Barnard., Investigation of ground engaging tool materials to improve on their wear and toughness characteristics. Private Technical Memorandum no. 19378. Mintek, 1999
86. Durferrit GmBh AS 140 Salt, www.durferrit.com E-Mail: ockert@durferrit.co.za, accessed in 2009
87. ASTM E915-96, Standard Test Method for Verifying the Alignment of X-Ray Diffraction Instrumentation for Residual Stress Measurement, ASTM International, West Conshohocken, PA, Published 2003.
88. SAE J784, *Standards to Determine the Volume Percentage of Retained Austenite,* SAE International Journal of Materials & Manufacturing, Published 2003.
89. ASTM E975-03, Standards practice for X-Ray Determination of Retained Austenite in steel with near random crystallographic orientation, SAE International Journal of Materials & Manufacturing, Published December 2003.
90. M Smith, The influence of the degree of transformation of M_7C_3 carbides to $M_{23}C_6$ carbides on the properties of high chromium white cast irons, *M.Sc. Thesis*, University of the Witwatersrand, Johannesburg, 1994
91. ASTM G65-85, Annual book of ASTM standards, Standard Test Method for Measuring Abrasion Using the Dry Sand/Rubber Wheel Apparatus, ASTM. Philadelphia, Published November 2004.
92. K.P. Ngwenya, Wear test and characterisation of 70mm diameter grinding balls. Mintek Service report no. 73009905 (28). Mintek, 2004

93. J.S. Moema, J. Zimba, G.A. Slabbert, M.J. Papo, *Development of Novel and Cost Effective Grinding Media for the Platinum Industry: Project T50049*, *(Technical Report No. 2), Mintek Report No. 4950*, 30th May 2008.

94. F.A. Maratray and R. Usseglio-Nanot, Factors affecting the structure of chromium and chromium-molybdenum white cast iron, Climax Molybdenum Publications, USA, 1970.

95. G. Laird., II. (1993): Some Comments on White Cast Iron Microstructures and Wear Properties, Transactions of the AFS, 101, 497-504.

96. P. Dupin and J.M. Schissler, Influence of addition of silicon, molybdenum, vanadium, and tungsten upon the structural evolution of the as-cast state of a high-chromium cast iron (20% Cr, 2.6% C). AFS Trans, 92, pp.355–360, 1984.

97. G.F. Vander Voort., Manilova E.P., Michael J.R. and Lucas G.M., Study of Selective Carbide Etching of Carbides in Steel.

98. R.A. Couperthwaite, , Guidelines for Optimal Operation of the EDAX Electron Backscatter Diffraction (EBSD) System, Mintek Internal Report No. 42625, March 2017.

99. G.A. Roberts, J.C. Hamaker and A.R. Johnson, Knoop hardnesses of some of the carbides as they relate to the expected hardness of the matrix, Tool Steels, Publication ASM (US) (1962).

100. M.X. Zhang, Kelly PM, Gates JD, Journal of Materials Science, Vol. 36, No16, pp3865-3875. 2001.

101. S.K Chang. D.G Kim and J.W. Choi, Effects of Alloying Elements and Austenite Destabilization Treatment on Graphitization of High Chromium Cast lron, ISIJ International, Vol. 32 (1992), No. 11, pp.1163-1169.

102. S. Turenne, F. Lavallee, J. Masounave., Matrix microstructure effect on the abrasion wear resistance of high-chromium white cast iron, Journal of Materials Science 24 (1989) pp3021-3028

103. P. Dhanapal and A.S Ibrahim, Production of Carbidic Austempered Ductile Iron [CADI] International Conference on Systems, Science, Control, Communication, Engineering and Technology 2016 [ICSSCCET 2016]

104. C. Siddaraju, N.D. Prasanna, M.K. Muralidhara., Abrasive Wear Studies on Austempered Ductile Iron Castings, International Journal of Emerging Technology and Advanced Engineering., Website: www.ijetae.com (ISSN 2250-2459, ISO 9001:2008 Certified Journal, Volume 3, Issue 6, June 2013)

105. T Jian-Min, Z. Yi-Zhong, S. Tian-Yi, D. Hai-Jin - The influence of retained austenite in high chromium cast iron on impact-abrasive wear, Wear, Vol. 135, pp217-226, 1990

9. CHAPTER 9: APPENDICES

Data Tables

Table A. Electron probe micro-analyses (EPMA) results of HCWCI alloys.

Alloy	Elemental (wt%)					Phase
	C	Si	Cr	Mn	Fe	
HCWCI	8.45	0.03	40.4	0.77	50.8	Carbide
875 FAQ	1.86	1.00	8.3	0.52	88.8	Matrix
875-350	1.82	1.00	8.3	0.54	89.0	Matrix
875-450	1.80	0.98	8.2	0.52	88.9	Matrix
925 FAQ	1.76	1.10	8.0	0.50	87.6	Matrix
925-350	1.88	1.28	8.1	0.56	89.1	Matrix
925-450	1.75	1.28	8.3	0.55	88.5	Matrix
1000-FAQ	1.78	1.23	8.5	0.55	88.4	Matrix
1000-350	1.80	1.29	8.1	0.56	88.9	Matrix
1000-450	1.94	1.25	8.0	0.55	88.8	Matrix
1050-FAQ	1.49	1.29	7.3	0.56	89.9	Matrix
1050-350	1.84	1.25	8.6	0.57	88.4	Matrix
1050-450	1.61	1.27	8.2	0.53	88.7	Matrix
1100-FAQ	1.31	1.34	6.9	0.57	90.3	Matrix
1100-350	2.05	1.19	8.0	0.56	88.2	Matrix
1100-450	1.50	1.28	7.5	0.57	88.4	Matrix

Table B. Electron probe micro-analyses (EPMA) results of CANI alloy.

Alloy	Elemental (wt%)					Phases
	C	Si	Cr	Mn	Fe	
CANI	5.77	0.28	2.6	1.87	91.8	Carbide
809 CANI	0.77	3.23	0.6	1.03	99.9	Matrix
809-275	0.76	3.25	0.5	0.86	94.4	Matrix
809-350	0.95	2.53	0.6	0.77	95.3	Matrix
809-375	0.94	3.19	0.5	0.92	94.4	Matrix
809-400	1.43	3.25	0.6	1.13	94.1	Matrix

Table C. Hardness values in Brinell (HB) for the high chromium white cast iron.

Condition	**Brinell hardness, from the surface to the centre (mm)**							**%RA**
	5mm	**10mm**	**15mm**	**20mm**	**25mm**	**30mm**	**35mm**	
As cast	550	550	550	525	525	518	500	-
875°C + FAQ	785	736	766	727	732	720	733	10.6
875°C + FAQ +350°C T	770	768	769	719	686	700	710	8.9
875°C + FAQ +450°C T	690	682	675	682	680	654	672	6.4
925°C + FAQ	796	681	711	696	637	679	681	9.2
925°C + FAQ +350°C T	782	779	782	780	770	773	768	10.6
925°C + FAQ +450°C T	686	678	683	680	677	655	678	2.9
1000°C + FAQ	772	758	754	725	618	672	643	32.0
1000°C + FAQ +350°C T	719	706	709	715	673	702	694	33.2
1000°C + FAQ +450°C T	697	695	692	672	690	695	691	11.5
1050°C + FAQ	739	731	733	710	717	711	696	40.5
1050°C + FAQ +350°C T	631	611	619	611	609	611	607	32.2
1050°C + FAQ +450°C T	615	613	589	593	587	601	591	22.6
1100°C + FAQ	558	536	525	513	487	511	498	38.1
1100°C + FAQ +350°C T	501	485	480	493	491	500	497	54.9
1100°C + FAQ +450°C T	474	484	436	473	468	465	467	50.8

Table D. Hardness values in Brinell (HB) for the carbidic austempered nodular iron (CANI).

Condition	**Brinell hardness from the surface to the centre (mm)**							**%RA**
	5 mm	**10 mm**	**15 mm**	**20 mm**	**25 mm**	**30 mm**	**35 mm**	
CNI_As-cast	365	311	302	307	308	307	304	-
CNI_275°C	582	546	546	554	536	529	526	17.4
CNI_300°C	415	397	405	404	404	407	404	21.8
CNI_350°C	392	377	383	385	389	380	378	26.1
CNI_375°C	433	422	433	406	417	399	404	16.4
CNI_400°C	472	468	415	424	415	399	402	16.6

Table E. Pin-on-belt abrasion results of HCWCI (tested on 120 grit SiC paper).

Alloy Identity	**% Mass Loss**	**% Retained Austenite**		**Change in %RA**
		Before	After	
875°C + FAQ	0.49	10.6	4.1	6.5
875°C + FAQ +350°C T	0.61	8.9	5.3	3.6
875°C + FAQ +450°C T	0.47	6.5	4.1	2.4
925°C + FAQ	0.49	9.2	5.4	3.8
925°C + FAQ +350°C T	0.61	10.6	6.6	4.1
925°C + FAQ +450°C T	0.49	3.0	4.1	-1.1
1000°C + FAQ	0.60	32.0	12.3	19.7
1000°C + FAQ +350°C T	0.46	33.2	13.9	19.4
1000°C + FAQ +450°C T	0.51	11.5	11.9	-0.4
1050°C + FAQ	0.54	40.5	28.2	12.4
1050°C + FAQ +350°C T	0.52	32.3	17.2	15.1
1050°C + FAQ +450°C T	**0.31**	22.6	13.2	9.4
1100°C + FAQ	0.38	**57.3**	35.9	21.4
1100°C + FAQ +350°C T	0.49	54.9	28.2	26.7
1100°C + FAQ +450°C T	**0.34**	50.9	18.2	32.7

Table F. Pin on belt abrasion results of CANI (tested on 120 grit Silicon carbide paper).

Alloy Identity	**Mass Loss (POB)**		**% Retained Austenite**		**% RA Change**
	(g)	**%**	Before	After	
CNI_As-cast	0.3088	2.1			
CNI_275°C	0.3275	2.0	17.4	9.7	7.7
CNI_300°C	0.3052	2.0	21.8	16.8	4.5
CNI_350°C	0.3341	2.4	26.1	11.8	14.2
CNI_375°C	0.2641	2.2	16.4	7.7	8.7
CNI_400°C	0.2411	2.2	16.6	6.02	10.6

Table G. Dry Rubber Wheel abrasion test results of HCWCI.

Alloy Identity	**Average Mass Loss (g)**					
	5 min	**10 min**	**15 min**	**20 min**	**25 min**	**30 min**
As-cast	0.171	0.262	0.345	0.392	0.445	0.461
875°C + FAQ	0.040	0.072	0.083	0.113	0.119	0.132
875°C + FAQ +350°C T	0.140	0.252	0.331	0.425	0.485	0.547
875°C + FAQ +450°C T	0.132	0.175	0.22	0.291	0.351	0.408

Table H. Dry rubber wheel abrasion test results of CANI.

Alloy Identity	Mass Loss (g)					
	5 min	10 min	15 min	20 min	25 min	30 min
CNI_As-cast	0.184	0.351	0.410	0.435	0.451	0.463
CNI_275°C	0.098	0.102	0.110	0.111	0.124	0.121
CNI_300°C	-	-	-	-	-	-
CNI_350°C	0.251	0.453	0.511	0.598	0.682	0.766
CNI_375°C	-	-	-	-	-	-
CNI_400°C	0.273	0.335	0.451	0.512	0.527	0.586

Table I. Influence of retained austenite on wear rate values of the HCWCI grinding balls.

Balls Identity	Initial Total Mass (g)	Total Mass Loss (g)	% Mass Loss	% RA
875°C + FAQ	4953.39	101.06	2.0*	10.6
875°C + FAQ +350°C T	4954.25	100.95	2.0*	8.9
875°C + FAQ +450°C T	5048.12	111.31	2.2*	6.5
925°C + FAQ	6314.04	112.66	1.8	9.2
925°C + FAQ +350°C T	6423.92	122.88	1.9	10.6
925°C + FAQ +450°C T	6214.82	131.31	2.1	3.0
1000°C + FAQ	6216.75	108.07	1.7	32.0
1000°C + FAQ +350°C T	6258.74	98.12	1.6	33.2
1000°C + FAQ +450°C T	6239.18	102.07	1.6	11.5
1050°C + FAQ	6189.49	218.24	3.5	40.5
1050°C + FAQ +350°C T	6304.04	155.88	2.5	32.3
1050°C + FAQ +450°C T	6214.10	208.48	3.4	22.6
1100°C + FAQ	6097.92	123.93	2.0	57.3
1100°C + FAQ +350°C T	6239.40	113.95	1.8	54.9
1100°C + FAQ +450°C T	6170.54	131.29	2.1	50.9

**One ball broke during the abrasive wear test (ball mill) due to casting defects*

Table J. Mass loss values of the 70mm diameter CANI grinding balls.

Balls Identity	Initial Total Mass (g)	Total Mass Loss (g)	% Mass loss)	% RA Before
CNI_275°C	13875.0	213.00	1.5	17.4
CNI_300°C	8595.0	222.79	2.6	21.8
CNI_350°C	3705.3	113.82	3.1	26.1
CNI_375°C	7331.5	243.50	3.3	16.4
CNI_400°C	8518.3	262.38	3.1	16.6